DE MATERIALS QUARTERLY PROGRESS REPORT

For the Period
April 1, 2004 to June 30, 2004

Prepared by:

David P. Stinton, Manager, and
Roxanne A. Raschke
DE Materials Research
Oak Ridge National Laboratory

For:

Department of Energy
Office of Distributed Energy

DE MATERIALS QUARTERLY PROGRESS REPORT

April—June 2004

TABLE OF CONTENTS

Mechanical Characterization of Monolithic Silicon Nitride Si_3N_4
R. R. Wills, S. Hilton, and S. Goodrich
University of Dayton Research Institute, Dayton, Ohio

Microstructural Characterization of CFCCs and Protective Coatings
K. L. More
Oak Ridge National Laboratory, Oak Ridge, Tennessee

DEVELOPMENT OF MONOLITHIC CERAMICS AND HIGH-TEMPERATURE COATINGS

Kennametal's Hot-Section Materials Development
R. Yeckley
Kennametal, Inc., Latrobe, Pennsylvania

Saint-Gobain Hot Section Materials Development
R. H. Licht
Saint-Gobain Ceramics & Plastics, Inc., Northboro, Massachusetts

Environmental Protection Systems for Ceramics in Microturbines and Industrial Gas Turbine Applications, Part A: Conversion Coatings
S. D. Nunn and R. A. Lowden
Oak Ridge National Laboratory, Oak Ridge, Tennessee

Environmental Protection Systems for Ceramics in Microturbines and Industrial Gas Turbine Applications, Part B: Slurry Coatings and Surface Alloying
B. L. Armstrong, K. M. Cooley, M. P. Brady, H-T Lin, and J. A. Haynes
Oak Ridge National Laboratory, Oak Ridge, Tennessee

Polymer Derived EBC for Monolithic Silicon Nitride
R. Raj
University of Colorado at Boulder
Boulder, Colorado

EBC Development for Silicon Nitride Ceramics for Enhanced Hydrothermal Corrosion Resistance
B. Nair, C. Lewinsohn and Q.Zhao
Ceramatec, Inc. Salt Lake City, Utah

Failure Mechanisms in Coatings
J. P. Singh, Kedar Sharma, and P. S. Shankar
Argonne National Laboratory, Argonne, Illinois

High-Temperature Diffusion Barriers for Ni-Base Superalloys
B. A. Pint, J. A. Haynes, K. L. More, and I. G. Wright
Oak Ridge National Laboratory, Oak Ridge, Tennessee

POWER ELECTRONICS

High Temperature Heat Exchanger
E. Lara-Curzio
Oak Ridge National Laboratory, Oak Ridge, Tennessee

Heat Exchange Concepts Utilizing Porous Carbon Foam
B. E. Thompson and A. G. Straatman
University of Ottawa, Ottawa, Ontario, Canada
University of Western Ontario, London, Ontario, Canada

MATERIALS FOR ADVANCED RECIPROCATING ENGINES

Spark Plug Erosion and Failure
M. P. Brady, H. T. Lin, J. H. Whealton, R. K. Richards, and J. B. Andriulli
Oak Ridge National Laboratory, Oak Ridge, Tennessee

Advanced Materials for Exhaust Components of Reciprocating Engines
P. J. Maziasz
Oak Ridge National Laboratory, Oak Ridge, Tennessee

Development of Catalytically Selective Electrodes for NOx and Ammonia Sensors
T. R. Armstrong
Oak Ridge National Laboratory, Oak Ridge, Tennessee

RECUPERATORS

Recuperator Alloys – Composition Optimization for Corrosion Resistance

B. A. Pint
Metals and Ceramics Division
Oak Ridge National Laboratory
Oak Ridge, TN 37831-6156
Phone: (865) 576-2897, E-mail: pintba@ornl.gov

Objective

In order to provide a clear, fundamental understanding of alloy composition effects on corrosion resistance of stainless steel components used in recuperators, the oxidation behavior of model alloys is being studied. The first phase of this study narrowed the range of Cr and Ni contents required to minimize the accelerated corrosion attack caused by water vapor at 650°-800°C. Other factors that continue to be investigated include the effects of temperature, alloy grain size, phase composition and minor alloy additions. These composition and microstructure effects also will provide data for life-prediction models and may suggest a mechanistic explanation for the effect of water vapor on the oxidation of steels. This information will be used to select cost-effective alloys for higher temperature recuperators.

Highlights

The oxidation behavior of model austenitic alloys is being studied in order to better understand the role of minor alloy additions on the accelerated attack (AA) observed in exhaust gas at 650°C-700°C. Initial characterization has been completed on 10,000h specimens of alloy 120 exposed for 10,000h at 650° and 700°C in humid air. At the lower exposure temperature, grain boundary Cr depletion was much more acute near the gas interface and may explain the formation of some Fe-rich oxide nodules that would not normally be expected on a highly alloyed material.

Technical Progress

Experimental Procedure

As outlined in previous reports, model alloys were vacuum induction melted and cast in a water-chilled copper mold, followed by hot forging and rolling to 2.5mm. The sheets were then cold rolled to 1.25mm and annealed under Ar + 4%H_2 for 2 min at 1000°C. Sheet specimens (12mm x 17mm x 1.2mm) were polished to 600 grit SiC finish. The oxidation tests were done in air + 10vol.% water vapor with 100h cycles at 800°C or 1h cycles at 700°C with 10 min cooling between cycles. After oxidation, selected specimens were Cu-plated, sectioned and polished to examine the oxide scale using electron microprobe analysis (EPMA).

Results of oxidation testing

A new series of model alloys was produced to further understand the role of Cr and Ni content on oxidation resistance and particularly lifetime. All of the alloys contain Mn and Si additions but no strengthening elements. Specimens of the new alloys have reached ≈3,000h of exposure and can be compared to the results for the previous series of model alloys, Figures 1 and 2. At 650°C, the most prominent observation is that discrete jumps (perturbations) in mass gain have been observed for

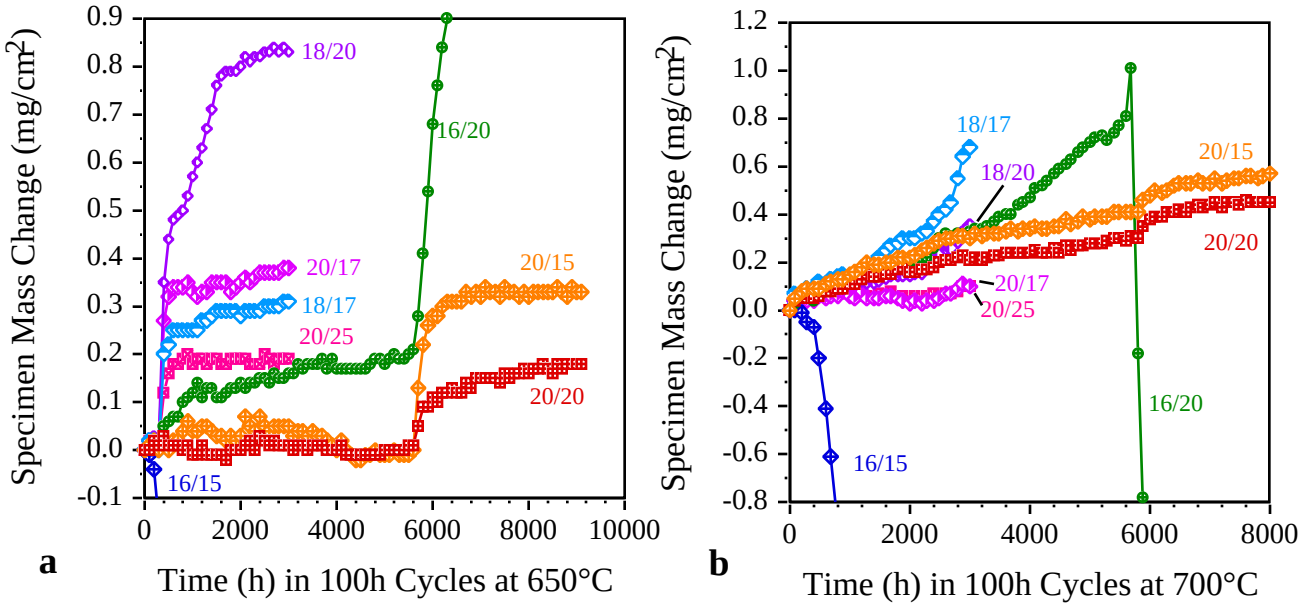

Figure 1. Specimen mass changes for model Fe-Cr-Ni alloys (designated by [Cr]/[Ni]) with Mn and Si additions during 100h cycles in air plus 10%H_2O at (a) 650°C and (b) 700°C. Especially at 650°C, perturbations have been observed in the mass gains.

these specimens at various times, Figure 1a. The reason for these increases is not clear. However, they can occur at relatively short or long times. Nevertheless, these singular events can be distinguished from a sustained rapid mass increase indicating the onset of accelerated attack (AA) such as was observed for the Fe-16Cr-20Ni specimen at ≈6,000h. In general, the mass gains for the new alloy specimens are consistent with the results for the earlier model alloys except for the

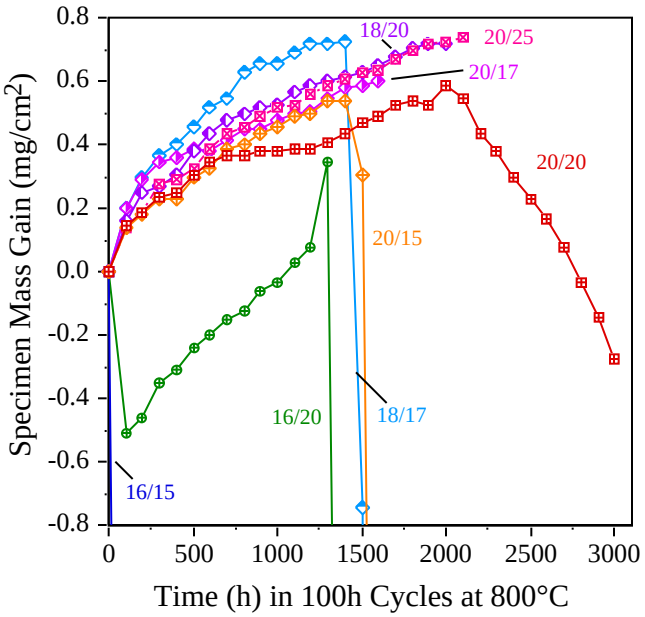

Figure 2. Specimen mass changes for model Fe-Cr-Ni alloys (designated by [Cr]/[Ni]) with Mn and Si additions during 100h cycles in air plus 10%H_2O at 800°C. Accelerated attacked has been observed for many of the lower Cr and Ni content specimens.

specimen of Fe-18Cr-20Ni has shown an unusually high mass gain. Figure 1b shows the specimen mass gains at 700°C. At this point, the mass gains for the new alloys at 700°C are generally consistent with the previous observations. The specimen of Fe-18Cr-17Ni has shown a continued mass increase consistent with the onset of AA at a relatively short time. Testing at 800°C has been used to illustrate the overall benefit of higher Cr and Ni contents, Figure 2. For the new series of alloys, the onset of AA for Fe-18Cr-17Ni at 800°C was consistent with observations for the previous series of alloys. Several of the new alloys have yet to reach AA.

Characterization of 10,000h foils

As presented previously, 10,000h testing has been completed for foil (100µm) specimens at 650° and 700°C in humid air, Figure 3. Initial characterization has been completed for the alloy 120 specimens from these tests. Figure 4a shows a secondary electron image of a polished cross-section of the alloy 120 specimen exposed for 10,000h at 650°C in humid air. Consistent with the mass gain increase noted during the test, some oxide nodules were observed on the foil. Several types of precipitates were observed in the foil: large Nb-rich carbides and Cr-rich sigma phase. Also, Si was enriched on all of the grain boundaries in the foil. The primary focus of the characterization was on the Cr depletion. Scans across the foil thickness at 1µm intervals were performed to assess the Cr depletion, Figure 4b. The scans revealed the Cr depletion was confined to the outer 12-16µm of material with the inner material largely unaffected. Figure 5a shows a higher magnification of the surface oxide which was mapped for the location of several elements. For example, Figure 5b is a Cr map of the same region. This map reveals that the inner oxide is rich in Cr but where the oxide is thicker, the outer oxide was primarily Fe-rich, consistent with nodule formation during AA. In the regions where the oxide remained relatively thin, the underlying metal was significantly depleted in Cr, especially along the alloy grain boundaries, Figure 5b. This behavior is attributed to the slow Cr diffusion at this temperature. The implication of these observations is that despite the high Cr and Ni content of this material, the foil was still susceptible to AA because the flux of Cr from the substrate was not sufficient to replenish the Cr consumed from the surface by a combination of oxidation and evaporation of the oxy-hydroxide.

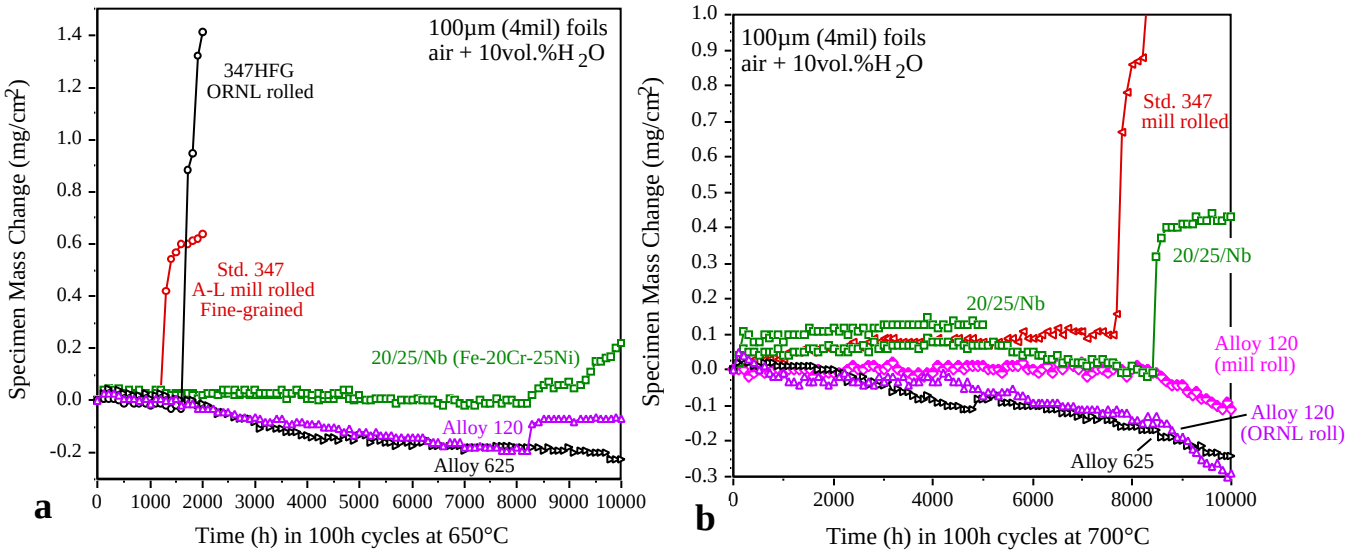

Figure 3. Specimen mass changes for foil specimens during 100h cycles in air plus 10%H_2O at (a) 650°C and (b) 700°C.

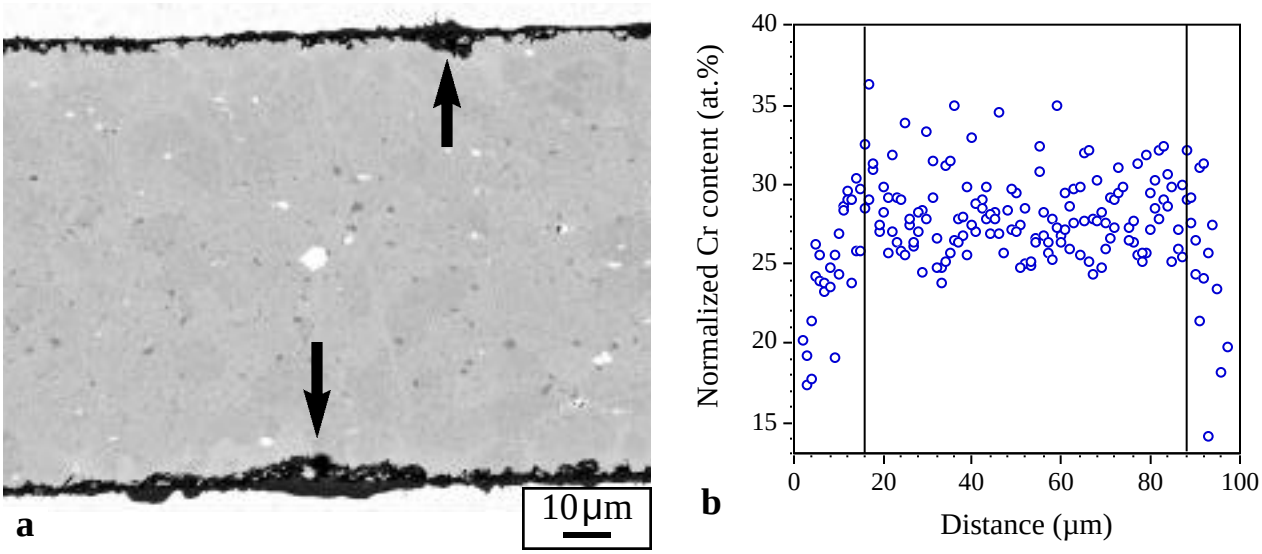

Figure 4. (a) EPMA secondary electron image of a polished cross-section of alloy 120 foil after 10,000h at 650°C in humid air (b) Normalized Cr content (at.%) across the foil thickness. Arrows in (a) mark oxide nodules.

Figure 6a shows a cross-section of the alloy 120 foil after 10,000h at 700°C in humid air. Consistent with the low mass loss in Figure 3b, few oxide nodules (arrow) were observed in the cross-section and a relatively thin compact scale developed. Similar particles were observed in the center of the foil as at 650°C and Si also was enriched at the alloy grain boundaries. Also consistent with the higher exposure temperature, more Cr was lost from the foil, Figure 6b. The depletion was to a greater depth (≈20μm) than at 650°C. Figure 7a shows a higher magnification of the oxide scale and Figure 7b shows a Cr map from the same region. Unlike at 650°C, the Cr depletion appeared to be more uniform. This suggests that as the exposure temperature increases, the alloy grain boundaries are no longer selectively depleted in Cr and the material is less likely to experience AA. However, from this single observation, it is not clear if a steady-state situation has arisen where Cr can diffuse from the interior of the foil to replenish Cr lost at the foil surface. If not, a similar situation could

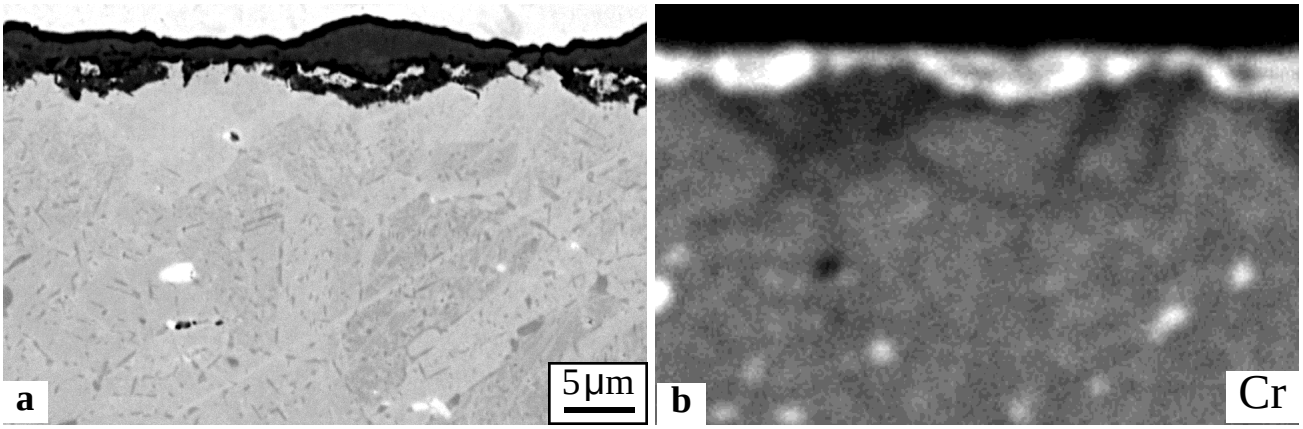

Figure 5. (a) EPMA secondary electron image of the specimen in Figure 4. (b) Cr map of the area in (a) showing a Cr-rich under scale and Cr depletion on the metal grain boundaries.

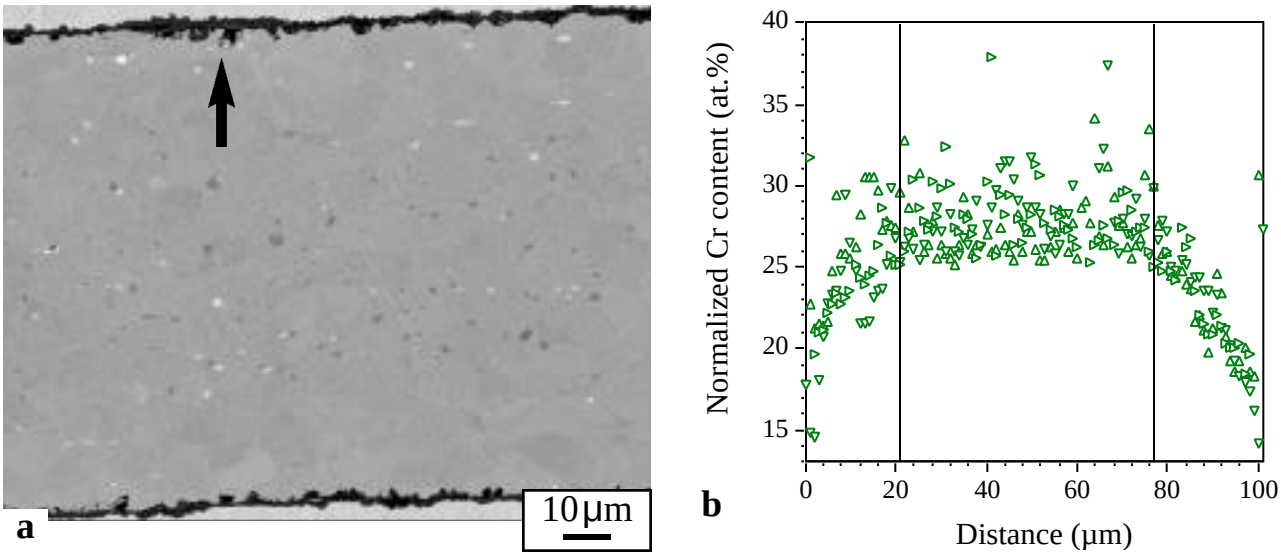

Figure 6. (a) EPMA secondary electron image of a polished cross-section of alloy 120 foil after 10,000h at 700°C in humid air (b) Normalized Cr content (at.%) across the foil thickness. Arrow in (a) marks oxide nodule.

arise as at 650°C where the surface becomes Cr depleted and the Cr flux from the center of the foil is insufficient to replenish it. Further work is required to understand this behavior. However, these results provide a great deal of information about the onset of AA as a function of temperature. In particular, the localized depletion at 650°C explains the observation that the onset of AA is nearly independent of specimen thickness. Only the outer 10-20µm of material was depleted.

It should be noted that extrapolation of these results to longer times is not recommended until the amount and type of depletion can be better quantified. Quantifying the amount of depletion detected is highly dependent on the assumed starting Cr content and this value needs to be measured more accurately in the processed foils. Depletion rates in other foil materials also are being measured for comparison. Additional characterization needs to be performed on these specimens to determine the composition of the various precipitates observed in the foils after extended high temperature

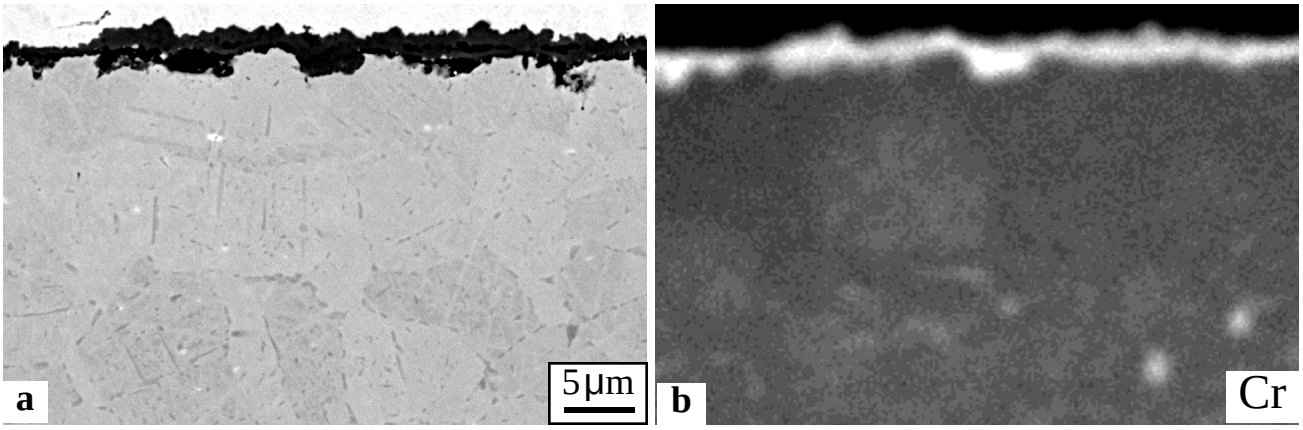

Figure 7. (a) EPMA secondary electron image of the specimen in Figure 6. (b) Cr map of the area in (a) showing a Cr-rich scale.

exposures.

Status of Milestones

Fabricate foil material of two most promising compositions for creep and corrosion testing that simulate conditions in a recuperator. (March 2004) COMPLETED

Industry Interactions

Discussed oxidation results with W. Matthews from Capstone in April and May 2004.

Discussed oxidation mechanisms with G. Hirko from United Technologies in April 2004.

Provided data to Dr. Menon at Honeywell in May 2004.

Problems Encountered

None.

Publications/Presentations

Presented paper entitled “Stainless steels with Improved Oxidation Resistance for Recuperators,” by B. A. Pint and K. L. More, ASME Paper #GT2004-53627, at the International Gas Turbine Institute Turbo Expo, Vienna, Austria, June, 2004.

Presented poster entitled “The Use of Model Alloys to Develop Corrosion-Resistant Stainless Steels,” by B. A. Pint, R. Peraldi and P. J. Maziasz, at the 6th International Conference on High Temperature Coatings and Protection of Materials, Les Embiez, France, May 2004.

R. Peraldi and B. A. Pint, "Effect of Cr and Ni Contents on the Oxidation Behavior of Ferritic and Austenitic Model Alloys in Air With Water Vapor," *Oxid. Met.*, **61** (2004) 463-83.

Recuperator Materials Testing and Evaluation

Edgar Lara-Curzio, Rosa Trejo and K. L. More
Metals and Ceramics Division
Oak Ridge National Laboratory
P.O. Box 2008, Oak Ridge, TN 37831-6069
Phone: (865) 574-1749, E-mail: laracurzioe@ornl.gov

Objective

The objective of this sub-task is to screen and evaluate candidate materials for the next generation of advanced microturbine recuperators. To attain this objective, a commercially available microturbine was acquired and in coordination and collaboration with its manufacturer, it was modified to operate at recuperator inlet temperatures as high as 843°C. The durability of candidate recuperator materials will be determined by placing test specimens at a location upstream of the recuperator, followed by determination of the evolution of the material's physical and mechanical properties as a function of time of exposure. During exposure tests inside the microturbine, it will be possible to subject test specimens to various levels of mechanical stress by using a specially designed sample holder and pressurized air. The selection of materials to be evaluated in the modified microturbine will be made in coordination and collaboration with other tasks of this program and with manufacturers of microturbines and recuperators.

Highlights

A 500-hr test campaign was completed to evaluate ORNL-modified stainless steels.

Technical progress

During the reporting period work continued to expose and evaluate candidate materials for microturbine recuperators in ORNL's microturbine recuperator test facility. Test specimens of Haynes alloys HR120®, HR230®, and HR214®, ORNL-modified stainless steels, and alloy LCF 625 were evaluated for periods of time up to 1000 hours (Figures 1 and 2). The microstructural characterization and evaluation of residual properties of these materials, according to procedures described in detail elsewhere,[1] is under way. The evaluation and characterization of ORNL-modified stainless steels in ORNL's microturbine recuperator test facility constituted one of the milestones for this project in FY2004.

[1] E. Lara-Curzio, "Recuperator Materials Testing and Evaluation" in DER Materials Program Quarterly Report, January-March, 2004

Figure 1. Photograph of ORNL's microturbine recuperator test facility operating with four sample holders.

Figure 2. Sample holder after 500-hr exposure in ORNL's microturbine recuperator test facility. From left to right, the foils that were evaluated are: alloy LCF-625, ORNL-modified stainless steel, ORNL-modified stainless steel, and alloy LCF-625.

During the reporting period, three Bowman microturbines (35 kW, 60 kW and 80 kW) were received from Southern California Edison (Figures 3 and 4). The microturbines had been installed and operated at the University of California-Irvine for different periods of time. The microturbines were dismantled and work is under way to determine the residual properties of the recuperators (Figure 5).

Figure 3. 80 kW Bowman microturbine received from Southern California Edison

Figure 4. 35kW and 60 kW Bowman microturbines received from Southern California Edison.

Figure 5. Recuperator box removed from Bowman microturbine.

Status of Milestones

1. Complete study of how the mechanical properties, microstructure and corrosion products of Haynes-214 and HR230 alloys evolve as a function of exposure time and applied stress in recuperator testing facility (09/04). Complete
2. (2) Complete evaluation of residual properties of five decommissioned microturbine recuperators (09/04). In progress.

Industry Interactions

Capstone Turbine Corporation provided some of the foils evaluated in ORNL's microturbine recuperator test facility. Southern California Edison graciously transferred three decommissioned Bowman microturbines to ORNL for evaluation of residual recuperator properties.

Problems encountered

None

Publications/Presentations

A paper entitled "Residual Properties of Microturbine Recuperators," was presented at ASME Turbo Expo 2004, Power for Land, Sea, and Air, June 14, 2004, Vienna, Austria. The manuscript was published as Paper Number GT2004-54255, Proceedings of ASME Turbo Expo 2004.

Advanced Alloys for High-Temperature Recuperators

P. J. Maziasz, B. A. Pint, K. L. More,
J. P. Shingledecker, and N. D. Evans
Metals and Ceramics Division
Oak Ridge National Laboratory
P.O. Box 2008, Oak Ridge, TN 37831-6115
Phone: (865) 574-5082, E-mail: maziaszpj@ornl.gov

Objective

The main objective of this program is to work with commercial materials suppliers (foil and thin sheet) and recuperator manufacturers to enable manufacture and evaluation of upgraded recuperators from cost effective alloys with improved performance and temperature capability. The near term goal is better performance to or above 704°C (1300°F), and the longer-term goal is reliable performance at 760°C (1400°F) and higher.

Highlights

Materials for use to 760°C (1400°F) or higher

Commercial recuperator sheet (0.010 in.) of alloy 625 was obtained from IRES earlier this year, and continues to show outstanding creep resistance, with no ruptures after over 5,000 h at 704 and 750°C. Testing will continue next quarter.

Technical Progress

Recuperator Component Analysis

Different microturbine OEMs have provided pieces of fresh and engine-tested PFR and PSR recuperators made from standard 347 stainless steel for analysis, testing, and characterization, which was completed previously. ORNL continued analysis of PFR recuperator air cells and related manufacturing process specimens with Ingersoll Rand Energy Systems, including braze alloy and processing evaluations, and this effort is nearly complete. Collaborative efforts between ORNL and the recuperator makers to provide or characterize advanced alloys (ie. HR120, 20-25Nb or alloy 625) with more temperature capability and reliability continued this quarter.

Selection and Commercial Scale-Up of Advanced Recuperator Materials:
a) Materials for use to about 704°C (1300°F)

Previous oxidation testing in 10% water vapor at 650-750°C continued this quarter, with testing at 650°C exceeding 12,000 h. HR 120, alloy 625 and NF709 (20-25Nb) all show good resistance in this temperature range. Creep testing of commercial foils (3.5-4.0 mils thick) and sheet (10 mils thick) at 704°C and 152 MPa continued, with commercial alloy 625 sheet exceeding 5000 h, as shown in Fig. 1. Standard 347 steel foil ruptured after

less than 100 h while HR120 lasted 900 h at this condition, but the alloy 625 still remains in the secondary creep regime with less than 1% strain after 5000 h.

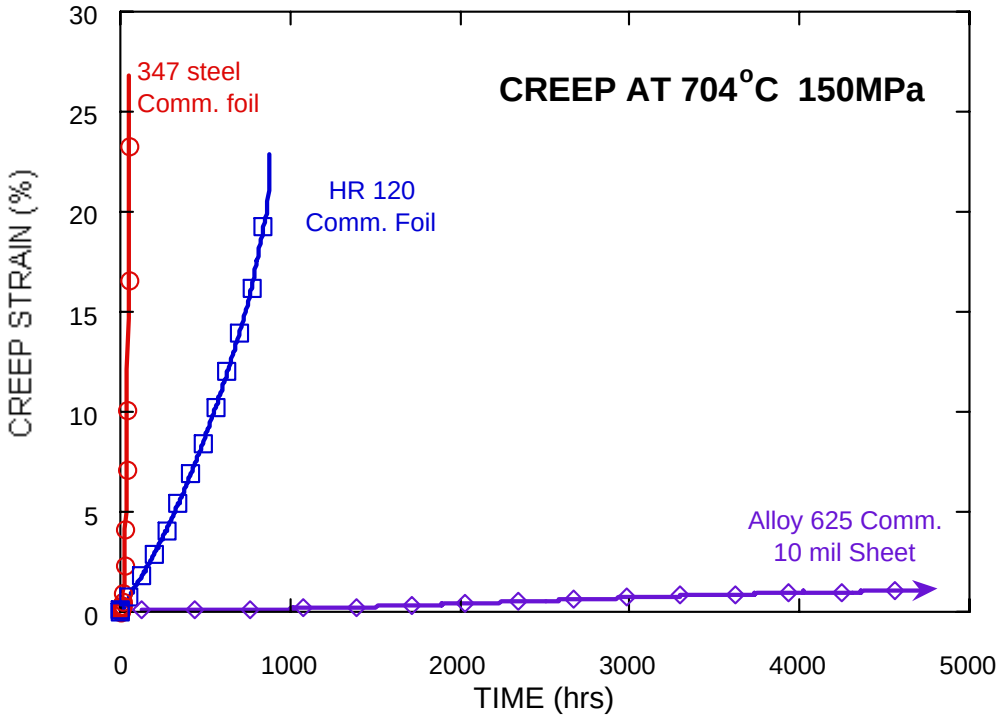

Figure 1 – Comparison of creep rupture curves for testing of commercial foils of standard 347 steel, HR120 and 10 mil sheet of alloy 625 at 704°C and 152 MPa (22 ksi).

b) Materials for use at 760°C (1400°F) or higher

HR 120 (Fe-25Cr-35Ni) is one of the more promising commercially available materials which has significantly better creep-resistance and corrosion-resistance in this temperature range at 3-4 times the cost of 347 stainless steel. Commercial 3.5 mil foil of

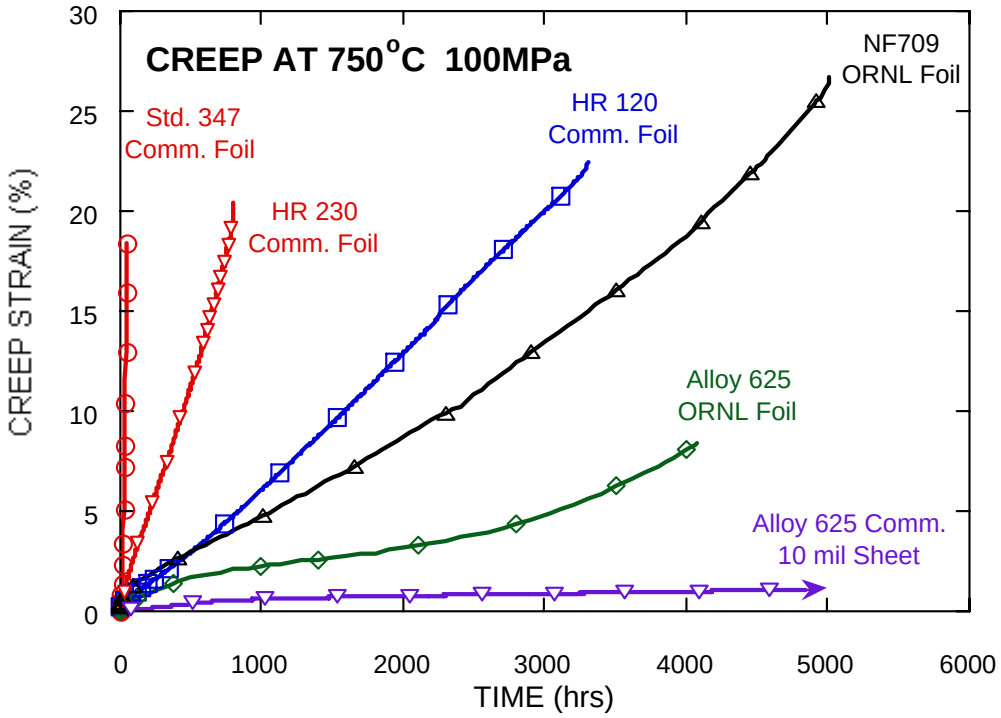

Figure 2 – Comparison of creep rupture curves for testing of commercial or ORNL processing of 4 mil foils of high performance alloys at 750°C and 100 MPa (14.5 ksi). Foils include prior data on commercial HR120 and new data on commercial HR230, and ORNL processed foils of NF709 and alloy 625. New data on continued testing of commercial 10 mil sheet of alloy 625 is also included.

HR120 was obtained by ORNL from Elgiloy Specialty Metals (Elgin, IL) and creep-tested at 704°C/152 MPa (as mentioned above), and at 750°C/100 MPa. The HR 120 foil lasted for 3300 h at 750°C, with very good rupture ductility. The creep resistance of HR 120 at 750°C is about 13 times better than standard 347 steel foil with standard commercial processing (Fig. 2). New creep data on similar commercial foil of HR230 (Ni-22Cr-14W-5Co) tested this quarter is also included. While HR230 alloy has good oxidation resistance and good strength as thicker section material, it's creep resistance is only several times better than 347 steel as foil, and it is about twice the cost of alloy 625. Creep data is also included for NF709 (Fe-20Cr-25Ni, Nb,N), from boiler tubing that was split and rolled into foil at ORNL. The NF709 shows about 50% longer rupture life than HR120. Alloys 625 foil shows roughly similar creep rupture life, but a much lower creep rate.

Last quarter, new samples of commercial 10 mil sheet of alloy 625 used for manufacturing PFR recuperator aircells were placed into creep tests at 704 and 750°C, and tests continued this quarter to beyond 5,000 h with no rupture (Figs. 1 and 2), and testing will continue next quarter.

The commercial HR 120 foil and ORNL foils of alloy 625 and NF709 have also been incorporated into the oxidation testing matrix, and at 650-750^{o}C are resistant to water-vapor enhanced oxidation, at least to about 8000 h. Oxidation testing will continue next quarter, and many of these steels and alloys have also been incorporated into the ORNL recuperator testing facility next quarter.

Finally, the new joint project that began last quarter between ORNL and Allegheny-Ludlum (AL) to produce a range of commercial foils and sheet for recuperator manufacturing of their new AL20-25+Nb stainless alloy continued this quarter. Sheets of 0.010 and 0.015 inches thick were produced this quarter and will be annealed early next quarter. Some of this sheet stock will be final product (for Ingersoll Rand Energy Systems (IRES) advanced recuperator manufacturing), while the other portion will be further processed into a range of foils (for both Capstone Turbine and IRES recuperator manufacturing) early next quarter. ORNL will creep test these sheets and foils next quarter.

Status of Milestones

FY2004 – In collaboration with Allegheny Ludlum, process a 5000 lb commercial heat of corrosion-resistant 20/25 Nb alloy into foils and sheet for high-temperature recuperators (August 2004). (On-Schedule)

Industry Interactions

Microturbine OEM Ingersoll-Rand Energy Systems sent ORNL a sample of commercial 10 mil sheet of alloy 625, used for PFR aircell manufacturing, for creep and corrosion testing. ORNL and Ingersoll Rand continued the studies of braze alloy in support of their advanced PFR recuperator manufacturing efforts. Commercial foil of HR230 was was sent to ORNL by Haynes International, Inc. this quarter. Plate and foil specimens of several heats of ORNL modified 347 steels and HR120 were sent to Fuel Cell Energy, Inc. last quarter, for corrosion testing for the fuel cell heat exchangers or structural materials applications. This was an action item from our earlier visit to the Fuel Cell Energy facility in Danbury, CT.

Problems Encountered

None

Publications/Presentations

P.J. Maziasz, B.A. Pint, J.P. Shingledecker, K.L. More, N.D. Evans, and E.Lara-Curzio, “Austenitic Stainless Steels and Alloys With Improved High-Temperature Performance for Advanced Microturbine Recuperators,” paper GT2004-54239 was presented orally and published in proceedings (CD by ASME with all papers) at the ASME Turbo Expo 2004, held 14-17 June, 2004 in Vienna, Austria.

CERAMIC RELIABILITY FOR MICROTURBINE HOT-SECTION COMPONENTS

Reliability Evaluation of Microturbine Components

H. T. Lin, M. K. Ferber, and T. P. Kirkland
Metals and Ceramics Division
Oak Ridge National Laboratory
P.O. Box 2008, Oak Ridge, TN 37831-6068
Phone: (865) 576-8857, E-mail: linh@ornl.gov

Objective

Evaluate and document the mechanical properties of very small specimens machined from ceramic components (e.g., blades, nozzles, vanes, and rotors) in as processed and after engine testing condition at ambient and elevated temperatures under various controlled environments. This work will allow microturbine companies to verify mechanical properties of components and apply the generated database in probabilistic component design and lifetime prediction methodologies. The work also provides a critical insight into how the microturbine environments influence the microstructure and chemistry, thus mechanical performance of materials.

Highlights

Studies of mechanical properties of biaxial discs machined from airfoils of NT154 silicon nitride microturbine rotor (fabricated by Saint-Gobain Ceramics & Plastics) was completed. The NT154 silicon nitride rotor, similar to the Kyocera SN237 rotor, was designed for Ingersoll-Rand 70 kWe PowerWorks^{TM} microturbine system. Biaxial discs with nominal dimensions of 7 mm in diameter x 0.5 mm in thickness were machined from airfoils. Ball-on-ring tests were carried out at room temperature with the as-processed surface under tension. Database generated has been provided to Saint-Gobain for processing refinement, and also to Ingersoll-Rand and UTRC for its probabilistic component design and life prediction effort.

Technical Progress

Studies of dynamic fatigue properties at elevated temperatures for SiAlON ceramics (Kennametal Inc., PA) were completed during this reporting period. Kennametal was awarded by DOE under Microturbine Materials Program to develop SiAlON ceramics for hot-section components for advanced microturbines. The SiAlON ceramics due to their superior wear resistance have been developed for metal cutting tools application, and might have great potentials for structural applications in microturbine systems. The purpose of this study is to generate database for down-selecting the candidate composition(s) and also for probabilistic component design and life prediction efforts carried out by microturbine companies. All of the materials, sintered with different chemical compositions, i.e., rare earth oxide content, contain a mixture of α- and β-SiAlON grain microstructure. The SiAlON ceramics were fabricated under the Phase I contract, and MOR bars were longitudinally machined per the revised ASTM C116 standard with 600 grit surface finish. The dynamic fatigue tests were carried out at 20 and 1204°C and at stressing rate of 30 and 0.003 MPa/s in air per ASTM C1465. The 30 MPa/s is used to evaluate the inert characteristic strength as a function of temperature, and 0.003 MPa/s is applied to measure the slow crack growth (SCG) susceptibility at temperatures.

Test results showed that four of the SiAlON materials evaluated at 1204°C and 30 MPa/s exhibited similar 32-42% decrease in characteristic flexure strength as compared with those

strength values obtained at room temperature (Table 1 and Fig. 1-5). Also, results showed that these SiAlON materials exhibited low Weibull modulus due to the presence of various sizes of metal particles introduced from processing contamination. These obtained low Weibull moduli were similar to the values reported at room temperature. The dynamic fatigue results at 1204°C showed that the AB132 material exhibited minor strength degradation with fatigue exponent of 65. Both AB831 and AB531 were down selected by Kennametal for further processing refinement and more complete database generation. AB831 bend bars with as-processed and machined surfaces have been received. Dynamic fatigue tests will be carried out at temperatures up to 1204°C in air. Initial test results will be described in the next quarterly report.

Table 1. Summary of uncensored Weibull and strength distributions for Kennametal SiAlON ceramic specimens with as-machined surface (longitudinally machined per the revised ASTM C1161 standard).

Material	# of Spmns. Tested	Stressing Rate (MPa/s)	Temp. (°C)	Uncens. Weibull Modulus	± 95% Uncens. Weibull Modulus	Uncens. Chrctstic Strength (MPa)	± 95% Uncens. Chrctstic Strength (MPa)
2308A	15	30	20	5.92	3.80, 8.55	651	589, 715
2308E	15	30	20	6.06	3.91, 8.73	783	710, 858
2308E	12	0.003	20	6.62	4.06, 9.90	807	729, 887
AB132	15	30	20	6.39	4.16, 9.14	878	801, 958
AB531	15	30	20	10.65	6.75, 15.55	801	757, 844
AB532	15	30	20	8.47	5.27, 12.65	721	673, 771
AB582	15	30	20	7.21	4.65, 10.34	567	523, 613
AB831	15	30	20	8.45	5.42, 12.29	960	894, 1025
AB832	15	30	20	10.70	6.83, 15.57	1029	973, 1084
AB132	**15**	**30**	**1204**	**8.60**	**5.65, 12.17**	**507**	**474, 541**
AB531	**15**	**30**	**1204**	**23.98**	**15.50, 34.49**	**497**	**485, 509**
AB582	**15**	**30**	**1204**	**8.88**	**5.68, 12.94**	**331**	**310, 353**
AB831	**15**	**30**	**1204**	**10.54**	**6.69, 15.32**	**607**	**575, 640**
AB132	**15**	**0.003**	**1204**	**11.43**	**6.87, 17.18**	**483**	**413, 463**
2308A	15	30	1204	9.79	6.52, 13.62	393	370, 415
2308E	15	30	1204	7.45	4.67, 11.05	540	489, 582
2308A	15	0.003	1204	10.68	6.87, 15.38	415	392, 437
2308E	14	0.003	1204	3.37	2.29, 4.55	440	369, 522

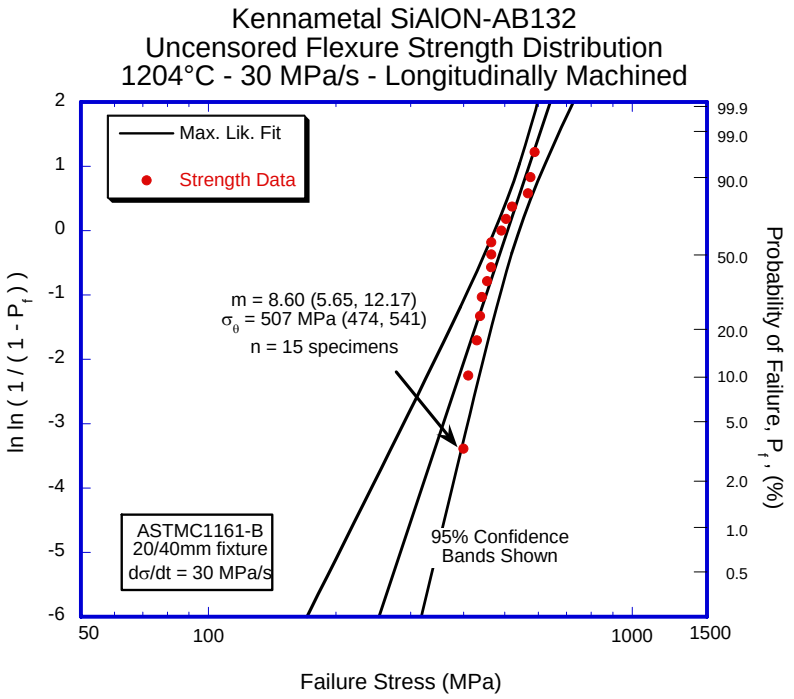

Figure 1. Uncensored flexure strength distribution at 1204°C and 30 MPa/s of SiAlON-AB132 ceramic with as-machined surface (bulk material).

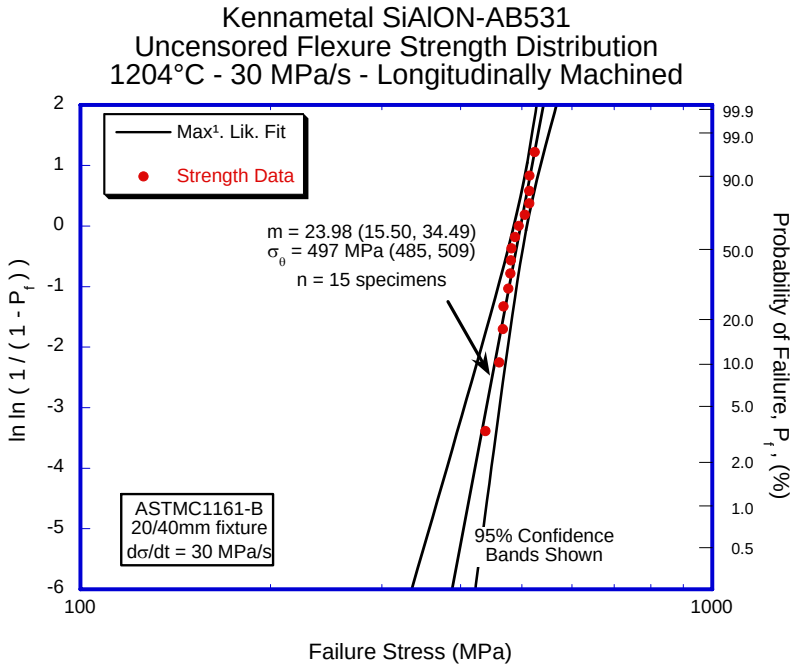

Figure 2. Uncensored flexure strength distribution at 1204°C and 30 MPa/s of SiAlON-AB531 ceramic with as-machined surface (bulk material).

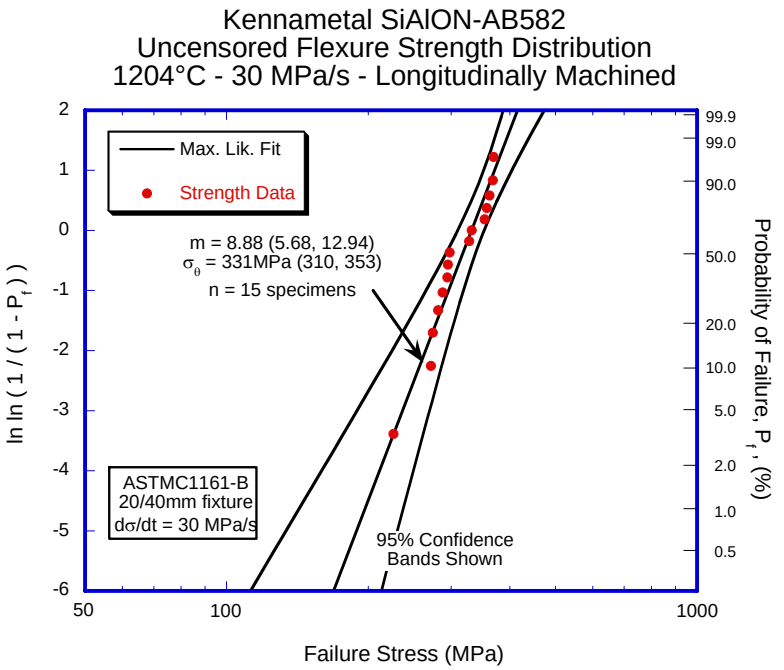

Figure 3. Uncensored flexure strength distribution at 1204°C and 30 MPa/s of SiAlON-AB582 ceramic with as-machined surface (bulk material).

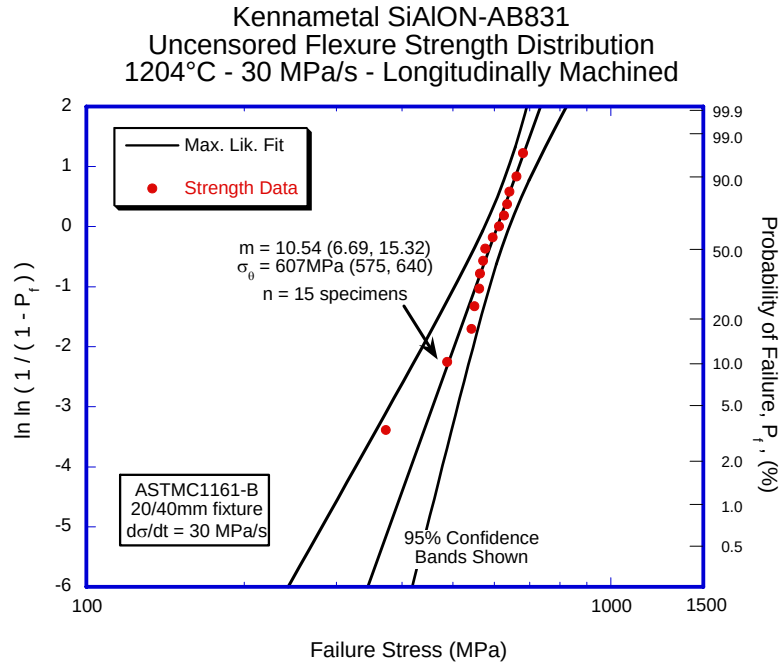

Figure 4. Uncensored flexure strength distribution at 1204°C and 30 MPa/s of SiAlON-AB831 ceramic with as-machined surface (bulk material).

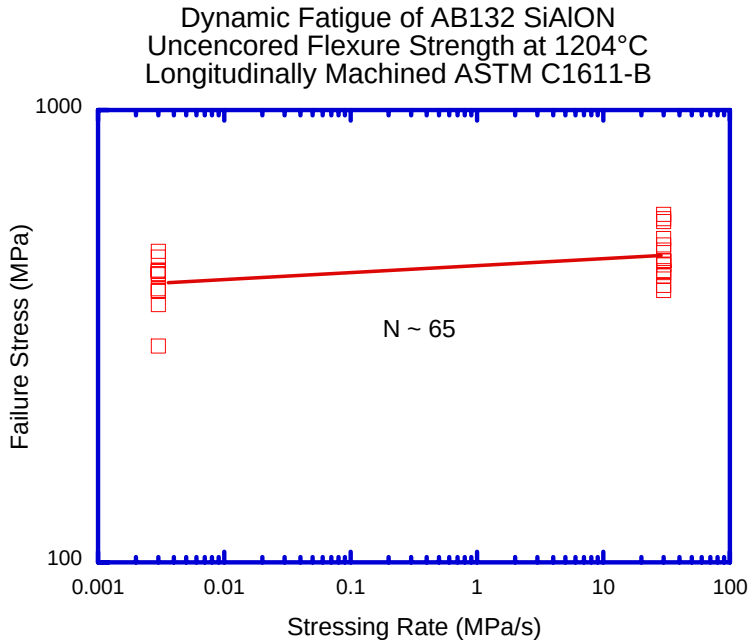

Figure 5. Flexure strength versus stressing rate for SiAlON-AB132 with as-machined surface (bulk material) tested at 1204°C.

Figure 6 shows the uncensored biaxial strength distribution of Kyocera SN282 integrated vane ring. The SN282 vane ring, acquired from UTRC, was designed for ST5+ advanced microtubine system. Results shows the biaxial discs machined from airfoils with as-processed surfaces exhibited moderate characteristic strength with a low Weibull modulus. Test results have been provided to UTRC for verification of probabilistic component design and life prediction.

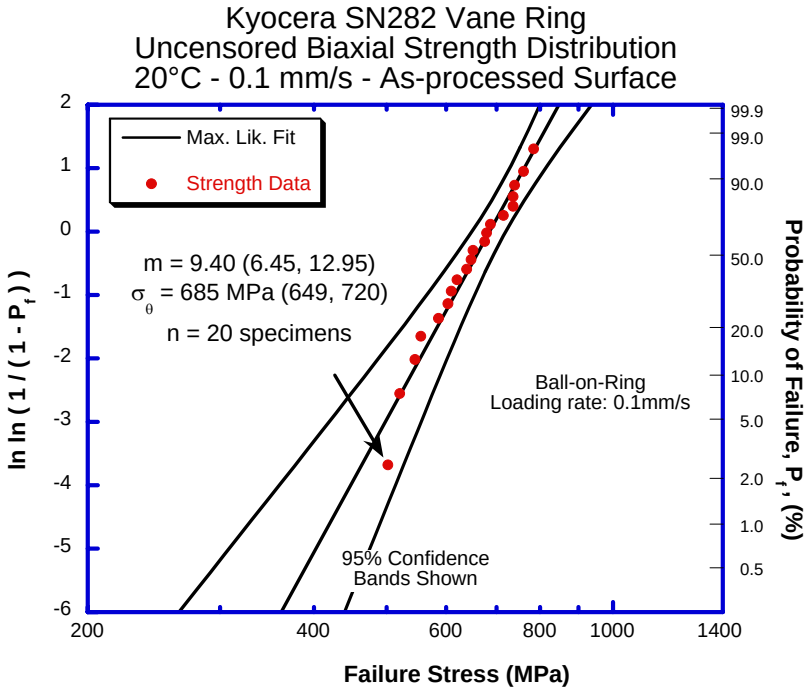

Figure 6. Uncensored biaxial strength distribution for discs machined from Kyocera SN282 vane ring with as-processed surfaces.

Status of Milestones

Complete evaluation of next generation Si_3N_4 with EBC from SMRC, Japan after long-term steam jet testing. September 2004. On schedule.

Industry Interactions

Communication with John Holowczak, Venkata Vedula, and Jun Shih at UTRC to discuss SEM analysis results for SN282 integrated vane ring samples.

Communication with Vimal Pujari and Ara Vartabedian at Saint-Gobain Ceramics & Plastics on the updates of the machining status for NT154 silicon nitride microturbine rotor.

Communication with Russ Yeckley at Kennametal on the high temperature dynamic fatigue test results of SiAlON ceramics manufactured during Task I effort.

Russ Yeckley at Kennametal visited ORNL on April 5th to review the up-to-date Phase I status on SiAlON ceramics development.

Problems Encountered

None

Publications/Presentations

H. T. Lin and M. K. Ferber, "Characterization of Mechanical reliability of Silicon Nitride Microturbine Rotors," presented and to be published in Proceedings of International Symposium on New Frontier of Advanced Si-Based Ceramics and Composites, June 20-23, 2004, Gyeongju, Korea.

S. M. Zemskova, H. T. Lin, M. K. Feber, and A. J. Haynes, "CVD Mullite Coatings Performance Under High Temperature High Load Conditions," presented and to be published in Proceedings of International Symposium on New Frontier of Advanced Si-Based Ceramics and Composites, June 20-23, 2004, Gyeongju, Korea.

M. K. Ferber and H. T. Lin, "Mechanical Characterization of Monolithic Ceramics for Gas Turbine Applications," **Invited Paper**, presented and to be published in Proceedings of International Symposium on New Frontier of Advanced Si-Based Ceramics and Composites, June 20-23, 2004, Gyeongju, Korea.

Development and Characterization of Advanced Materials for Microturbine Applications

M. K. Ferber and H-T Lin
Metals and Ceramics Division
Oak Ridge National Laboratory
P.O. Box 2008, Oak Ridge, TN 37831-6069
Phone: (865) 576-0818, E-mail: ferberk@ornl.gov

Objective

The primary objective of this project is to evaluate the long-term mechanical and chemical stability of advanced materials of interest to the DER program. Currently the project is evaluating (1) structural ceramic, which are being considered for use as hot-section components in microturbines and (2) thick thermal barrier coatings (TTBCs) being developed for thermal management in combustor liners used in industrial gas turbines. The structural ceramics effort focuses on the development and utilization of test facilities for evaluating the influence of high-pressure and high-temperature water vapor upon the long-term mechanical behavior of monolithic ceramics having environmental barrier coatings. In the case of the TTBCs, the primary focus is on the evaluation of changes in microstructure and thermal properties arising from long-term aging tests.

A secondary objective of the program is to develop and characterize the toughened silicon nitride ceramics with the following attributes:

- Fracture toughness ≥ 10 MPa•m$^{1/2}$ with fracture strengths > 1 GPa, and
- High mechanical reliability at low and intermediate temperatures coupled with creep resistance at the desired operating temperatures,
- Enhanced resistance to elevated temperature environmental damage, and
- Thermal expansion coefficients tailored to enhance the effectiveness of environmental barrier coating (EBC) systems.

Highlights

Dilatometry was used to evaluate the extent of sintering occurring in thick thermal barrier coatings exposed at elevated temperatures for extended times. This technique, which also has the potential to identify phase transformations, is being used to study the long-term stability of these materials. Results will be compared to those obtained from previous aging tests conducted at Solar Turbines.

Technical Progress

Thick Thermal Barrier Coatings

As reported previously [1], the thermal physical properties of thick thermal barrier coatings (TTBCs), which were aged at temperatures of 1800, 1900, 2000, 2100, 2150, 2200, 2250, and

2300°F (982, 1038, 1093, 1149, 1177, 1204, 1232, and 1260°C), were measured as a function of time (for 100, 500, 1000, 2000 and 5000 h).

As shown in Figure 1, the apparent density of these specimens increased with aging time and temperature. As discussed previously, SEM showed that sintering was the primary cause of these density variations. It is also likely that sintering of the TTBC was a major cause of the increase in thermal conductivity.

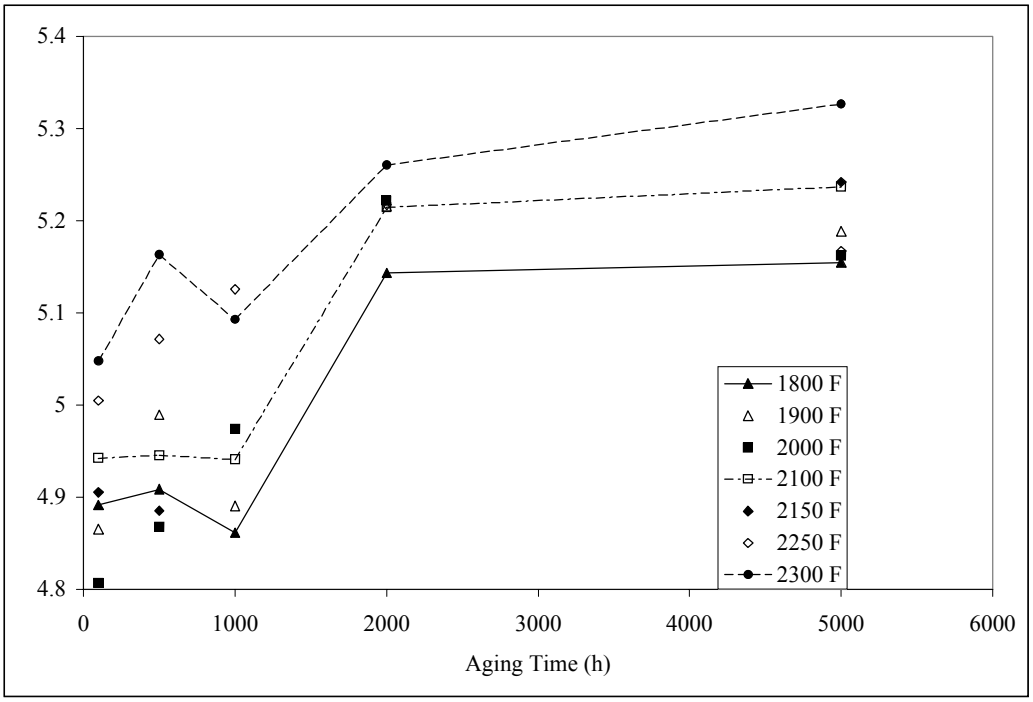

Figure 1: Apparent density as a function of aging temperature and time.

Subsequent dilatometry studies were used to evaluate the extent of sintering occurring during aging. Specifically, thin rectangular free-standing TTBC specimens having a nominal length of 25 mm, were aged at 1310°C in commercial dual-rod system (Theta Industries, Inc., 26 Valley Road, Port Washington, NY 11050. The dilation of each specimen was measured relative to that of a single crystal sapphire reference specimen. The resulting data were used to calculate the percent relative shrinkage, $\Delta L/L_o$ (%), as a function of time at temperature (Figure 2). The density of the specimen was also calculated as a function of time by assuming that the shrinkage was isotropic (Figure 3). The increase in density occurring during the first 60 h is comparable to that for the TTBC specimen aged at 1260°C (Figure 1).

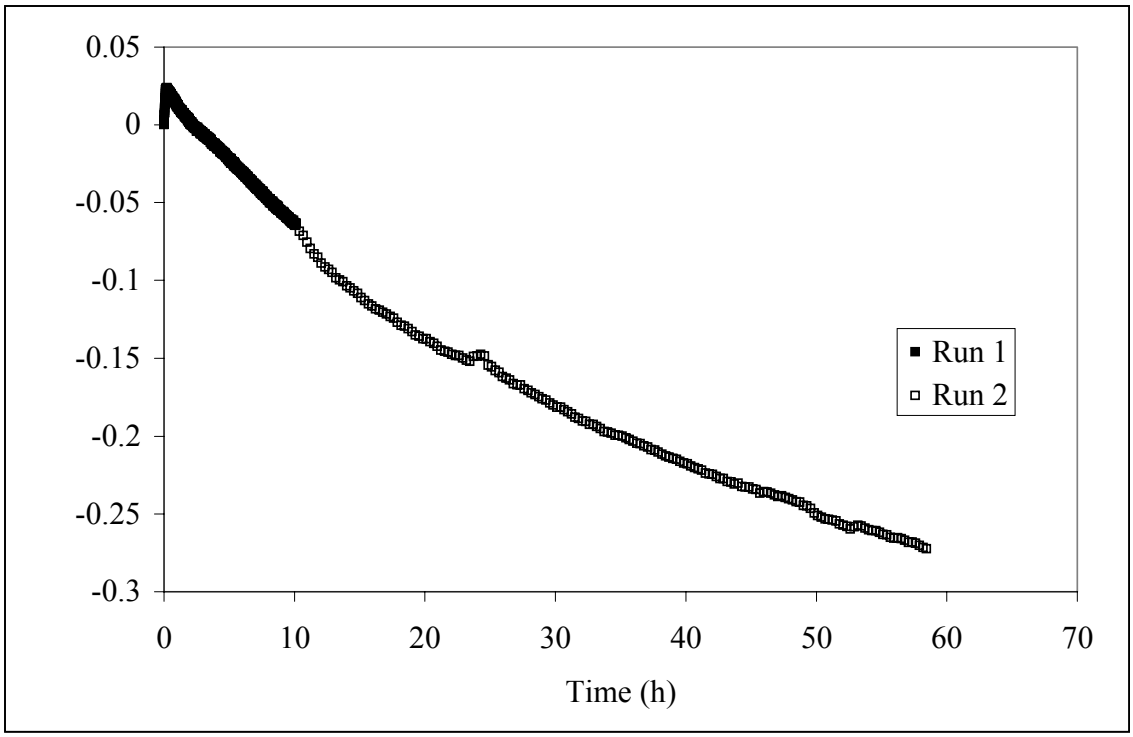

Figure 2: Shrinkage versus time data generated at 1310°C using a dual-rod dilatometer.

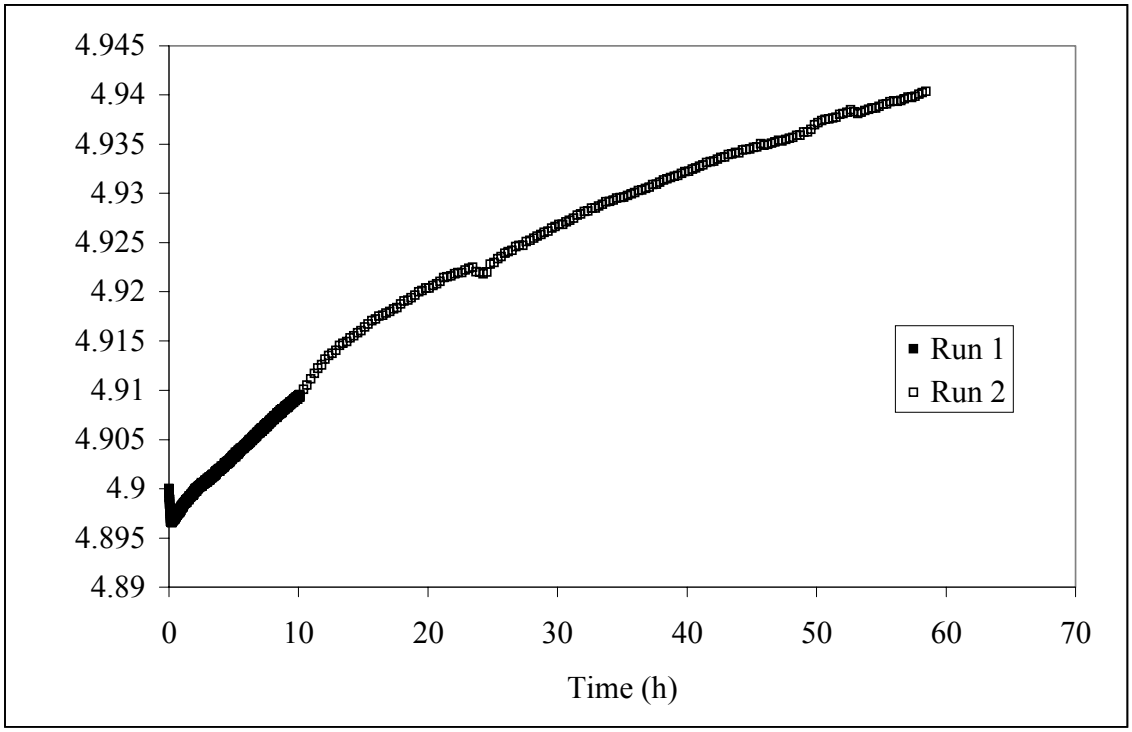

Figure 3: Density versus time curve at 1310°C calculated from the data in Figure 2.

Toughened Silicon Nitride

During this reporting period, mechanical property data were collected for the seeded Al-Y silicon nitride composition described in Refs. [2-5]. The room-temperature results for the toughness, Weibull modulus, and four-point flexure strength are shown in Figures 4-6, respectively. For purposes of comparison, data are also provided for several varieties of silicon nitride [reaction sintered (RS SN), hot pressed (HP SN), sintered (early vintages-S SN), hot isotatically pressed (HIPed SN), and self-reinforced (SR SSN)] as well as several types of silicon carbide [reaction sintered (RS SiC), hot pressed (HP SiC), and (c) sintered silicon carbides (SSiC)].

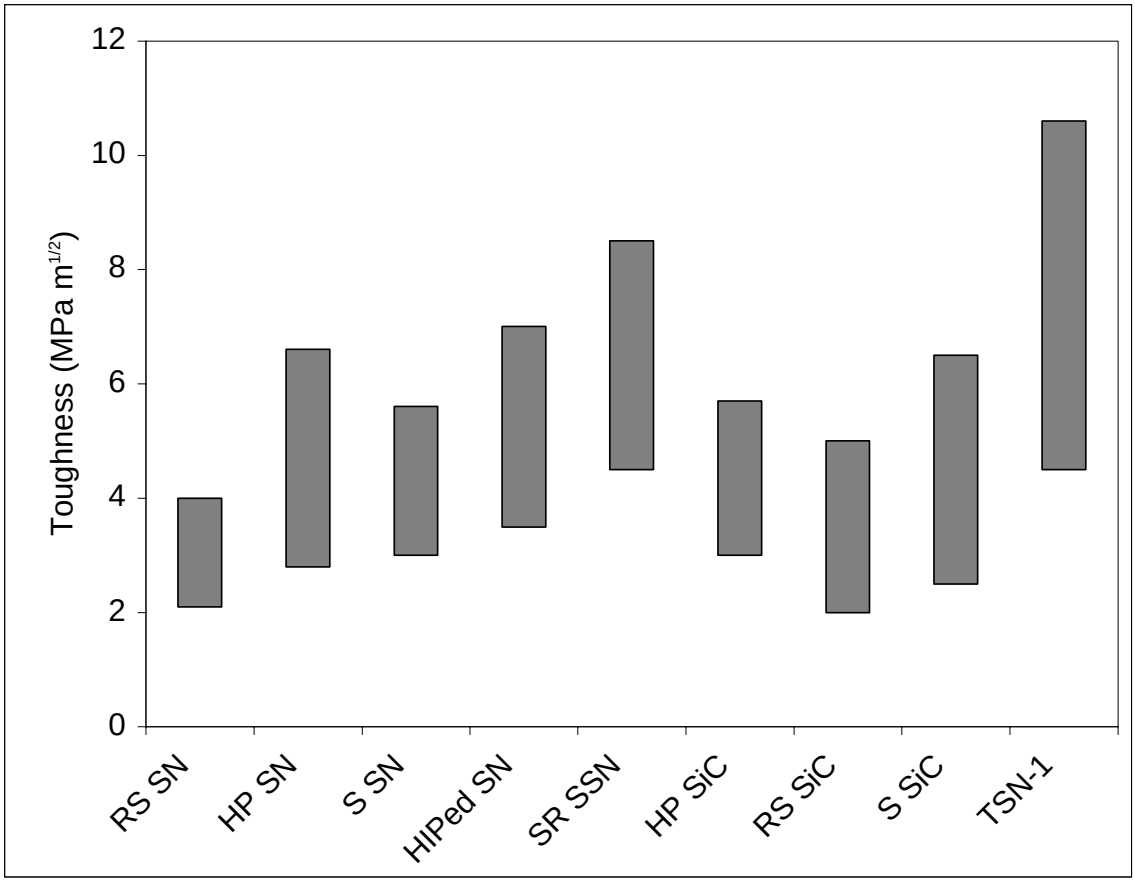

Figure 4: Comparison of fracture toughness of various silicon nitrides and silicon carbides at room temperature. The TSN-1 represents the toughened silicon nitride described in [2-5].

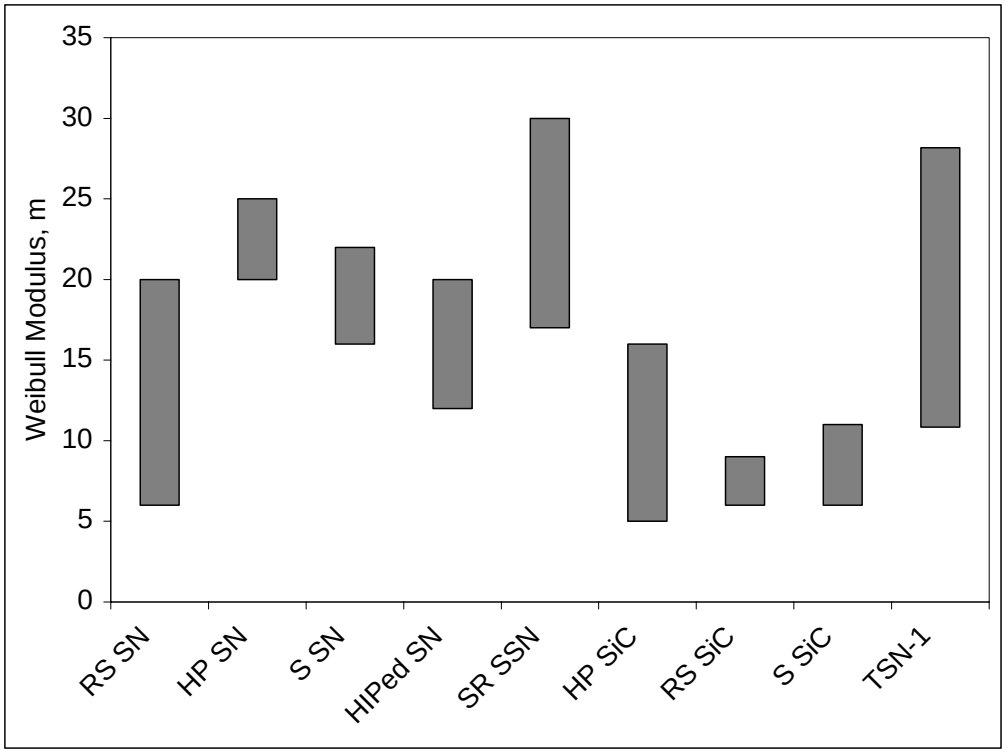

Figure 5: Comparison of four-point flexure Weibull modulus of various silicon nitrides and silicon carbides at room temperature. The TSN-1 represents the toughened silicon nitride described in [2-5].

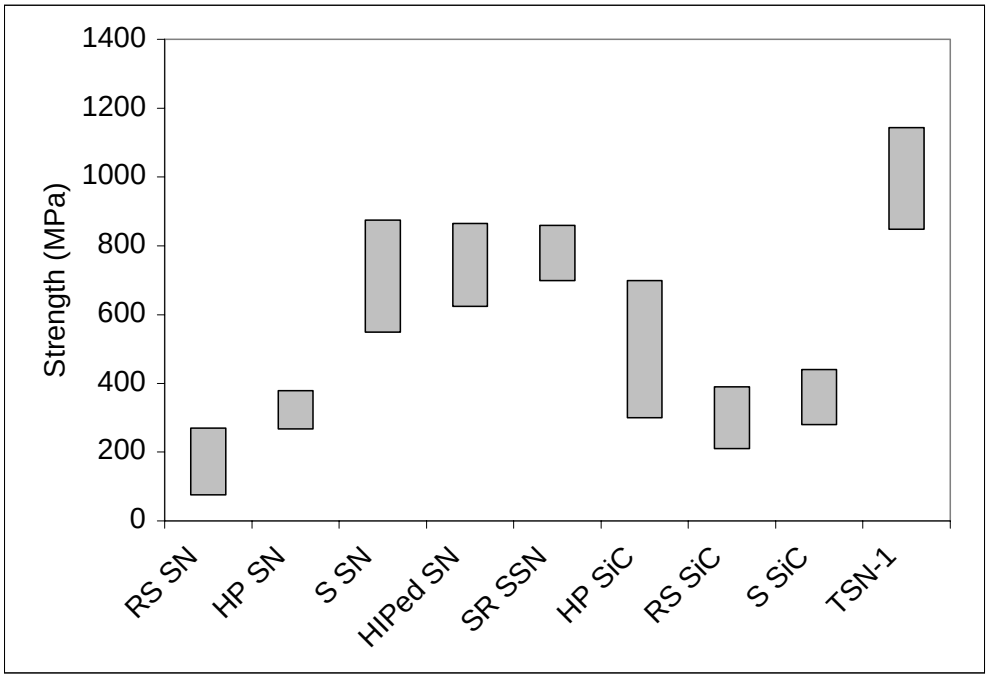

Figure 6: Comparison of flexure strength of various silicon nitrides and silicon carbides at room temperature. The TSN-1 represents the toughened silicon nitride described in [2-5].

Status of Milestones

(1) Complete the characterization of thick thermal barrier coatings (supplied by Solar Turbines) aged for periods up to 5000 and issue report-March 2004 Completed

(2) Complete mechanical property assessment of toughened silicon nitride ceramics and incorporate into database-October 2004

(3) Complete the characterization of commercially available environmental barrier coatings and issue report-March 2005.

Industry Interactions

Discussions were held with Mark van Roode of Solar Turbines concerning future material characterization needs with respect to their Advanced Materials program.

Problems Encountered

None

Publications

M-K Ferber and H-T Lin, "Mechanical Characterization Of Monolithic Ceramics For Gas Turbine Applications," presented at the International Symposium on New Frontier of Advanced Si-Based Ceramics and Composites held on June 20-23, 2004 in the Hotel Hyundai, Gyeongju, Korea (to be published as a proceedings by Trans Tech Publications Ltd.).

References

[1] M. K. Ferber And H. -T. Lin, "Long-Term Testing," DER Quarterly Progress Report for the period April 1, 2003 through June 30, 2003.

[2]. P. F. Becher, E. Y. Sun, C. H. Hsueh, K. B. Alexander, S. L. Hwang, S. B. Waters, and C. G. Westmoreland, "Debonding of Interfaces Between Beta-Silicon Nitride Whiskers and Si–Al–Y Oxynitride Glasses," *Acta Metall.*, 44(10) 3881-93 (1996). b. E. Y. Sun, P. F. Becher, C. H. Hsueh, G. S. Painter, S. B. Waters, S. L. Hwang, and M. J. Hoffmann, "Debonding Behavior Between □-Si_3N_4 Whiskers and Oxynitride Glasses With And Without An Epitaxial □-SiAlON Interfacial Layer," *Acta Mater.*, 47(9) 2777-85 (1999).

[3]. E. Y. Sun, P. F. Becher, C-H Hsueh, S. B. Waters, K. P. Plucknett, K. Hirao, and M. Brito, "Microstructural Design of Silicon Nitride with Improved Fracture Toughness, Part II: Effects of Additives," *J. Am. Ceram.* Soc., 81(11) 2831-40 (1998). b. P. F. Becher, G. S. Painter, E. Y. Sun, C. H. Hsueh, and M. J. Lance, "The Importance of Amorphous Intergranular Films in Self-Reinforced Si_3N_4 Ceramics," *Acta Mater.*, 48 (12) 4493-99 (2000).

[4]. P. F. Becher, E. Y. Sun, K. P. Plucknett, K. B. Alexander, C-H Hsueh, H-T Lin, S. B. Waters, C. G. Westmoreland, E-S Kang, K. Hirao, and M. Brito, "Microstructural Design of Silicon Nitride with Improved Fracture Toughness, Part I: Effects of Grain Shape and Size," *J. Am. Ceram. Soc*., 81(11) 2821-30 (1998).

[5]. H. T. Lin, Oak Ridge National Laboratory, data to be published.

Reliability Analysis of Microturbine Components

S. F. Duffy, E. H. Baker & J. L. Palko
Connecticut Reserve Technologies, LLC
2997 Sussex Court
Stow, Ohio 44224
Phone: 330-678-7328, E-mail: sduffy@crtechnologies.com

Objective

Connecticut Reserve Technologies, LLC (CRT) is continuing to develop and enhance the methodology to determine Weibull distribution metrics for complex shaped microturbine components (for example the Ingersol Rand (IR) microturbine rotor). The combination of service stress state and a requisite probability of survival for a Si_3N_4 microturbine rotor are being used to determine Weibull modulus - characteristic strength pairs for any arbitrary Si_3N_4 scaled to standard mechanical test coupons and test methods.

CRT has also developed the ability to compute effective area, effective volumes, and reliability prediction confidence bounds using the *CARES* algorithm and the *WeibPar* software for arbitrary component geometries.

Technical Progress

As noted in the previous quarterly report the finite element model of the IR rotor originally provided to CRT had the surface geometry removed at some point in the creation of the model. CRT has modified an *ANSYS* macro under this contract that is designed to extract surface information (stress states and geometry) for elements that were attached to areas created in the solid modeling phase. The original rotor is depicted in Figure 1.

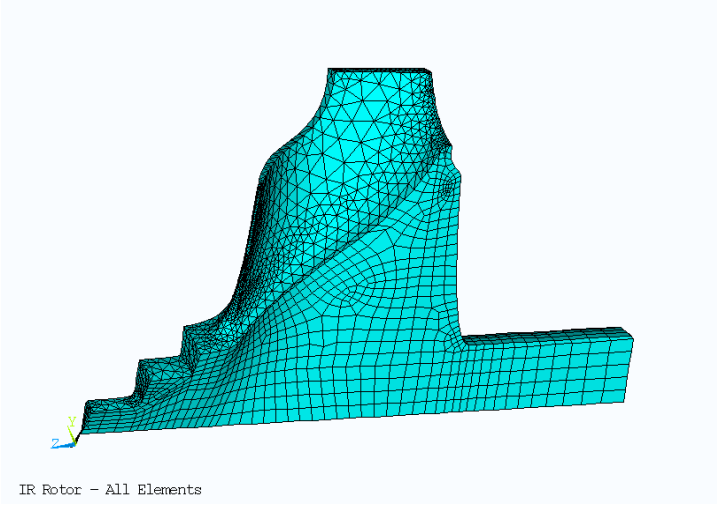

Figure 1. Entire Mesh - Ingersoll Rand Rotor

In extensively modifying an existing surface macro originally developed at NASA Glenn Research Center, CRT was subsequently able to identify elements from within the mesh that have an element surface coincident with a surface of the rotor. These selected elements are depicted in Figure 2.

Note that for elements with surfaces coincident with the surface of the rotor the entire element is shown, not just the face of the element coincident with the surface of the rotor.

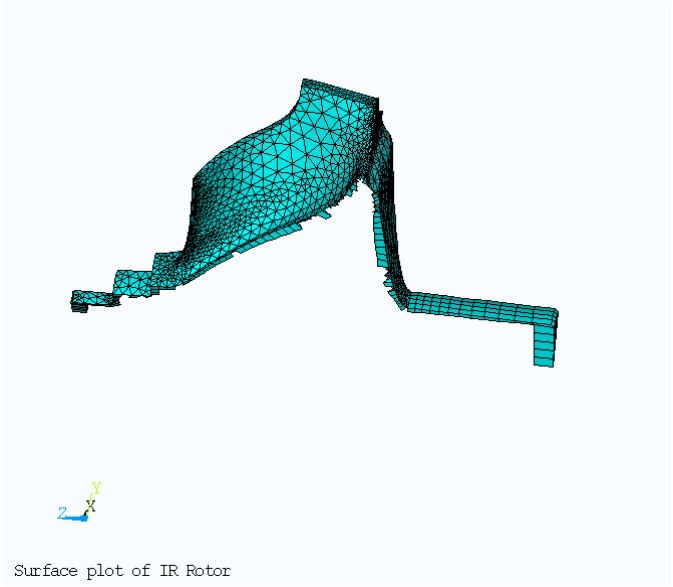

Figure 2. Elements with Surfaces Coincident with the Surface of the IR Rotor

With the capability of isolating element surfaces and capturing stress states as well as surface geometries, CRT can now generate Weibull metrics relative to a surface flaw analysis. CRT has begun generating results relative to defining material parameters for the Ingersoll Rand rotor. Figure 3 depicts a family of curves that represent the relationship between the Weibull modulus and the material characteristic strength (σ_0) for failure rates of 1 in 500,000; 1 in 50,000; 1 in 5,000; and 1 in 500.

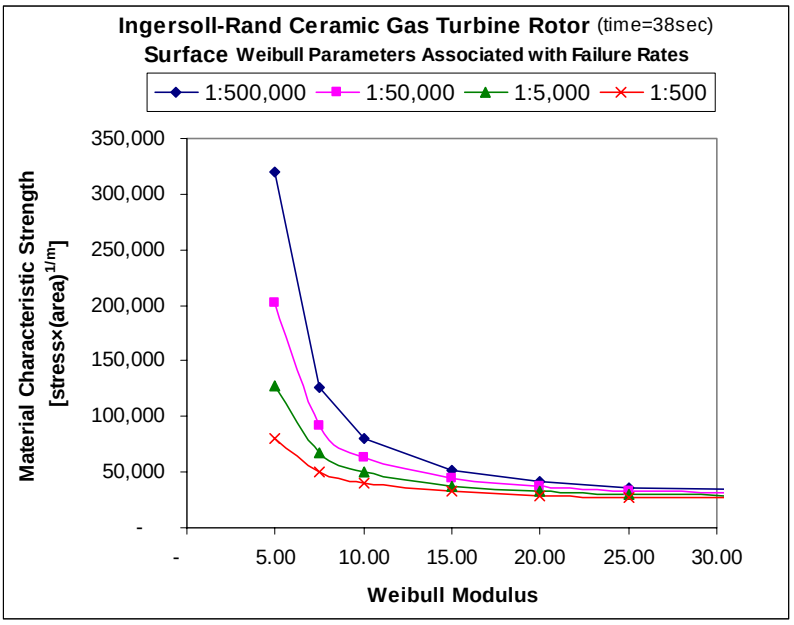

Figure 3. Material Characteristic Strength as a function of Weibull modulus And Failure Rate

The information in Figure 3 can be cast in a more relevant context if the relationship between the material characteristic strength (σ_0) and Weibull characteristic strength (σ_θ) is utilized. This requires adopting a specific test specimen which then stipulates a relationship between (σ_0) and (σ_θ). In this report a modulus of rupture (MOR) bar test specimen was adopted to illustrate results. In Figure 4 the characteristic strength (σ_θ) of a MOR bar specimen (ASTM C1161B) is graphed as a function of the Weibull modulus and the failure rates stipulated above.

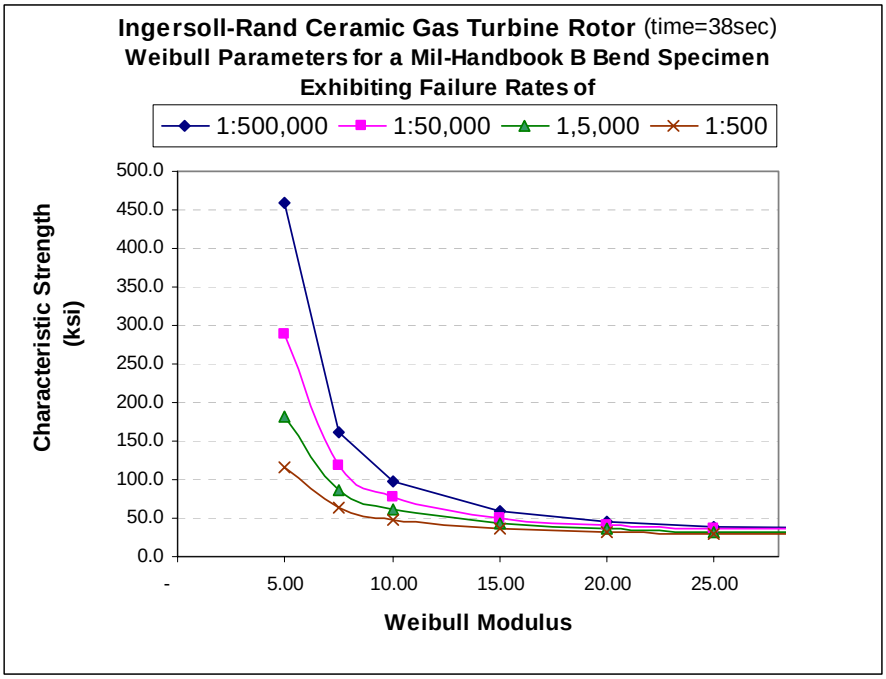

Figure 4. Characteristic Strength of a MIL-HNBK-B Bend Bar Specimen as a Function of the Weibull modulus

Not all common test specimens currently used in ceramic testing have closed form relationships between (σ_0) and (σ_θ). At the present time CRT is developing a curve for the disk specimen H.T. Lin (ORNL) is utilizing to assess strength for the as-processed and as-machined Kyocera material. This curve will establish a functional relationship between $k_A \bullet A$ and Weibull modulus for the biaxial stress state developed in ball on ring specimens. Once the relationship between $k_A \bullet A$ and Weibull modulus has been established, the relationship between (σ_0) and (σ_θ) can be computed using the expression

$$\left(\sigma_0\right)_A = \left(\sigma_\theta\right)_A \left(k_A A\right)^{1/m_A} \quad \textbf{(1)}$$

where the subscript A denotes area. This effort will be presented in the next quarterly report.

Status of Milestones

Determine characteristic strength - Weibull modulus "maps" for both surface- and volume-based flaws that limit strength in ASTM C1161B and ASTM C1161C bend bar and ASTM C1273 Button-head tensile specimen geometries. Use the stress state of the Ingersol-Rand rotor to direct those

calculations and compose and submit a publication-ready ORNL/TM Report summarizing those methods and results. [30Sep04] *On schedule.*

Provide ORNL with latest versions of CARES and WeibPar. [30Sep04] *On schedule.*

Industry Interactions

None

Publications Encountered

None

NDE Technology Development for Microturbines

W. A. Ellingson, C. Deemer, E. R. Koehl, R. Visher, and Z. Metzger
Argonne National Laboratory
9700 South Cass Avenue
Argonne, IL 60439
Phone: (630) 252-5058, E-mail: Ellingson@anl.gov

Objective

The objective of this project is development of low-cost, reliable nondestructive evaluation/characterization (NDE/C) technologies for: (1) evaluating low-cost monolithic ceramics for hot section components of microturbines or industrial gas turbines, (2) evaluating environmental barrier coatings (EBCs) for monolithic ceramics and ceramic matrix composites, and (3) evaluating other materials which are part of the technology to advance the programs for the Distributed Energy Resources-Electrical Reliability (DE-ER) technologies. The project is directly coupled to other Office of Distributed Energy and Electrical Reliability projects focused on materials developments.

Highlights

There are two highlights this period. First, we made significant progress on the automated feature detection for flaws in ceramic parts and second we significantly improved the reliability and speed of reconstruction from the 3D x-ray CT data sets.

Technical progress

Automated Feature Detection and Visualization of Flaws in Ceramic Rotor

Efforts this period focused on development of automated feature detection for ceramic microturbine components using X-ray computed tomographic (XCT) data. For automated feature detection, efforts have concentrated on development and implementation of automated edge detection methods. Several edge detection algorithms were investigated: 1) grey level hysteresis threshold with an "edge crawl" for feature detection, 2) Sobel filtering, and 3) Canny optimal edge detection. XCT image data from a section of a gelcast Si_3N_4 AS800 rotor (see Fig 1) was used to evaluate the capabilities of the edge detection routines to perform automated feature detection. The section was cut from an unbladed rotor which had a diameter of 112 mm. Three flat-bottom holes (having diameters of 0.4 mm, 0.6 mm, and 1.5 mm) were machined into the section using an ultrasonic drilling system (see first Microturbine quarterly report from 2004).

Three edge detection routines were applied to the XCT reconstruction as shown in Fig. 2. The results of the various operations are shown in Figs. 3-5. It was determined that the grey level hysteresis threshold was extremely sensitive to input parameters (i.e. the gray levels chosen for

the thresholding). This implies that the hysteresis thresholding technique lacks the robustness required for automated feature recognition. This technique was also sensitive to noise, causing false positive results because of data acquisition and reconstruction artifacts. The Sobel filter (see Fig. 4) was less sensitive to input parameters but was extremely sensitive to noise. Multiple noise reducing filters were attempted, including median and Gaussian filters, in an attempt to reduce the effects of the data acquisition and reconstruction artifacts prior to applying the Sobel filter. However, it was determined that these noise reducing filters could not compensate for the

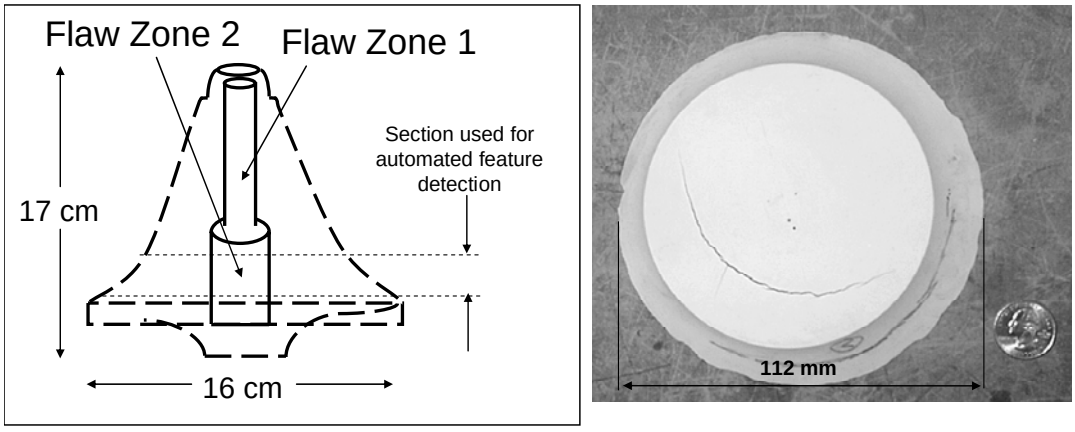

Fig. 1. Specimen used for automated feature detection. a) Schematic diagram of unbladed gelcast AS800 microturbine rotor showing location of section and b) digital photograph showing the seeded defects in sections.

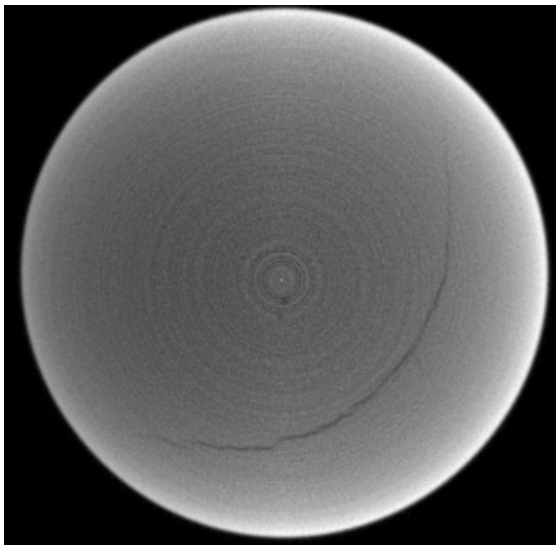

Fig. 2. XCT reconstruction of the 112 mm diameter section showing the the seeded defects and an internal crack.

Sobel operator's high sensitivity to noise. The most robust investigated method was the Canny edge detection method (see Fig. 5). This technique was comparatively more stable in response to

artifacts and noise in the reconstructed image. The Canny edge detection technique was not able to completely discriminate the seeded defects and internal cracking from the data acquisition and reconstruction artifacts causing the feature edge to be broken and incomplete. To counteract this effect, the Canny

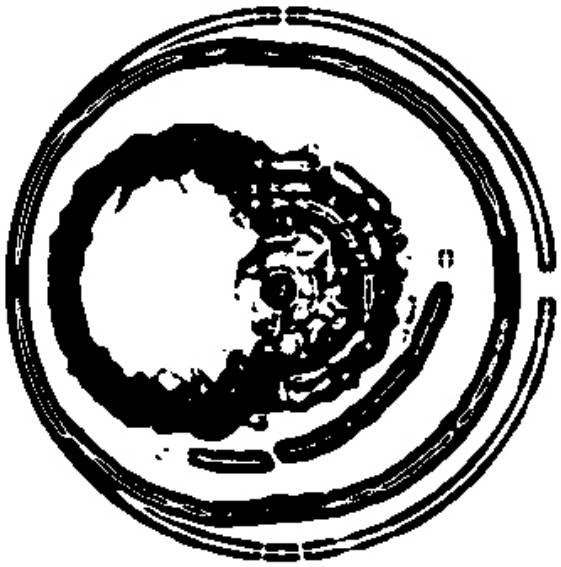

Fig.3. Edges of the XCT reconstruction shown in Fig. 2 determined by the threshold method

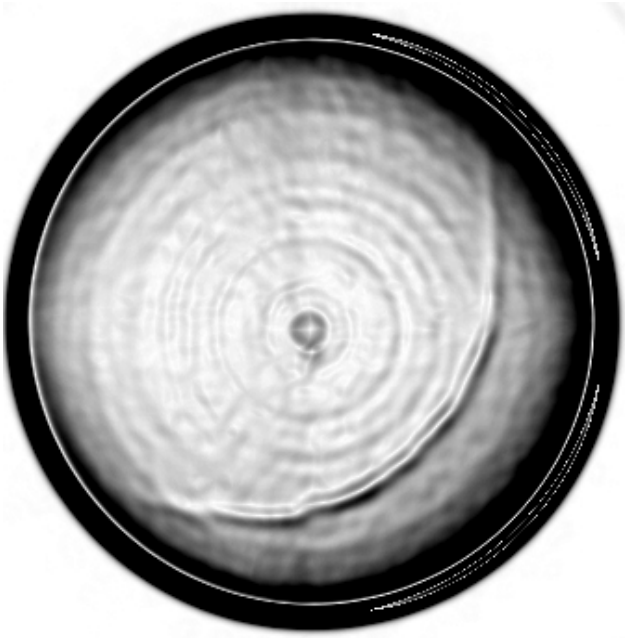

Fig. 4. Edges of the XCT reconstruction shown in Fig. 2 determined by the Sobel operator

method is being modified to incorporate the “crawl” technique (used in the hysteresis threshold method) to provide a complete description of the feature. Additional efforts are under way to decrease the prominence of the artifacts in the reconstructed image. These efforts will

concentrate on applying noise reducing filters to the data prior to data reconstruction. Work will also be done to determining the optimal parameters for the edge detection algorithms.

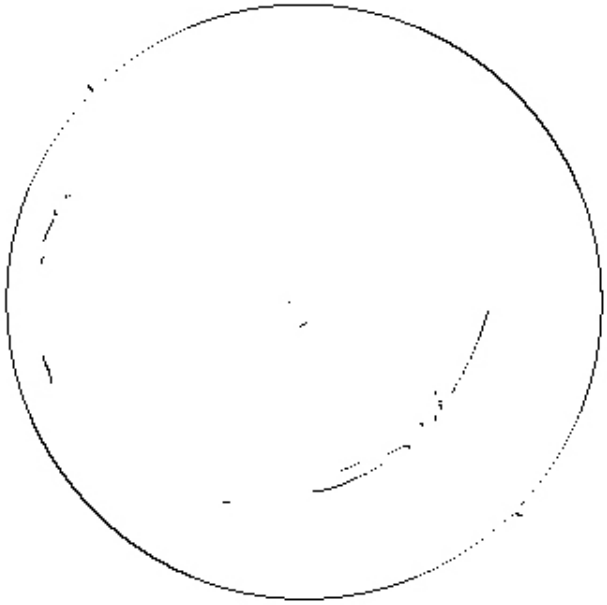

Fig. 5. Edges of the XCT reconstruction shown in Fig. 2 determined by the Canny method

High Speed Image Reconstructions using the Beowulf Computer cluster

The advances in the area of large area, high resolution flat panel X-ray detectors has enabled X-ray computed tomography (CT) to detect features much smaller in real components than were possible less than 3 years ago. However, the larger size and high resolution of these detectors, such as the RID 1620 detector (17" square with a 200 μm Pixel size) used at ANL, causes the time for data reconstruction to increase dramatically. The number of calculation required to compute an XCT reconstruction is on the order of magnitude of N^3, where N is the number of columns in the data set. For the RID 1620, the floating point operations (FLOPs) required for reconstruction is on the order of 100 GigaFLOPs. For a detector with half the resolution, only 10 GigaFLOPs would be required.

Work this period focused on improving the computational time by upgrading the hardware and making modifications to the reconstruction software. The 18 nodes previously using the Intel PIII 450 MHz processors were upgraded to Intel P4 2.8 GHz processors. Additional computers were also added bringing the total number to 50. Three nodes containing the PIII processors were not upgraded but removed from the large cluster and formed into a three node development cluster. All modifications to the reconstruction software are developed on this smaller cluster to eliminate extensive time used for debugging code on the main cluster.

The software upgrades focused on several major issues: A)- recovering data lost because of a program crash, B)- reducing reconstruction time, C)- improving the functional reliability, and D)- improved diagnostic error reporting. Upon closer investigation of the code and reconstruction results, it was evident that these problems were linked. A Beowulf cluster uses an Ethernet communication channel—a random communication protocol. This random nature means that if a node attempted to send a message over a busy channel, it would wait a random amount of time, then

make another attempt at communication. After several failures, the node would abort the communication attempt and respond with an error message. Such a situation causes the complete failure of the reconstruction code, all reconstructed data to be lost and a misleading error message to be displayed. The hardware upgrades have helped resolve some of these issues by improving hardware timing performance, however, software modifications were necessary to resolve the rest of the issue.

Modifications were made that have allowed the cluster to perform reconstructions of large data sets with more reliability. For instance, a reconstruction of a 75 slice block with 121 MB could not be reconstructed before the upgrades discussed above. To reconstruct this volume, it needed to be reconstructed in 3 smaller subsets. After the upgrades, this block was reconstructed successfully without the need to segment. Reconstructions times have decreased to approximately 8 seconds per slices with these changes.

Status of milestones

Demonstrate high-speed 3D-X-ray computed tomography to detect critical sized flaws in full-sized monolithic rotors. The new CMOS 80μm detector has allowed detection of necessary flaws. However, we continue to work on speed of reconstruction for 3D volumes with the Beowolf Cluster.

Complete installation of software for modeling laser scatter and demonstrate the ability to predict sensitivity of detection in EBCs. The software, Emflex, installed on a Sun Blade 100 computer, has now been run successfully. However, we had to add memory up to 2 gigabytes. Parameteric variables studied included thickness and laser input power.

Industry/National Lab Interactions

Additional discussions took place this period relative to interactions with staff from Saint-Gobain Industrial Ceramics and Plastics, Solar Turbines , Siemens-Westinghouse and COI relative to oxide/oxide composites

Problems encountered/resolved

The RID1620 large area x-ray detector had to again be returned to Germany for more repairs. It is also being upgraded to allow 3 frames per second which is an increase over the 0.8 frames per second previously.

Trips/meetings

1. W. A. Ellingson attended the International Gas Turbine Conference held in Vienna, Austria, June 13-17, 2004. He presented a paper titled ” Optical Coherence Tomography as a Nondestructive Evaluation method for Ceramic Coatings.” He has visited several other laboratories in Germany, Switzerland and Sweden.

CHARACTERIZATION OF ADVANCED CERAMICS FOR INDUSTRIAL GAS TURBINE/ MICROTURBINE APPLICATIONS

Oxidation/Corrosion Characterization of Microturbine Materials

K. L. More and P. F. Tortorelli
Metals and Ceramics Division
Oak Ridge National Laboratory
Oak Ridge, Tennessee 37831-6064
Phone: (865) 574-7788, E-mail: morekl1@ornl.gov

Objectives

Characterization and corrosion analyses of Si_3N_4 materials provided to ORNL as part of the Hot-Section Materials/Component Development Program

Exposures of candidate Si_3N_4 materials to high water-vapor pressures (in Keiser Rig) to simulate high-temperature, high-pressure environmental effects associated with microturbines

Evaluate the reliability of environmental barrier coatings (EBCs) on silicon nitrides for selected microturbine applications

Highlight

During this reporting period, Keiser Rig exposures of Saint Gobain Ceramic's NT-154 Si_3N_4 were completed at 1200°C. The Si_3N_4 materials were exposed at 1200°C, 10 atm total pressure, and two different water-vapor contents, 0.3 and 2.0 atm, for a total of 2000 h. The exposure conditions used for these Si_3N_4 specimens were also used to expose other manufacturer's Si_3N_4 and Sialon compositions (Honeywell Ceramic Components AS-800, Kennametal Sialon, and Kyocera SN-282). Thus, direct comparisons of recession behavior at high water-vapor pressures can be made.

Technical Progress

Coupons of three different Saint Gobain Ceramic's NT-154 Si_3N_4 (similar NT-154 compositions produced via different processing routes) were exposed in ORNL's Keiser Rig for a total of 2000 h (in 500 h increments) at 1200°C, 10 atm total system pressure, and two different H_2O pressures, 0.3 and 2.0 atm. Differences in oxidation performance were observed between the three NT-154 Si_3N_4 materials following exposure up to 1000 h (only 1000 h data analyzed to date and presented here).

The oxidation performance for the three NT-154 Si_3N_4 materials exposed for 1000 h at 1200°C are compared in Figure 1. For this graph, the thickness of the silica scale that forms on the

NT-154 specimen surface is plotted versus the square root of the specimen exposure time at 1200°C. These data quantify the oxidation rates for the different NT-154 Si_3N_4 materials, which were exposed under similar conditions in the Keiser Rig. As Figure 1 shows, clear differences in oxidation rates were measured for the specimens exposed to 20% H_2O whereas the difference in rates between the specimens exposed to 3% H_2O were not nearly as distinct. The reason for the difference in oxidation rate observed for exposure to 20% H_2O depends on the starting Si_3N_4 microstructure, which is produced as a result of the Si_3N_4 processing (all three Si_3N_4 materials contained the same amount of additives). The Si_3N_4 microstructure and surface oxide scale formed on the three NT-154 Si_3N_4 specimens are shown in Figure 2 a-c (these Si_3N_4 specimens are the same ones used to generate data plotted in Figure 1, 500 h exposure at 1200°C and 20% H_2O). Note that the NT-154 specimen that had the highest oxidation rate (designated as 20B-9-1, Fig. 2c) had the smallest overall Si_3N_4 grain size and a finer secondary phase size (finer-scale distribution) and that the NT-154 specimen that had the lowest oxidation rate (designated 20A-1-1, Fig. 2a) had the largest overall Si_3N_4 grain size and a much wider/larger dispersion/distribution of the secondary phase. Additional characterization and data reduction will be conducted.

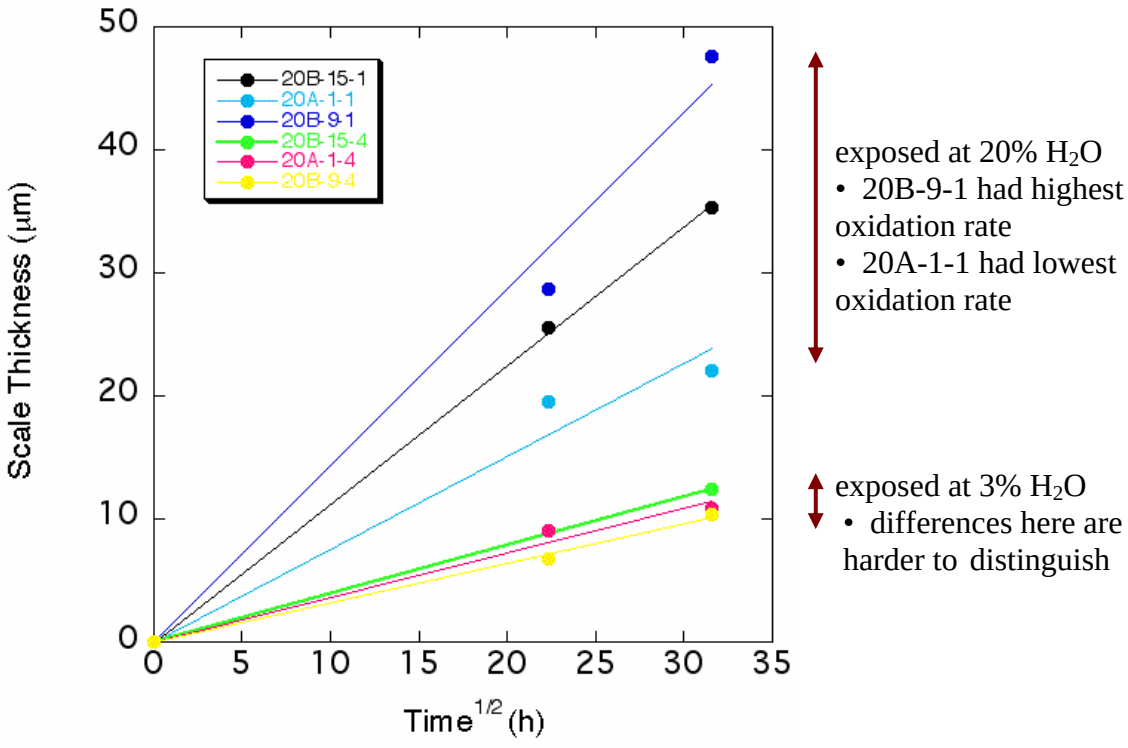

Figure 1. Scale thickness vs. exposure time+H_2O pressure for different Saint Gobain NT-154 Si_3N_4 materials. Exposures conducted at 1200°C, 10 atm total pressure, and H_2O pressures of 0.3 and 2.0 atm, for 2000 h.

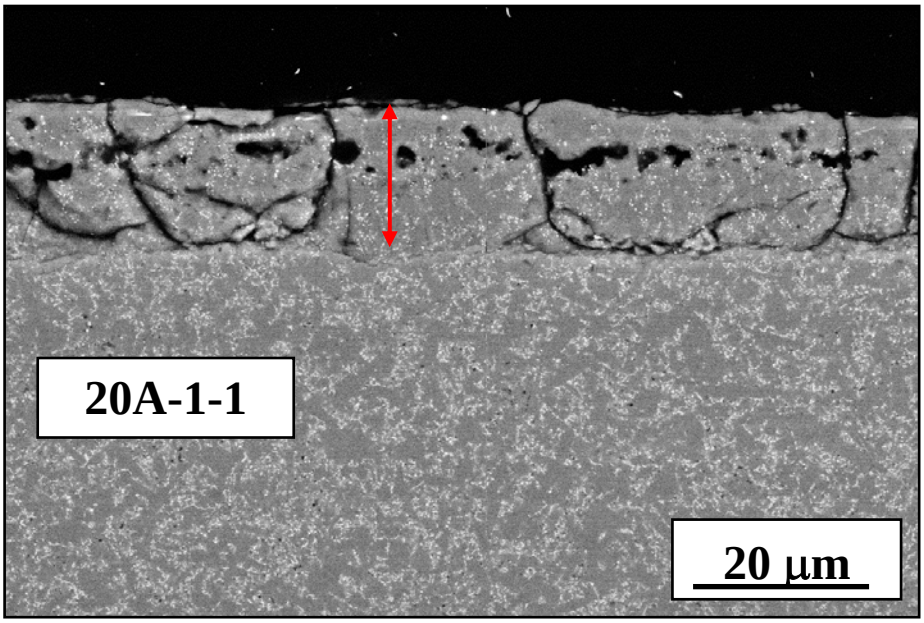

(a)

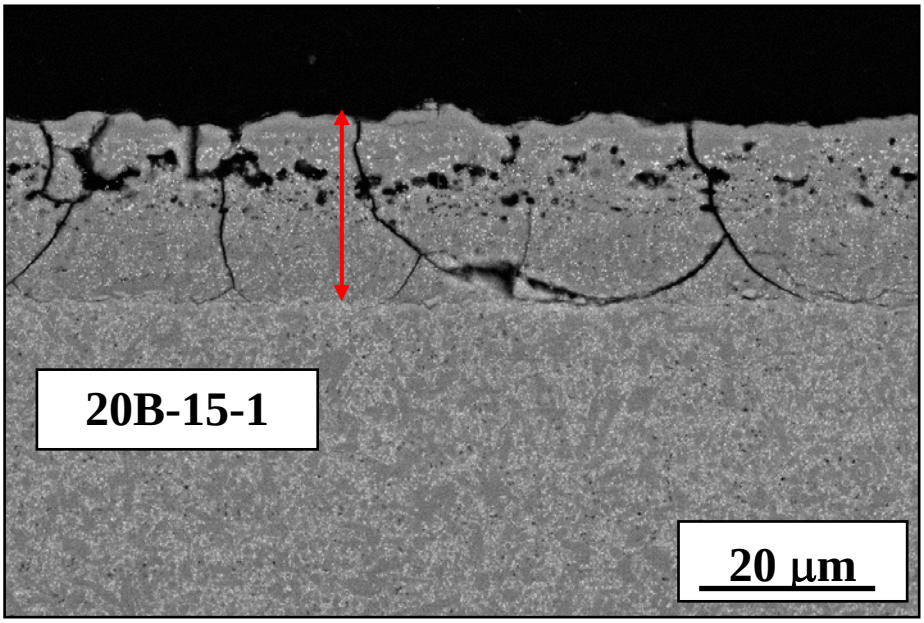

(b)

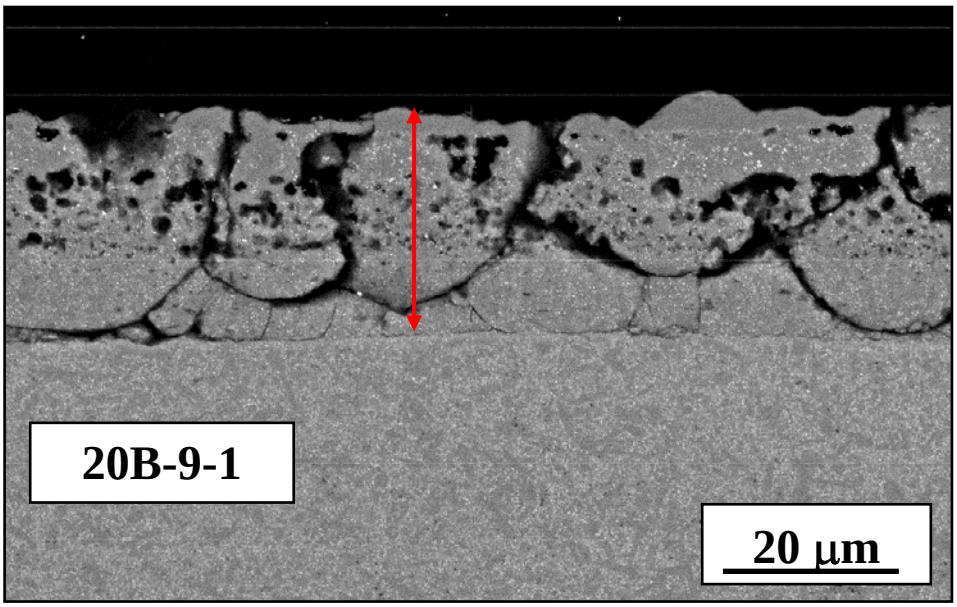

(c)

Figure 2. SEM images of Si_3N_4 cross-sections showing microstructure of three different NT-154 specimens tested in ORNL's Keiser Rig for 500 h at 1200°C and 20% H_2O. For comparison with oxidation data presented in Figure 1.

Status of Milestones

07/2004 Compile and report the results of the evaluation and comparison of uncoated Si_3N_4 (manufactured by Honeywell, Kyocera, St. Gobain, and Kennametal) exposed in the Keiser Rig for two different temperatures and two water-vapor pressures after 1000 h exposure.
Work is currently in progress.

Industry Interactions

1. Visit to ORNL by R. Yeckley and D. Siddle from Kennametal and K. Fox from Penn State to discuss status of Kennametal/ORNL collaboration on characterization of Sialon. April 5, 2004.
2. Visit to ORNL by Ara Vartebedian, Vimal Pujari, and Charles Bateman from Saint Gobain Ceramics to discuss status of Saint Gobain/ORNL collaboration on characterization of NT-154 Si_3N_4. June 2-3, 2004.
3. Exposures of Saint-Gobain Si_3N_4 and Kennametal Sialon in Keiser Rig are ongoing.

Problems Encountered

None

Publications/Presentations

None

Mechanical Characterization of Monolithic Silicon Nitride Si_3N_4

R. R. Wills and S. Goodrich
University of Dayton Research Institute
300 College Park, KL-165, Dayton, OH 45469-0162
Phone: (927) 229-4341, E-mail: roger.wills@udri.udayton.edu

Objective

The objective of this project is to work closely with microturbine materials suppliers to characterize monolithic ceramics and provide the data obtained to microturbine manufacturers via a website database. User-friendly software, that will allow prospective users to readily compare different silicon nitrides, will also be developed. This project consists of the following four tasks.

Task 1: Evaluate Strength and Mechanical Properties of New Materials

This task is motivated by the materials needs of the microturbine manufacturers and the ceramic component suppliers. Consequently, Task 1 will focus on the generation of key mechanical property data for these materials with emphasis on strength, strength distribution, time-dependent failure, elastic properties, and fracture toughness. In particular, the effects of water vapor are very important.

Continued testing and evaluation of SN281/282 at 1400 °C will be conducted by dynamic stressing and creep in air and water vapor. Baseline mechanical property data will also be measured for materials supplied by Kennametal and Saint Gobain Advanced Ceramics as part of their materials development effort funded by ORNL. The initial focus will be on measuring creep flexure strength. For new materials and EBC systems the focus will be on determining other properties such as thermal expansion, thermal diffusivity, hardness, elastic modulus and fracture toughness. This type of data is needed to support finite elements analyses.

Task 2: Develop "User Friendly" Software for Searching Existing Mechanical Properties Database

UDRI has received a number of requests from microturbine manufacturers for strength and time-dependent mechanical property data for current silicon nitride and silicon carbide ceramics. The current database contains a number of searchable PDF files and an Excel database containing the individual strength and creep data points by material for different temperatures. Integration of the site, with the National Aeronautics and Space Administration (NASA) Glenn's Ceramics Analysis and Reliability Evaluation of Structures (CARES)/Life software, will allow the user to predict reliability and life of various advanced ceramic materials. This tool will aid designers in their search for application-appropriate advanced ceramic materials.

The CARES computer code has a specific input format, but the existing data format used in the website is not compatible with this format. This task will focus on generating these input files for all the existing data and for data generated on new materials. In addition, the website will be redesigned and given a new URL to facilitate easier access.

Task 3: Screening of Novel Oxidation Resistant and EBC Compatible Silicon Based Ceramics

Above 1100 °C, the long-term reliability of structural ceramic components is limited by loss of material through water vapor enhancing the corrosion of silicon based structural ceramics. This has necessitated the development of multilayer environmental barrier coatings (EBCs) to protect the underlying structural ceramic. In this task, UDRI will screen potential new EBC coating materials such as the aluminum silicon carbides for which little or no data currently exists. The primary screening test will be oxidation in water vapor. For new materials and EBC systems, focus will also be on determining other properties such as thermal expansion, thermal diffusivity, hardness, elastic modulus and fracture toughness, which are needed to support design work using finite element analyses.

A second approach to solving this problem is not to coat the silicon nitride but to fabricate composite silicon nitrides that contain 10-30 mol % of an oxidation resistant second phase. Studies on silicon nitride-barium aluminosilicate ceramics have shown that good mechanical properties can be obtained despite the relatively high amount of second phase. This task will concentrate on the preparation and characterization of two-phase silicon nitrides containing alkali aluminosilicates. Emphasis will be on determining the oxidation behaviour of such composites in water vapor.

Highlights

The kinetics of oxidation of Al_4SiC_4 in both air and air/saturated water vapor atmospheres at 1500°C are similar. This is in agreement with the oxidation of other materials that form alumina scales. Compressive creep rates of SN281 are similar to those found in tensile creep validating the argument that SN281 does not exhibit cavitation during tensile creep. Lanthanum phosphate, a potential oxidation barrier material, was compatible with silicon at elevated temperature but reacted with silicon nitride at 1200 °C.

Technical Progress

Properties of Kyocera SN-281 Silicon Nitride

In the last report it was concluded that slow crack growth in this form of silicon nitride occurred by a different mechanism than normally exhibited by other silicon nitrides. Furthermore it was suggested that crack propagates along the grain boundary by a process of surface and grain boundary diffusion in which adjoining grains behave elastically. In order to test this hypothesis crack growth studies need to be conducted. A high temperature Double Torsion fixture has been designed and an estimate for its construction is being obtained.

Compression creep studies have been conducted over the temperature range 1400°C to 1500 °C, and stress range of 5000psi to 10000psi. The temperature and stress was varied within these conditions principally to determine the activation energy (Q) and stress exponent(n) values for secondary creep found in the Orr Sherby Dorn equation.

$$\varepsilon = A\sigma^{n}(e^{-Q/RT}) \qquad (2)$$

Where A is a constant, ε is the strain, Q the activation energy, R the gas constant and T the temperature.

In Table 1 these values are compared with those of Lofaj et al[1] derived from tensile creep experiments.

Table 1 Comparison of Sherby Dorn Creep Parameters For SN281

	Compressive Creep	Tensile Creep[1]
Activation Energy(kJ/mole)	776.1	757
Stress Exponent	1.003	5

The activation energies are very similar indicating identical mechanisms are operating in both tensile and creep experiments. However the stress exponent values differ considerably. Communications with Dr. Weiderhorn[2] have indicated that the stress exponent value of 5 is incorrect, the correct value being 1.89. At 1500 C this material was found to exhibit a compressive steady creep rate of 0.00279 microstrain/s, very similar to the rate found by Weiderhorn under tensile loading. Thus it is apparent that the creep mechanism is similiar in both tension and compression, and consistent with the observation that cavitation is not exhibited by this material[1] during tensile creep.

Properties of NT154

Thermal expansion, heat capacity and thermal diffusivity properties of the latest St. Gobain material were measured. The graphs and data have been sent to Dr. Ferber at ORNL and to Dr. Pujari at St. Gobain.

Upgrading the Website

The dynamic fatigue graphs have been added to the PDF file for SN281.

Aluminum Silicon Carbide: a Potential EBC

Aluminum containing ceramics generally possess good oxidation resistance and are thus worthy of consideration as EBCs. While many of these have been considered or are currently under investigation as potential EBCs, one group of aluminum containing ceramics that has received little attention to date is the aluminum silicon carbides. Although little property data exists for

these materials, initial oxidation studies on Al_4SiC_4[3] indicate the formation of a thin protective oxide layer of alumina and mullite. The objective of the current task is to determine the oxidation resistance of these materials in water vapor and to determine some of their basic properties and, hence, ascertain whether or not these materials can be considered as viable EBC materials.

Small rectangular plates approximately 0.6 in x 0.3 in x 0.04 in were cut out of the hot pressed billet. After cleaning, the Al_4SiC_4 was subjected to oxidation at 1500 °C in an air/ saturated water vapor atmosphere. The oxidation kinetics were determined over 156 hours by weighing the sample at several intervals.

The data was examined for linear, parabolic and logarithmic kinetics. Excellent correlation with parabolic kinetics (see Figure 1) was found. This is similar to the oxidation kinetics in air. Furthermore the same dual layer oxide layers consisting of Al_2O_3 and $3Al_2O_3.2SiO_2$ were formed. Superimposing the weight gain data for oxidation in both atmospheres(see figure 2) shows the kinetics to be identical. Thus the addition of water vapor had no effect on the oxidation kinetics. This is in agreement with studies on the oxidation of other materials, such as NiAl, that result in alumina formation (4). In contrast silicon based ceramics, which form a silica oxidation layer, show increased reaction rates in water vapor containing atmospheres due to volatilization of $Si(OH)_4$. A sample of Al_4SiC_4 oxidized at 1500 °C in water vapor saturated air has been sent to Dr. Ferber for further evaluation in the Keiser Rig.

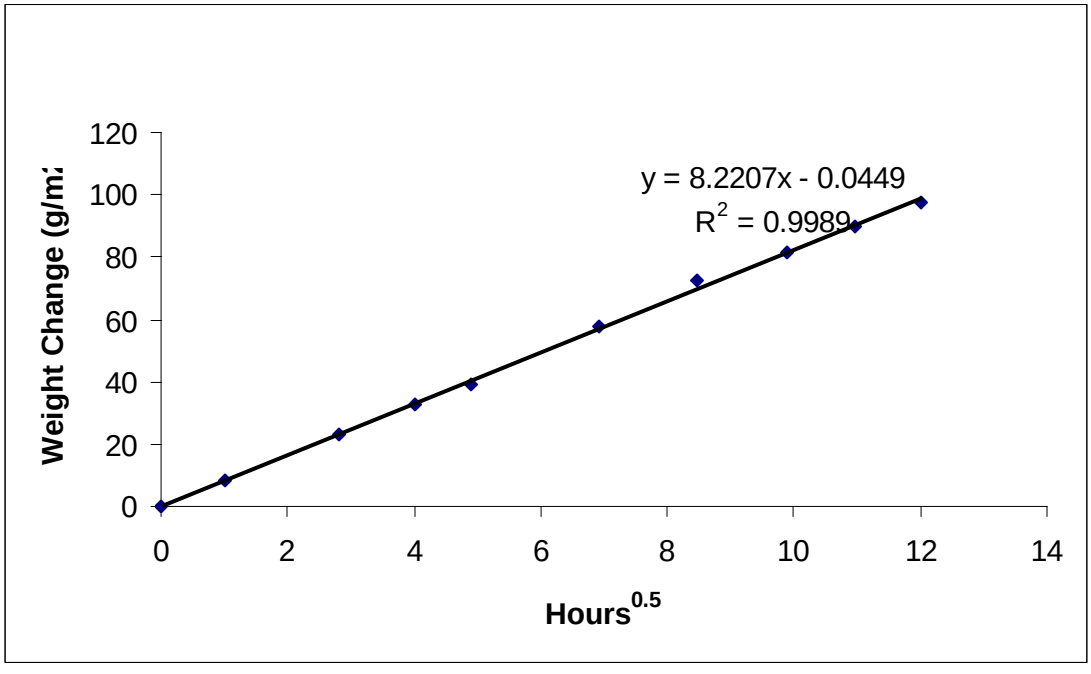

Figure 1 Parabolic Oxidation of Al_4SiC_4 in water saturated air at 1500 °C

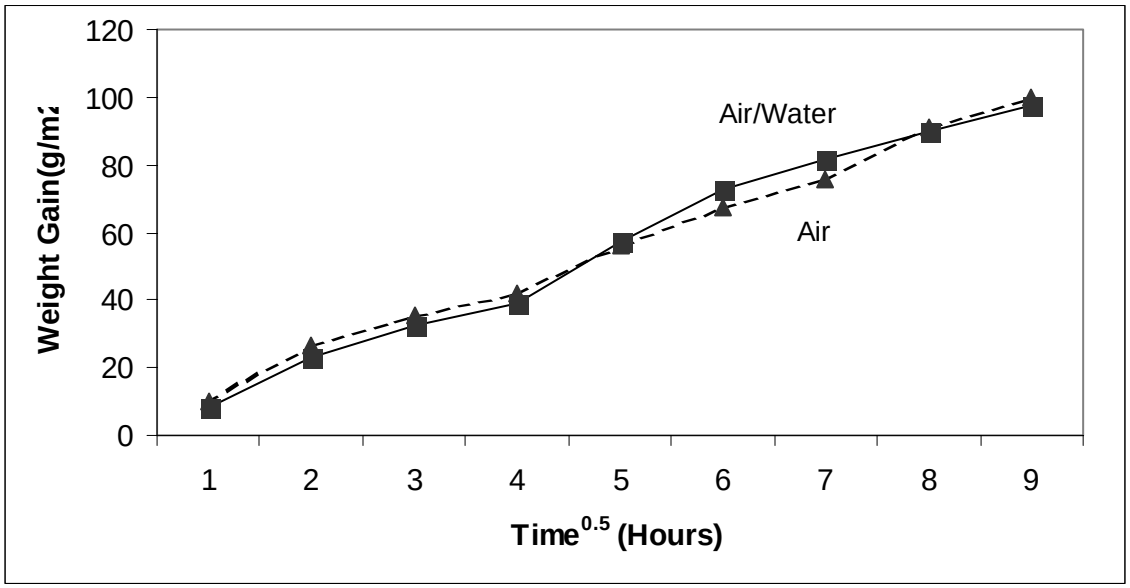

Figure 2 Similar Oxidation Behaviour of Al_4SiC_4 in air and air/saturated water vapor atmospheres at 1500°C

Interaction of Silicon And Silicon Nitride With Lanthanum Phosphate

Certain phosphates are refractory ceramics with high melting points. For example, lanthanum phosphate has become the preferred coating for alumina alumina composites because of its stability in air and water vapor and its ability to form a weak interfacial bond , thus promoting a high work of fracture. Samples of silicon nitride and lanthanum phosphate powders were mixed and hot pressed at temperatures from 1200 °C to 1700 °C to determine their mutual compatibility. Even at 1200°C the lanthanum phosphate volatilised from the mixture, showing that a strong reaction occurs between these two compounds. In contrast silicon metal did not react with the lanthanum phosphate even at 1400 °C.

Status of Milestones

1) Publish a paper on the oxidation of the aluminum silicon carbides. Sept 2004

Paper will be presented at the Cocoa Beach meeting in January 2005.

Industry Interactions

Briefly discussed GE status on engine testing of microturbine materials with Dr.Reza Sarrafi-Nour. Discussed status of St Gobain's contract on developing NT154 silicon nitride with Dr. Vimal Pujari and sent him the property measurements we have made on the new NT154.

.

Problems Encountered

None

Publications/Presentations

The creep data was included in a paper given by Dr. Sheldon Weiderhorn at the ISASC meeting June 20-23rd in Gyeongju, Korea.

References

1. Frantisek Lofaj, Sheldon M. Weiderhorn, Gabrielle G. Long, Bernard J Hockey, Pete R. Jemian, Lisa Browder, Jonathan Andreason, and Ulrike Taffner," Non Cavitation tensile creep in Lu doped silicon nitride," J. Europ Ceram. Soc [22],(2002), 2479-2487.

2. S. M.Weiderhorn, Private Communication

3. J. Schoennahl, B. Willer, and M. Daire, "Preparation and Properties of Sintered Materials in the Systems Si-Al-C and Si-Ti-C," p. 338 in Materials Science Monographs 4: Sintering-New Developments, Elsevier Science Publishing, Amsterdam (1979).

4. E. Opila, N. Jacobsen, D. Humphrey, T. Yoshio and K. Oda, "The Oxidation of AlN In Dry and Wet Oxygen", Electrochemical Proceedings [98-9], 430-437,(1998)

Microstructural Characterization of CFCCs and Protective Coatings

K. L. More and P. F. Tortorelli
Metals and Ceramics Division
Oak Ridge National Laboratory
P.O. Box 2008, Oak Ridge, Tennessee 37831-6064
Phone: (865) 574-7788, E-mail: koz@ornl.gov

Objectives

Characterization of CFCC materials and CFCC combustor liners after exposure to simulated (ORNL's Keiser Rig) and actual (engine tests) combustion environments

Exposures of candidate environmental barrier coatings (EBCs) to high water-vapor pressures (in Keiser Rig) to determine thermal stability and protective capability

Work with CFCC and coating suppliers/manufacturers to evaluate new/improved ceramic fibers, protective coatings, and composite materials

Highlights

During this quarter, work was continued on the exposure of BSAS-based EBC formulations and Si-based standards to very high (18atm) water-vapor pressures in ORNL's Keiser Rig to evaluate volatilization mechanisms of potential EBCs. To date, BSAS, BAS, SAS, SiO_2, and CVD SiC have been exposed for a total of 1000 h at 1250°C, 20atm total system pressure, and 18atm H_2O.

Technical Progress

The underlying principles of using the Keiser Rig for evaluating a material's volatility resistance were summarized in the DE Quarterly Report for 10/03-12/03. It was shown that very high water-vapor pressures could be used to compensate for the slow-flow gas velocities (~5-33 X 10^{-4} m/s) used in the Keiser Rigs. These high water-vapor pressure exposures (20atm total system pressure, 18atm H_2O compared with "standard" exposure conditions of 10atm total system pressure, 1.5atm H_2O) can be used to provide for a low-cost screening of the volatility of potential EBC compositions in addition to characterizing an EBC material's permeability, thermal stability, and chemical stability.

In this study, hot-pressed specimens of BSAS ($Ba_{0.75}Sr_{0.25}Al_2Si_2O_8$), BAS ($BaAl_2Si_2O_8$,), SAS ($SrAl_2Si_2O_8$), SiO_2, and CVD SiC were simultaneously exposed at 1250°C, a total system pressure of 20atm, and H_2O pressure of 18atm (500 h increments.) The hot-pressed specimens were supplied by UTRC and the standard materials (SiO_2 and CVD SiC) were the same as used previously to characterize oxidation of Si-based ceramics in the Keiser Rig. After 1000 h exposure at these conditions, significant weight losses were measured for all materials exposed, as shown in Figure 1, which plots % mass change vs. time (h). Note that both the SiO2 and SiC standards exhibited major mass losses – mass losses have not been observed in these two

materials after exposure for 1000s of hours in the Keiser Rig using "standard" exposure conditions.[1] The three oxide materials showed a mass increase after exposure for ~300 h followed by a continuous mass loss. The significant weight losses indicate that volatilization of the BSAS, BAS, and SAS occurred during the very high water-vapor exposures in the Keiser Rig. The primary goal of this work was to establish volatilization rates high enough in the Keiser Rig to differentiate between candidate EBCs, not necessarily to quantify the volatilization rates for individual EBC compositions. The measurable weight losses observed when the Keiser Rig was operated at very high water-vapor pressure (and slow gas-flow conditions) demonstrate that these exposures can be used to differentiate EBC volatilization-resistance.

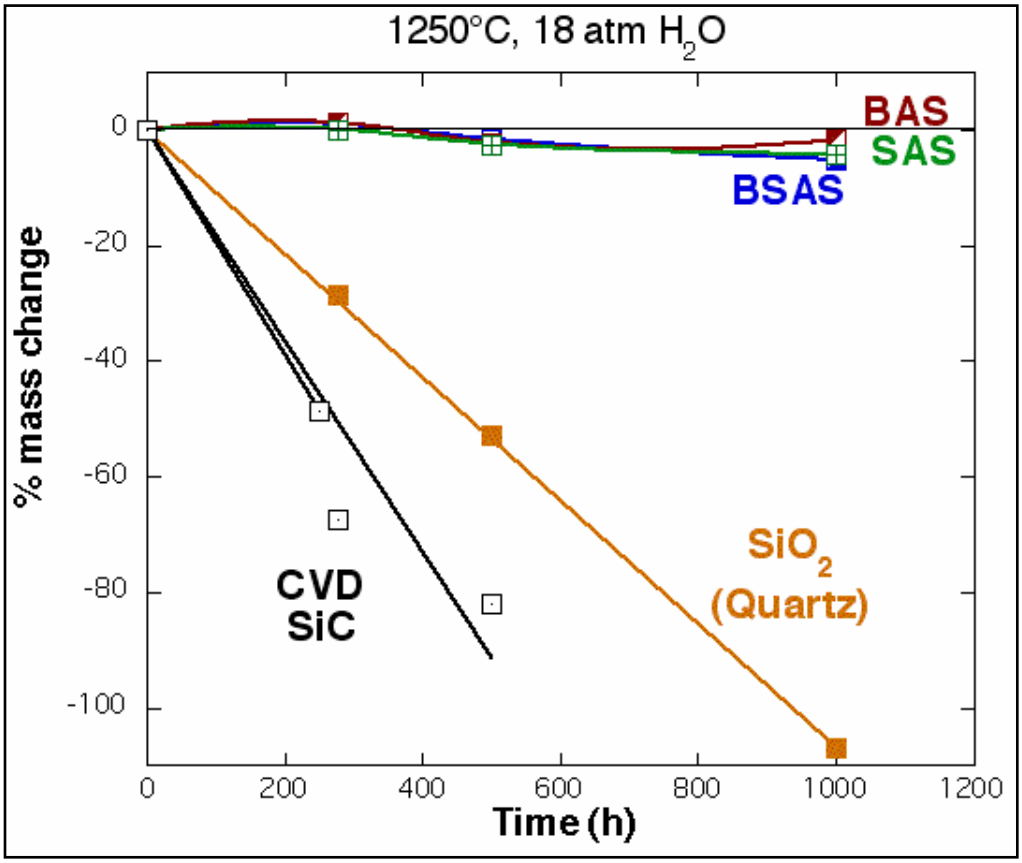

Figure 1. % mass change vs. exposure time for BSAS, BAS, SAS, SiO_2, and SiC exposed in ORNL Keiser Rig for 1000 h at 1250°C and very high H_2O pressure.

Status of Milestones

06/04 Milestone — Prepare a report and present results on the evaluation of oxide/oxide composite materials exposed in the Keiser Rig for use as microturbine or stationary gas turbine combustor liners. (June 2004)

This milestone is completed. ATK-COI Ceramics, Inc. oxide/oxide composite material, A/N720, has been exposed under simulated

microturbine exhaust conditions in ORNL's Keiser Rig at two temperatures, 1135°C and 1200°C, for 3000 h at each temperature. Results were presented at the 28th Annual Advanced Ceramics and Composites Conference held January 26-29, 2004 in Cocoa Beach, FL. A report was also prepared for ATK-COI Ceramics, Inc. and Capstone Turbines, Inc.

Industry Interactions

1. Study continues with Andy Szweda of ATK-COI Ceramics, Inc. to expose A/N720 oxide/oxide composites in the Keiser Rig at 1250°C for 3000 h in 1000 h increments. Post-exposure characterization (microstructural and mechanical) will be conducted.

2. Microstructural and mechanical evaluation of CFCC/EBC combustor liners recently removed from engine tests at Chevron and Malden Mills will be conducted at ORNL in collaboration with Solar Turbines, Inc. Characterization work will be completed by September 27, 2004.

3. Collaboration is ongoing with UTRC to expose BSAS, BAS, and SAS coupons and Si-based standards in the Keiser Rig at very high (~20 atm) water-vapor pressures to induce volatilization (see DE Quarterly Report for 10/03-12/03).

4. Work recently started on the evaluation of short-term engine tested "hybrid" oxide/oxide combustor liners in collaboration with ATK-COI Ceramics, Inc. and Siemens. Similar liners are currently running in a Solar Turbines Centaur 50S engine at the Texaco test site.

Problems Encountered

None

Publications/Presentations

1. P.F. Tortorelli and K.L. More, "Evaluation of EBCs in the Keiser Rig," presented at the DER EBC Workshop, Nashville, TN, Nov. 18-19, 2003.
2. K.L. More, E. Lara-Curzio, P.F. Tortorelli, A. Szweda, D. Carruthers, and M. Stewart, "Evaluating the High Temperature Stability of an Oxide/Oxide Composite Material at High Water-Vapor Pressures," presented at the 28th Annual Advanced Ceramics and Composites Conference, January 26-29, 2004, Cocoa Beach, FL.
3. K.L. More, P.F. Tortorelli, T. Bhatia, and G.D. Linsey, "Evaluating the Stability of BSAS-Based EBCs in High Water-Vapor Pressure Environments," presented at IGTI Turbo Expo 2004, June 14-17, 2004, Vienna, Austria. Published as ASME Paper #53863.

DEVELOPMENT OF MONOLITHIC CERAMICS AND HIGH-TEMPERATURE COATINGS

Kennametal's Hot-Section Materials Development

R. Yeckley, J. R. Hellmann, K. M. Fox, D. J. Green, and E. C. Dickey
Kennametal Inc.
1600 Technology Way, P.O. Box 231, Latrobe, PA 156-0231
Phone: (724) 539-4822, E-mail: Russ.yeckley@kennametal.com

Objective

Determine potential of an existing structural sialon that is being manufactured for other applications that, commensurate with the requirements of advanced microturbines shows potential for strength, environmental stability, and manufacturability for complex shapes.

Highlights

The Penn. State University subcontract 'Dispersion of sialon formulations' is complete. Very high solids loading are achieved in water and isopropanol slurries. Flexure bar sets with machined and as processed surfaces are complete for each of the two sialons selected from the sialon matrix for more extensive characterization. ORNL will conduct the mechanical testing.

Technical Progress

In early June Prof. J. Adair visited Kennametal to present and demonstrate the colloidal system developed for sialon processing. This meeting completed the Penn State contract 'Dispersion of Sialon Formulations'. A summary of this work is summarized in this quarterly.

Sialon presents a special challenge for complex shape forming. The powder mixtures contain AlN powders. The AlN is very unstable in water, reacting to form aluminum hydroxide. The solids content in solvent slips are rather low. The Penn State program made significant and impressive improvements in both water based and isopropanol sialon slurries.

Aluminum nitrides reactivity in water is depicted in Figure 1. The left side shows the change in crystalline structure of the AlN with time in water. The AlN quickly reacts with water to form Bayerite. Conversion to Bayerite is complete within approximately 24 hours.

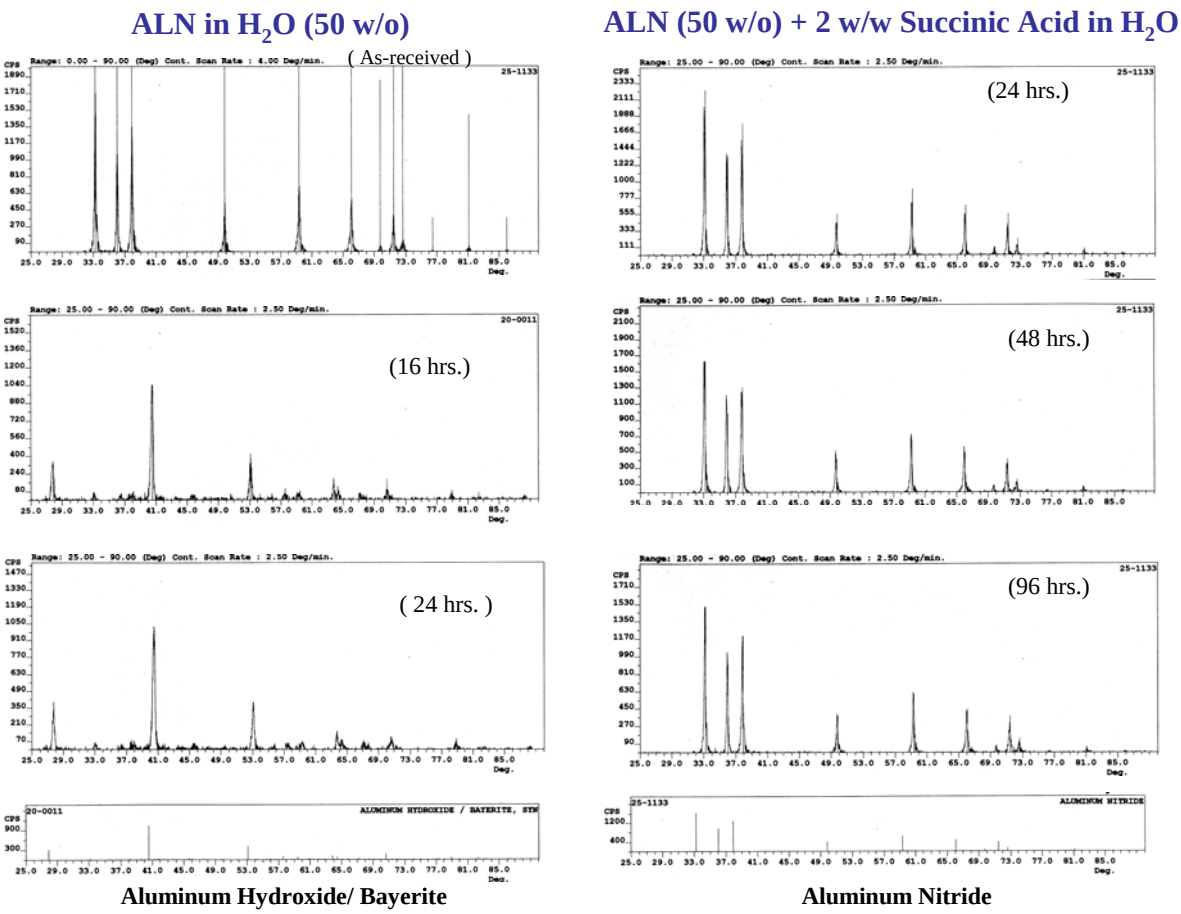

Figure 1. Diffraction patterns showing AlN conversion to bayerite in water and improved AlN stability in water with 2% succinic acid.

Prof Adair had shown that AlN could be processed in water by passivating the surface with succinic acid. This reacts at the surface forming a protective layer of aluminum succinate. The effectiveness of the passivation is shown on the right side Figure 1. AlN remains stable for approximately 96 hours with succinic acid.

A passivation-dispersion approach is developed to achieve high solids loading in sialon slurries. The uniform dispersion of heterogeneous powders is achieved by establishing a positive surface charge on each of the powders in the mixture. This is accomplished through the pH control, selection of the correct passivating agent and a dispersant to create the positive surface charge. This approach is illustrated in Figure 2. Polyethyleneimine (PEI) is chosen in part because PEI lays flat on the particle surface rather than extending out from the surface. This orientation should improve solids loading and viscosity because the organic molecule will have less tendency to interact with each other between particles.

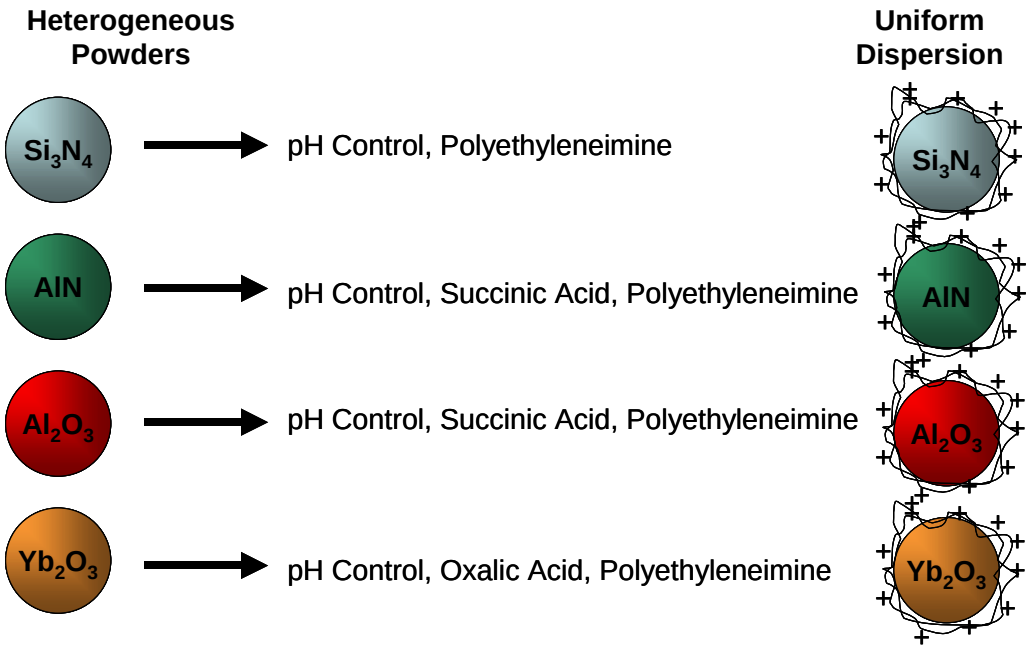

Figure 2. Illustrates the passivation-dispersion approach to achieve a uniform surface charge on a heterogeneous powder mixture.

Zeta potential measurements were completed on all powder used to form the sialon slurry. The Zeta potential measurements were completed in water and isopropanol. Examples of the Zeta potential measurements are shown for silicon nitride and aluminum nitride powders.

Polyethylenimine is used to disperse the silicon nitride powder. Succinic acid is not required for the silicon nitride powder since a native negative charge is already present. A zeta potential curve of the Si_3N_4 powder in an aqueous suspension with varying amounts of PEI was generated using the ZetaPALS. The pH was adjusted using 1.0 M nitric acid and 1 M tetramethylammonium hydroxide. The results can be seen in Figure 3. The 1 w/w PEI in suspension seems to be the ideal amount with the concentration and size of the PEI molecule and the surface area of the powder available for adsorption ideally matched at this concentration.

Aluminum nitride powder in isopropanol does not have a large enough magnitude for the zeta potential over the pH range evaluated to create a stable suspension. However, the addition of a dispersant, polyethylenimine (PEI), to the powder creates electrosteric stabilization with the added benefit of electrostatic repulsion of the particles and steric hindrance. PEI is a cationic polyelectrolyte, which develops a large surface charge at relatively low pH values. However, a negative charge on the surface of the particle is necessary for the absorption of the PEI onto the particle surface. The negative charge is produced by the addition of the succinic acid, which reacts with the alumina to form a thin layer of aluminum succinate causing a negative surface charge. The PEI will strongly absorb to this surface. In order to determine the concentration of succinic acid and PEI needed in the isopropanol suspension, zeta potential curves for the 0.1 wt. percent aluminum nitride powder in isopropanol from pH 3 to pH10 were generated using the ZetaPALS (Brookhaven Instruments) with the addition of 0.5 w/w succinic acid and varying the amount of polyethylenimine from 0.1 to 3.0 w/w based on the amount of AlN in solution. The pH was adjusted using 0.1 M nitric acid in methanol and 0.1 M tetramethylammonium hydroxide in methanol. The pH values measured are based on a pH probe calibrated in an aqueous

environment; therefore they can only be used as a qualitative value. The results of the zeta potential measurements can be seen in Figure 4. Figure 4 indicates the optimal amount of PEI is a 0.5 weight percent suspension based on the amount of powder in solution. Thus, the combination of correct concentration of PEI for the adsorption surface indicates that the 0.5 wt. percent concentration provides the ideal surface coverage with minimal PEI in the bulk solution. Below the 0.5 wt. percent concentration the PEI can flocculate the aluminum nitride.

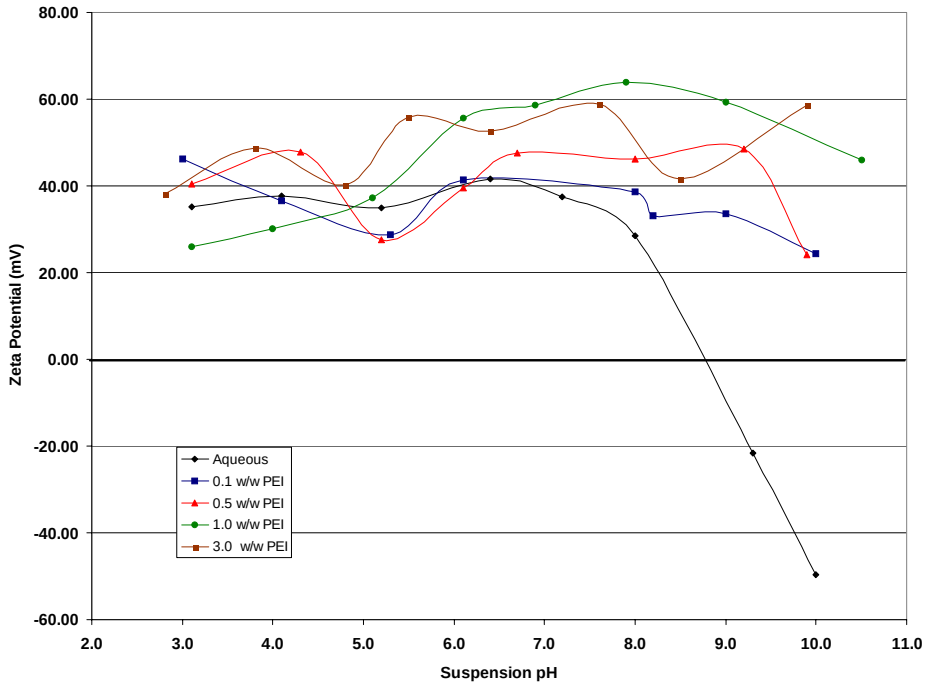

Figure 3. Zeta potential versus pH curve of 0.1 wt.% Si_3N_4 powder in an aqueous suspension with varying amounts of polyethylenimine.

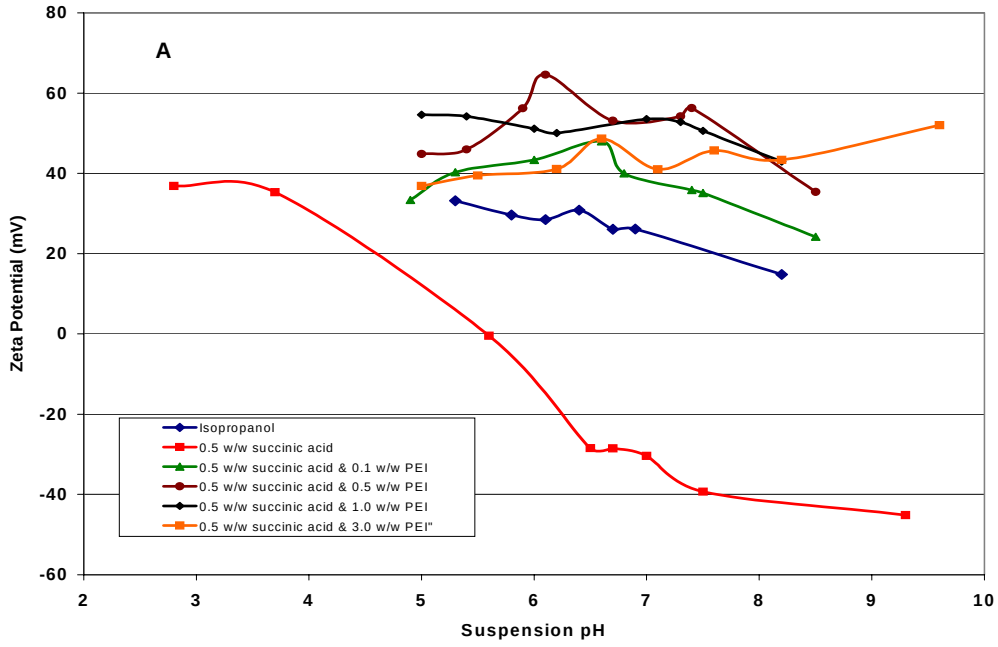

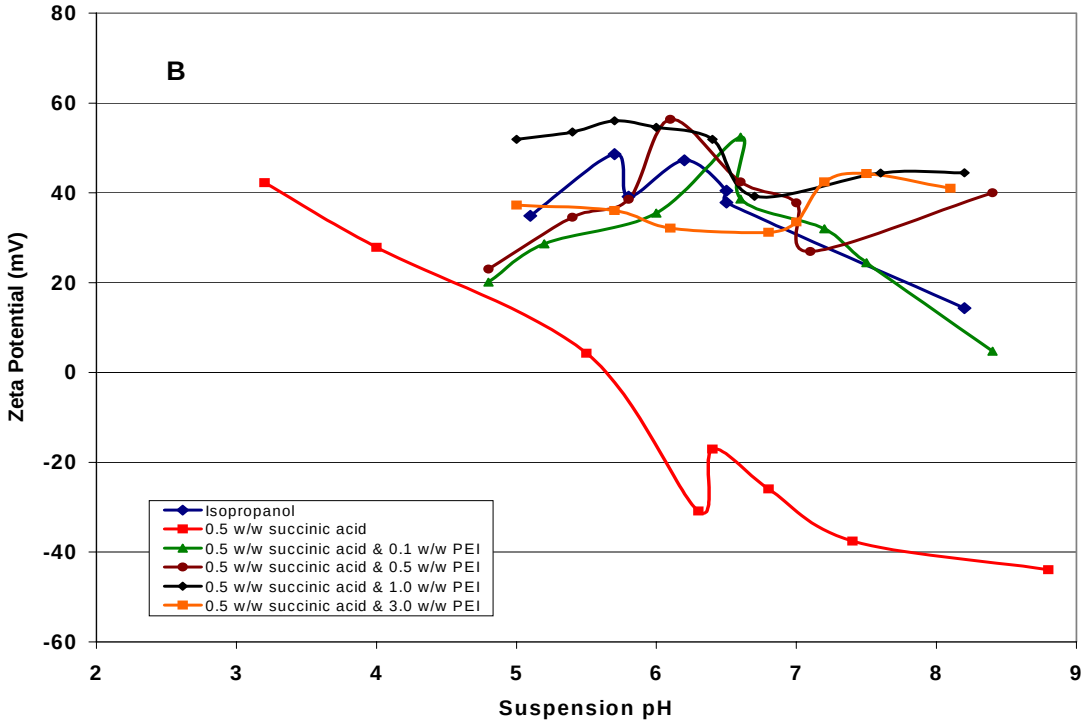

Figure 4. Zeta potential versus pH of 0.1 wt.% AlN powder in isopropanol with 0.5 w/w succinic acid and varying amounts of Polyethylenimine (PEI). A. Zeta Potential curve after 1 hour in solution. B. Zeta potential curve after 24 hours.

The optimal conditions of pH, succinic acid and PEI concentrations are used in the preparation of the concentrated suspensions for Kennametal. Solids contents up to 50 v/o were prepared using water as the carrier. The slip viscosity is relatively low up to 40 v/o solids. This is exceptional for sialon or silicon nitride slurries. Figure 5 plots the shear stress rate for a 40 v/o aqueous slip. Figure 6 plots the viscosity for the 40v/o slip. Table 1 summarizes results for three slurries prepared at 40 v/o solids. The viscosity is reproducible and could be used for slip casting or gel casting processes. Aqueous slips prepared at 50 v/o solids were dilatant and offer the potential for vibration casting approach. Based on the Zeta potential measurements completed in isopropanol similar high solids loadings were expected. In the initial trials the highest solids loading attained is 30 v/o and viscosities were higher. Including 2 w/o water in the isopropanol slurries resulted in slips equivalent to the aqueous slips. Forty volume percent slips were prepared with isopropanol – 2% water. Also initial tests indicate the water does not affect the AlN stability. The passivation – dispersion system developed for sialons should lead to better tolerances, less shrinkage and more uniform shrinkage of complex components because of the improved dispersion of heterogeneous powders. Plans are to produce a set of mechanical test specimens using the sialon colloidal system.

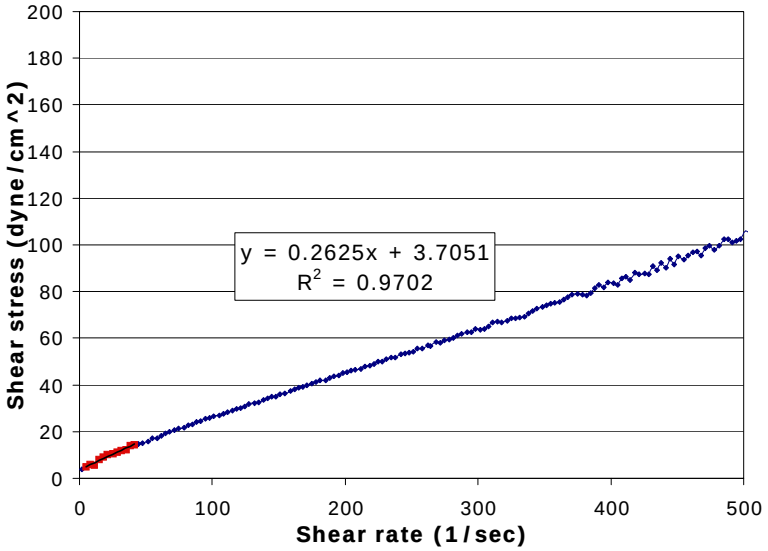

Figure 5. Shear stress rate for a 40 v/o aqueous sialon slurry.

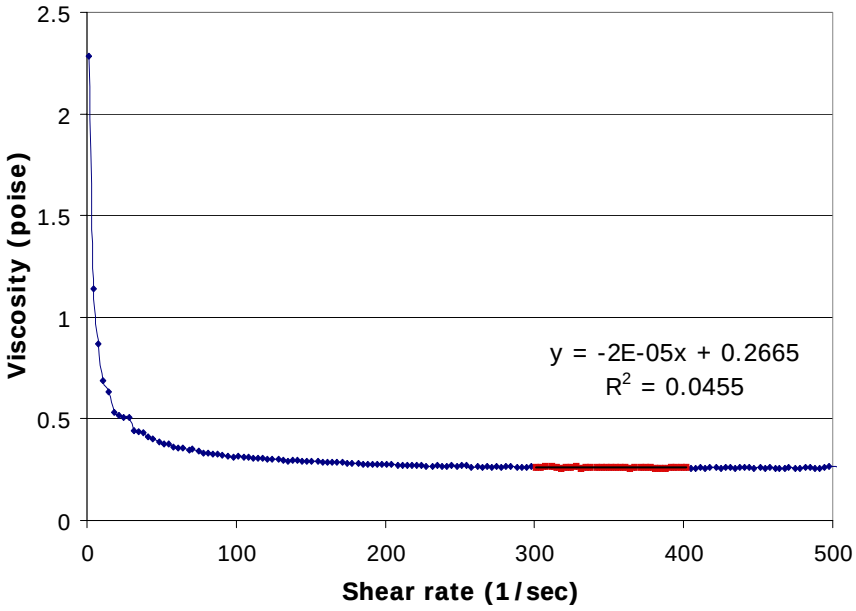

Figure 6. Slurry viscosity versus shear rate for a 40 v/o aqueous sialon slurry

Table 1. Summary of viscosity and Bingham yield with a 40 v/o slurry.

Trial	η_a (cP)	τ_B (dyn/cm2)
1	23.0	5.5
2	21.8	3.7
3	26.7	4.2
average	23.8±6.3	4.5±2.2

Status of Milestones

1) Sialon compositional preliminary matrix - completed
2) Complete mechanical and microstructural characterization of initial Sialon compositions.

Sept ‘04

a. Prepare flexure bars (ground and as processed surface) – Complete, sent to ORNL for testing

b. Tile for Kaiser Rig testing – complete, sent to ORNL

c. Deliver tensile rods to ORNL – Densification scheduled for completion in June.

d. Flexure bar Mechanical Testing at ORNL

3) Colloidal Processing of Silicon Nitride Apr. ‘04
Complete, Presentation made to Kennametal first week in June.

4) Role of Microstructure and Crystalline Phase Evolution on Thermo-mechanical Properties of Sialon Ceramics for Microturbine Applications Oct. ‘04
This effort is on schedule.

Problems Encountered

Kennametal ceramic sales posted strong growth the past several months. Our technology group pilot capacity is now supporting manufacturing to meet the high demands. This is expected to continue through August and is delaying the tensile rod sintering.

Publications/Presentations

None this quarter

Saint-Gobain Hot -Section Materials Development

R. H. Licht, Vimal K. Pujari, William T. Collins, James M. Garrett, Ara M. Vartabedian
Saint-Gobain Ceramics & Plastics, Inc.
Goodard Road, Northboro, MA 01532
Phone: (508) 351-7815, E-mail: Robert.h.licht@saint-gobain.com

Objective

The goal of this program is to develop and optimize a high temperature silicon nitride based ceramic material and process suitable for microturbine hot section component applications.

Highlights

The technical effort during this period focused on a) Reproducibility of improved (40%) as-processed (AP) surface strength in the production HIP unit, b) Development and evaluation of recession resistant solutions based upon the two selected approaches of HEEPS (HIP Engineered Environmental Protection System) and pack cementation (PC) and c) Mechanical property evaluation of net shape formed Integral Bladed Rotor (IBR) component.

AP strength (of NT154 high temperature silicon nitride) exceeding 700 MPa was reproduced utilizing the production HIP.

PC modified NT154 test specimens have been shown to exhibit a factor of 3 improvement in weight loss rate over baseline silicon nitride in an internal NRDC recession test rig.

Bi-axial flexure AP strength measured on an NT154 IBR was found to be comparable to those obtained previously from other competitive gas turbine grade materials.

Technical Progress

The technical effort involves a two-pronged approach:

1. Material development
2. Net Shape Forming Development (NSFD)

1. MATERIAL DEVELOPMENT:

1.1 AP Strength Reproducibility

The reproducibility of AP strength in the production HIP was verified. The four point flexure AP strength of 700 MPa was duplicated utilizing the proprietary new HIP process and the production HIP. The reproducibility of AP strength was found to

correlate directly to the AP surface finish which in turn is strongly impacted by the surface finish of the green components prior to HIPing.
A set of new NT154 test tiles were prepared with the desired green surface finish (duplicating that of CNC machined rotors) prior to HIP. These tiles will be delivered shortly to ORNL for AP strength evaluation.

1.2 Recession Mitigation

Material recession, due to volatilization in humid gas turbine environments, is an issue for silicon nitride and has been reported on in the literature. Phase II of the contract investigates recession resistant solutions for NT154. Three different approaches are currently being investigated:

- **a)** HEEPS - HIP Engineered Environmental Protection Surface
- **b)** Pack Cementation
- **c)** EBC Coating

1.2.1 HEEPS

Additional samples were prepared by a new impregnation technique. A significant improvement in the penetration depth in the green sample was achieved with this approach. HEEPS samples were prepared utilizing this approach. Initial characterization again suggests that there is a migration of the coating material. Work is underway in an attempt to minimize the migration of the coating material during HIPing.

1.2.2 Pack Cementation

As described in the previous quarterly report, the PC approach was successfully employed to help modify the surface of NT154 up to depths of 8-10 um. However, the surface modification was found (SEM, EDX) to be non uniform. During this reporting period, PC parameters (temperature, time, bed composition) were adjusted to improve the quality (depth and continuity) of the modified surface layer. High PC temperature was found to have the most significant beneficial effect. A factor of 3 improvement (over baseline NT154) in the weight loss rate was measured (Table 1) utilizing the recession rig at NRDC. XRD analysis showed an additional phase in all PC samples which exhibited a reduced weight loss.

Table 1: Internal NRDC Recession Test Results

Samples	Normalized mass change (mg/cm2/hour) Recession Run #4 and #5 Combined
Y2O3 Sample	**-1.0E-03**
NT154 Pack Cementation Sample #25	-1.0E-03
NT154 Pack Cementation Sample #24	-1.4E-03
NT154 Pack Cementation Sample #21	-1.9E-03
NT154 Pack Cementation Sample #17	-2.1E-03
NT154 Pack Cementation Sample #20	-2.3E-03
Baseline NT154	**-2.3E-03**
NT154 Pack Cementation Sample #22	-2.4E-03
NT154 Pack Cementation Sample #15	-2.5E-03
NT154 HEEPS #4	-3.0E-03
Fused Quartz	**-3.8E-03**

A set of baseline NT154 tiles was supplied to Steve Nunn at ORNL for additional pack cementation experiments. A set of new PC coupons will also be fabricated for Keiser rig testing.

1.2.3 EBC Coating

This effort is being pursued in collaboration with the Ceramatec, Inc. Geomimetic-based, as well as other materials are being investigated as candidate EBC materials.

Silicon carbide/silicon nitride based polymer precursors are being employed with appropriate fillers to apply graded multi-layer bond coats and the recession resistant top coat. Use of appropriate fillers is expected to grade the CTE of various layers to accommodate mismatch in expansion and the resulting residual stresses. NT154 tiles were supplied to Ceramatec for use in their coating development.

EBC coated and bulk material samples have been received from Ceramatec for some additional HEEPS based processing followed by recession screening tests.

Additionally, NT154 tiles were supplied to UTRC for their EBC development.

2. NET SHAPE FORMING DEVELOPMENT (NSFD):

Two green-machined Ingersoll-Rand design rotors (Figure 1) have been densified with the proprietary new HIP process. The two rotors have an excellent average surface roughness of 30-33 in on the AP surfaces. Based on the CMM measurements taken, the two rotors exhibited a maximum part to part variation of 0.006", which is an indication of the consistency of the process. Also, a measured concentricity within 0.003" for the two rotors is an indication of the uniform shrinkage seen with this process.

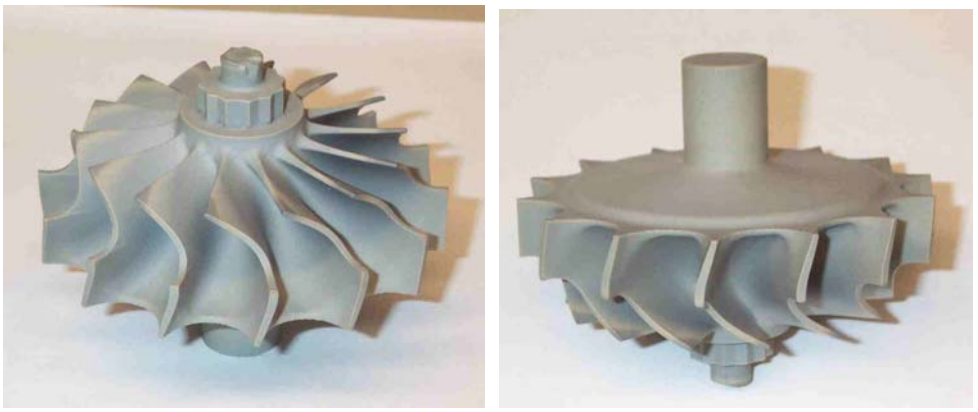

Figure 1: Dense NT154 Rotor of an Ingersoll-Rand Design

The two rotors have been delivered to ORNL for mechanical property evaluation. Disks core-drilled from individual blades are tested in biaxial flexure to establish the AP and bulk strength of actual components. To date, the AP test data for the first rotor has been received from ORNL and is shown in Figure 2. The average AP strength of 527 MPa is comparable to those of other candidate gas turbine grade

silicon nitride materials. Biaxial flexure disks machined from the hub section of the rotor will also be tested to establish properties representing the bulk material strength of thick cross-section components. We are trying to understand the discrepancy between the biaxial strength of the AP rotor surfaces and the higher MOR strength of AP tiles. One approach planned is to evaluate biaxial flexure disks machined from AP tiles.

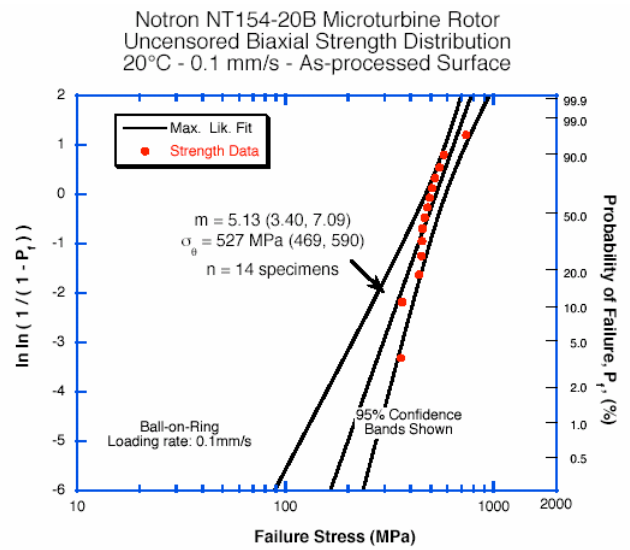

Figure 2: AP Biaxial Flexure Results from First NT154 Rotor (provided by HT Lin of ORNL)

The second dense rotor was prepared with an improved green machining procedure. As a result, the rotor shows a 10% surface roughness improvement, which should help to improve the AP strength. This rotor will also be tested at ORNL.

Status of Miletones

(1) Demonstrate a 40% improvement in the as-processed strength of Saint-Gobain NT154 silicon nitride (July 2004): COMPLETED

Our baseline or starting average AP flexure strength for NT154 was 450-500 MPa, which we showed in Phase I and which is consistent with earlier ATTAP data. We have repeatably achieved improved AP flexure strength of at least 650-700MPa, which would achieve the 40% DOE Milestone Goal.

We are encouraged that we can achieve the upper average 700 MPa goal as we have done so in both a laboratory and production scale HIP. Over the reporting period, we have gained further understanding that will help to consistently achieve our target AP strength. We are in the process of making specimens for qualification at ORNL.

(2) Evaluate baseline recession resistance for uncoated and surface-modified NT154 (September 2004) and

(3) Develop a suitable surface modification procedure or EBC for test tiles and components to improve the recession resistance (December 2004): ON SCHEDULE

The development of an internal NRDC recession test has been instrumental in screening candidate solutions. The baseline NT154, as well as surface-modified NT154 has been tested in the internal recession test. Up to a factor of 3 reduction in weight loss rate has been seen with surface-modified NT154. There are plans to deliver promising candidates to ORNL for Keiser Rig testing.

Industry Interactions

NT154 tiles delivered to ORNL, UTRC and Ceramatec for EBC development.

Vimal Pujari, Ara Vartabedian and Charles Bateman and Vimal Pujari visited ORNL on June 2nd and 3rd to review progress and conduct technical discussions.

Problems Encountered

None

Publications/Presentations

None

Environmental Protection Systems for Ceramics in Microturbines and Industrial Gas Turbine Applications Part A: Conversion Coatings

S. D. Nunn and R. A. Lowden
Metals and Ceramics Division
Oak Ridge National Laboratory
Oak Ridge, TN 37831

Objective

Monolithic silicon nitride ceramics are currently the primary ceramic material being used in combustion engine environments and are under consideration as hot-section structural materials for microturbines as well as other advanced combustion systems. Under oxidizing conditions, silicon nitride will typically form a surface oxidation (silicate) layer. In a combustion environment, this silicate layer can undergo rapid degradation because of the corrosive and erosive effects of high temperature, high pressure, and the presence of water vapor. This degradation can severely limit the useful life of the ceramic in this environment. Thus, the development of an environmental protection system for the ceramic has become an essential goal for enabling the long-term utilization of these materials in advanced combustion engine applications.

One approach that is being pursued to produce an environmental protection system for silicon nitride is the formation of a surface conversion layer using the pack cementation process. Pack cementation has been used for many years to develop an oxidation protection coating on nickel-based superalloys that are used for hot-section components in gas turbine engines. A reactive gas atmosphere is used to change the composition and microstructure of the metal alloy at the surface of the component so that it will form a protective oxide film under normal operating conditions. The same approach can be used to form a modified surface region on silicon nitride ceramic components. By selecting an appropriate reactive atmosphere for the pack cementation process, the surface region can be modified to form ceramic compounds that may provide enhanced corrosion and erosion resistance in the combustion engine environment.

Highlights

Visitors from Saint-Gobain came to ORNL to present an update on their progress in establishing production of the new NT154 silicon nitride material. During the visit we were able to discuss in-house efforts underway at Saint-Gobain to produce protective coatings on NT154 by a pack cementation process similar to that which is being evaluated at ORNL. The discussions were helpful to compare the specifics of the coating methods being explored and the status of the results of the coating experiments. Saint-Gobain has agreed to provide ORNL with a quantity of the latest NT154 material for use in the continuing coating studies that are ongoing at the Lab.

Technical Progress

Coatings on silicon nitride substrates of strontium aluminate or strontium aluminosilicate show good potential as protective barriers in gas turbine environments based on reaction products that have been observed on the surface of BSAS-coated silicon nitride samples after completion of environmental exposure testing. Although the BSAS broke down during high temperature and high moisture exposure, Sr compounds were detected on the substrate after the completion of the tests. Pack cementation is being used to form Sr-containing compounds on the surface of silicon nitride materials. Samples of Honeywell AS800, Kyocera SN281, and Saint-Gobain NT154 silicon nitrides were coated in air, argon, or nitrogen at either 1200ºC or 1400ºC. Three different Sr-containing compounds were used in the packing beds for the coating runs to react with the surface of the silicon nitride substrates. Alumina was also present in the pack beds. Some of the coating products that were formed are shown in Table 1.

Table 1. Processing variations and coating phases identified by XRD.

Silicon Nitride Substrate	Sr-Containing Compound in Pack	Sr Compounds Identified by X-ray Diffraction
AS800	$SrCO_3$	$SrSiO_3$, Sr_2SiO_4, $SrAl_2O_4$
AS800	$SrCl_2$	$SrAl_2Si_2O_8$
AS800	$Sr(NO_3)_2$	$SrSiO_3$, Sr_2SiO_4, $SrAl_2Si_2O_8$
NT154	$SrCO_3$	$SrSiO_3$, $SrAl_2Si_2O_8$
NT154	$Sr(NO_3)_2$	$SrSiO_3$, $Sr_3Al_2O_6$, $SrAl_2Si_2O_8$
SN281	$Sr(NO_3)_2$	$SrSiO_3$, $Sr_2Al_2SiO_7$

Analysis of the silicon nitride samples after pack cementation showed that several different Sr compounds could be formed on the substrate surfaces. The compounds included silicates, aluminates, and aluminosilicates. Development of the coating process is continuing to refine the coating layers that are produced. The durability and the protective characteristics of the coatings will be evaluated in a simulated turbine engine environment.

Coating development work is also continuing for producing ytterbium silicate on silicon nitride substrates. The most recent experiments involve the pre-oxidation of the substrates prior to pack cementation coating. A silica layer is formed by exposing the silicon nitride materials to air at 1400ºC. The presence of silica is expected to promote the formation of the rare earth silicate during pack cementation. Samples that have completed the coating run are presently being examined by X-ray diffraction to identify the surface compounds that have been formed.

In addition to silicon nitride ceramics, there is some interest in the gas turbine engine community in the use of SiC, particularly SiC/SiC composites, for some high temperature engine components. These components will be subject to corrosive degradation that is similar to what is observed with silicon nitride. To address this issue, some preliminary testing has been started to evaluate protective coating formation on SiC. Initially, test samples of CVD SiC are being used, but subsequent tests will include SiC CMCs. Early results have shown that surface layers of

compounds such as Yb_2SiO_5, $SrAl_2Si_2O_8$, and $SrSiO_3$ can be formed on the surface of SiC using the pack cementation coating process. Additional tests are planned to continue the evaluation of coating formation and to assess the protective characteristics of the coatings on SiC.

Status of Milestones

Evaluate the corrosion resistance of strontium aluminate-type and ytterbium-containing surface conversion coatings on silicon nitride in a simulated combustion atmosphere. (Sept. 2004)

Industry Interactions

Participated in a meeting with Saint-Gobain at ORNL to discuss the production status of the new generation NT154 silicon nitride and the use of pack cementation to form protective coatings.

Samples of the new-production NT154 silicon nitride have been received from Saint-Gobain for evaluation in pack cementation coating experiments.

Discussed preliminary results of pack cementation coatings on SiC with an airfoil materials engineer from General Electric Aircraft Engines. GEAE agreed to send a sample of SiC/SiC CMC to ORNL for use in coating experiments.

Problems Encountered

None

Publications and Presentations

None

Environmental Protection Systems for Ceramics in Microturbines and Industrial Gas Turbine Applications: Slurry Coatings

B. L. Armstrong, K. M. Cooley, and G. H. Kirby
Oak Ridge National Laboratory
P. O. Box 2008, Oak Ridge
Tennessee 37831-6063
Phone: (865) 241-5862, E-mail: armstrongbl@ornl.gov

Highlights

The rheological behavior of concentrated Y_2SiO_5 suspensions (ϕ = 0.45) was characterized to optimize their use in a dip-coating process.

Technical Progress

Previously, zeta potential experiments were carried out in order to characterize the surface of yttrium silicate particles in dilute aqueous suspension. From this work, poly(ethylene imine) (PEI) was determined to be an effective dispersant for the fabrication of concentrated suspensions. We have studied the rheological behavior of concentrated Y_2SiO_5 suspensions of varying PEI concentration, which is optimized for the dip-coating process at linear elastic modulus values ranging between 300 Pa – 20 kPa and yield stress values ranging between 2 Pa - 7 Pa. It was not possible to simultaneously achieve these parameters with dispersant additions only, thus, additional measures will be taken, e.g., the addition of a binder, pH modification, etc, to achieve optimum slurries for dip-coating.

Rheological Behavior

Work began on the optimization of Y_2SiO_5 (Praxair, Woodinville, WA) slurry rheology for a dip coating process. A cationic polyelectrolyte (polyethylenimine, Polysciences, Warrington, PA), with a weight average molecular weight (M_w) of 10,000 g/mole and one amine group (NH) per monomer unit was implemented as a rheological modifier for this system. Concentrated Y_2SiO_5 suspensions (45 vol% solids) were prepared at a constant pH of 7 and varying PEI concentration. The suspensions were ultrasonically treated for 5 min to break up weak agglomerates and mixed on a shaker table to obtain equilibrium behavior. Rheological measurements were carried out using a controlled stress rheometer (Rheometric Scientific SR5, TA Instruments, New Castle, DE) in stress viscometry and oscillatory stress modes to measure the apparent viscosity and elastic modulus, respectively.

The apparent viscosity is plotted as a function of applied shear stress in Fig. 1 for suspensions of varying PEI concentration. The degree of shear-thinning decreased with increasing PEI concentration until only slightly shear-thinning behavior was obtained at a PEI concentration of 0.25 mg/m^2 Y_2SiO_5. The elastic modulus is plotted as a function of applied shear stress in Fig. 2 for suspensions of varying PEI concentration. Solid-like behavior (i.e., a linear viscoelastic region and yield stress) was observed for all suspensions; however, the linear elastic modulus

and yield stress decreased with increasing PEI concentration until minimum values of 10 Pa and 2 Pa, respectively, were observed at 0.25 mg PEI/m^2 Y_2SiO_5.

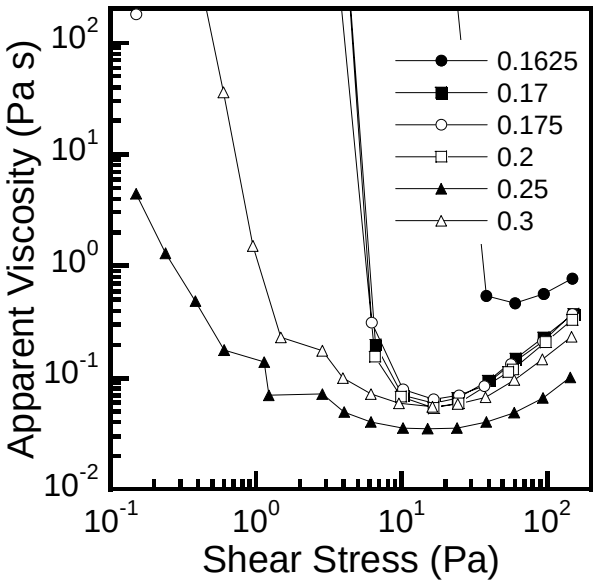

Fig. 1. Apparent viscosity as a function of shear stress for concentrated Y_2SiO_5 suspensions (45 vol% solids) of varying PEI concentration. Note, the solid lines merely guide the eye.

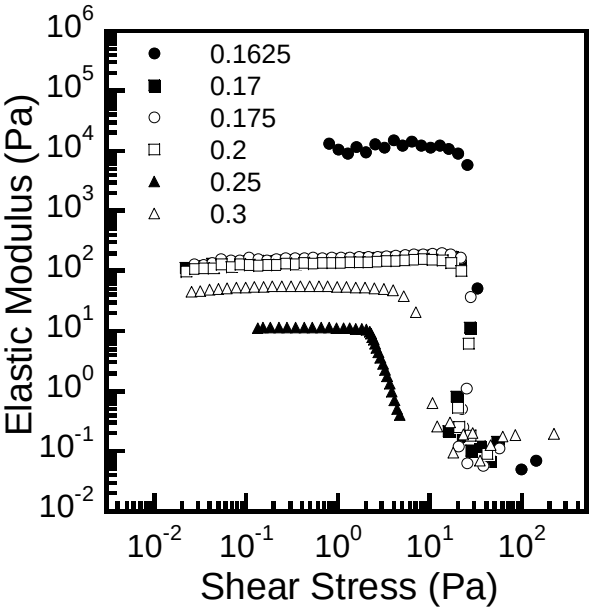

Fig. 2. Elastic modulus as a function of shear stress for concentrated Y_2SiO_5 suspensions (45 vol% solids) of varying PEI concentration (in mg PEI/m^2 Y_2SiO_5).

According to prior work on mullite-PEI suspensions, excellent dip coating suspensions are fabricated when the linear elastic modulus is between 300 Pa – 20 kPa and the yield stress is between 2 Pa - 7 Pa. The appropriate linear elastic modulus range was achieved over a very narrow range of PEI concentration, i.e., 0.1625 – 0.17 mg PEI per m^2 Y_2SiO_5. However, the appropriate yield stress is achieved at higher PEI concentrations ranging between 0.2-0.25 mg PEI per m^2 Y_2SiO_5. Clearly, it is not possible to simultaneously optimize the linear elastic modulus and yield stress with PEI additions alone. As a result, further rheological modification is required via the addition of a binder, pH modification, etc., to achieve optimal results.

Status of Milestones

Evaluate the protective capacity yttrium disilicate deposited by a slurry-based process on silicon nitride in a simulated combustion environment. (September 2004)

Industry Interactions

Discussions with UTRC and other industrial collaborators have continued. This project has also collaborated with an ARTD Fossil Energy project on Corrosion Resistant Coatings.

Problems Encountered

Due to the large quantity of substrates preferred and required for an accurate evaluation, the availability of silicon nitride substrates for coating studies has become an issue in this project. Frequently, substrates that are utilized for dipping studies are recycled from previous testing and evaluation experiments so substrate surface baselines (surface roughness and compositions) are difficult to maintain.

Publications

None

Polymer Derived EBC for Monolithic Silicon Nitride

Rishi Raj and Sudhir Brahmandam
University of Colorado
Boulder, Co
Phone: (303)492-1029, E-mail: Rishi.Raj@Colorado.EDU

Objective

The primary aim of the work during this period was to test the phase evolution and microstructural changes in the Zirconia – SiCN composites during dry and wet oxidation. The secondary aim was to conduct preliminary studies on coating these composites on silicon nitride.

Highlights

In contrast to weight-loss exhibited by hyrothermal oxidation of silicon nitride, the Zirconia – SiCN composite indicated a weight gain (which appeared to saturate with time).

XRD results showed that the amount of Zircon formed by a reaction between Zirconia and SiCN attained saturation, when oxidized under hydrothermal conditions.

XRD results on the hydrothermal tested sample also revealed that there was no silica on the surface, but appreciable amount of silica was present in the interior even after 100 hr. testing at 1300 °C. This indicates that the volatilization of silica is significantly suppressed in the composite.

Microstructural analysis indicated there was good adhesion between zirconia and SiCN due to the formation of zircon at the interface.

Preliminary coating studies indicated that a slurry of the composite gives defect free coatings of nearly 5 μm thickness on silicon nitride. Further efforts are on increasing the coating thickness.

Technical Progress

The primary emphasis during this period was on testing the oxidation behavior of a porous composite at one composition: 10mol% YCZ (6 μm) – 50 vol% SiCN (6 μm). The mixture was prepared by ball milling zirconia and SiCN powders and then cold compacting the resulting powder and sintering the compact at 1300 °C for 2 hr. in air. The sintered compact was ~ 77% dense. This compact was subjected to oxidation studies in both dry air and hydrothermal conditions. The hydrothermal testing apparatus was initially tested on silicon nitride samples; these results are detailed first.

(i) Hydrothermal Testing of Silicon Nitride

Silicon nitride samples were tested at a temperature of 1300 °C at two vapor flow rates of 4.4 and 17.6 cm s^{-1}. Figure 1 shows the change in weight per unit area vs. testing time. It should be noted that a negative value indicates weight loss. As seen in the figure, silicon nitride shows the expected para-linear weight change. Figure 2 shows a plot of the linear weight loss rate constant (K_l) as a function of the vapor flow rate. Also shown in the figure is the data from Opila *et al.* (2003). The relation between the linear rate constant, vapor pressure (P_{H2O}) and vapor flow rate (ν) may be written as:

$$K_l \propto \frac{\nu^{1/2} P_{H_2O}^2}{P_{total}^{1/2}} \quad (1)$$

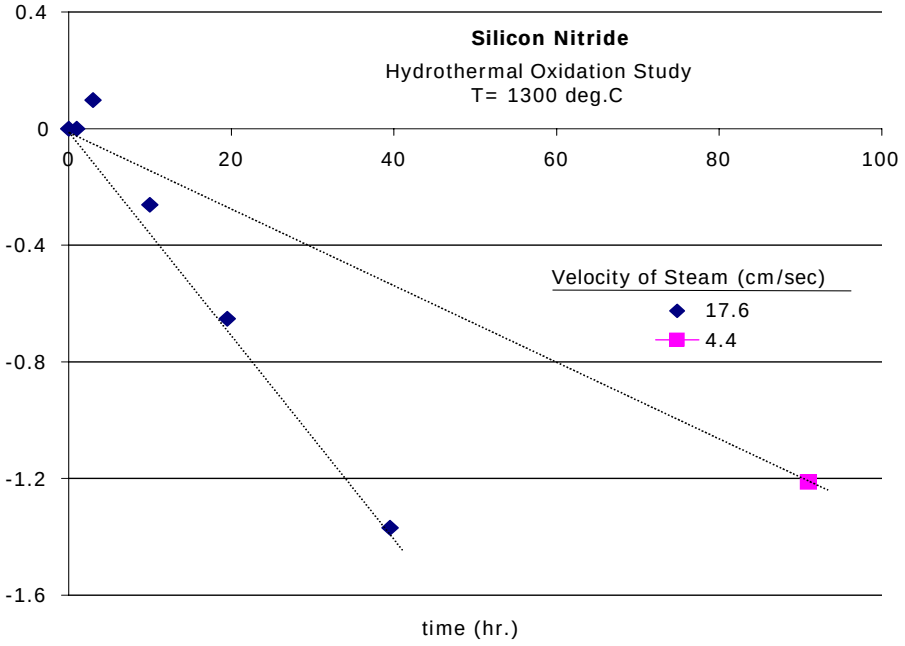

Figure 1: Tests on silicon nitride using the indigenously designed hydrothermal oxidation setup.

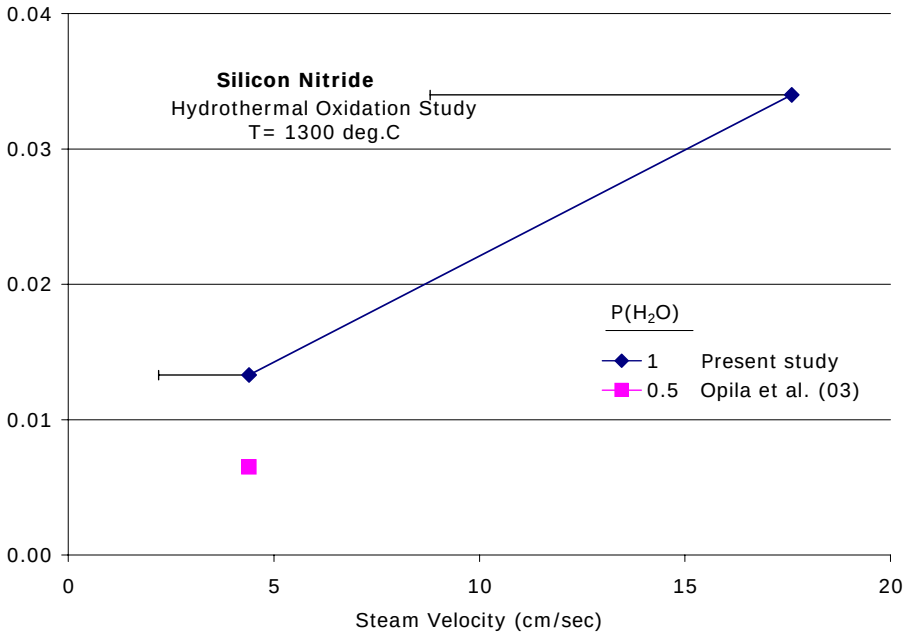

Figure 2: Linear weight loss rate as a function of steam velocity. Also shown is the data from Opila *et al.* (2003).

As seen in the figure, as the vapor flow rate quadruples, the rate constant nearly doubles. As shown in the figure, the vapor flow rate has an error of 50%. This is because when the water is injected into the hot chamber, the rapid volume expansion during the generation of steam can force nearly half the volume in the downward direction, away from the sample. Subsequent studies on the composite were conducted at the higher flow rate of 17.6 cm s^{-1}.

(ii) Oxidation Studies on 10YCZ(6μm) – 50v SiCN(6μm)

(a) Weight Change Studies:

Figure 3 shows a plot of the change in weight per unit area vs. time for the Zirconia – SiCN composite tested in dry air at 1250 and 1300 °C and in water vapor at 1300 °C, with a vapor velocity of 17.6 cm s^{-1}. A positive value indicates weight gain. As seen in the figure, the composite shows a weight gain even in hydrothermal conditions. As expected, the dry oxidation weight change increases with increasing temperature. However, it is interesting to note that the weight gain is much higher under hydrothermal conditions for times up to 30 hrs., at 1300 °C. This indicates that water vapor enhances the oxidation kinetics. In both instances the weight gain appears to reach saturation indicating a self-limiting reaction between Zirconia and SiCN into Zircon.

(b) Quantitative XRD Analysis:

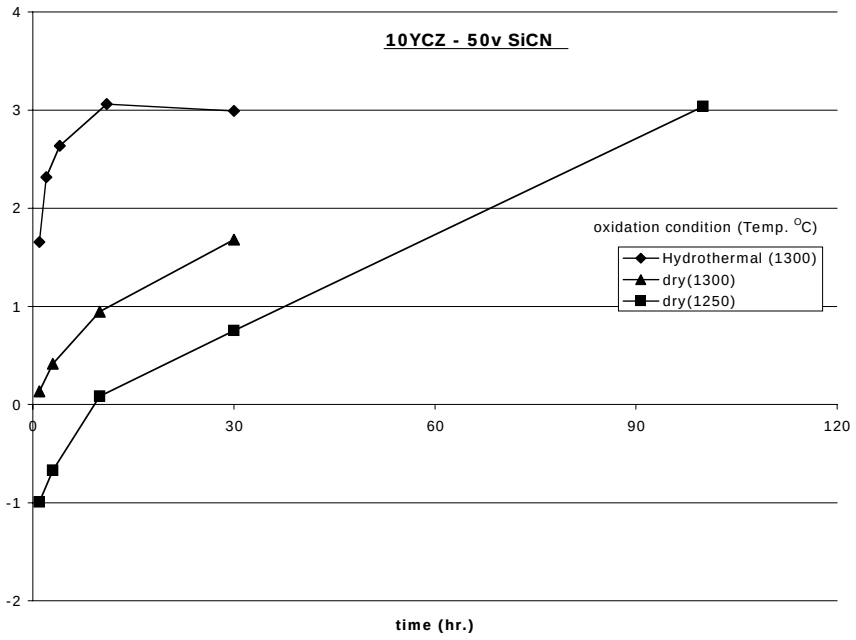

Figure 3 Weight change in the composite under dry and wet oxidation conditions.

The reaction products under both dry and wet oxidation were zirconium silicate (Zircon) and silica. The evolution of these phases was quantified by X-ray Diffraction (XRD) by the internal standard method. In this method, a crystalline material, is added in known amount to the composite and mixed thoroughly and a XRD scan is then performed on the resulting powder. The ratio of the integrated intensity of the peak corresponding to the phase of interest to the peak corresponding to the internal standard is proportional to the weight fraction of the phase of interest. Care must be taken in choosing the internal standard so that its major peaks do not overlap with those of the phase(s) of interest. In the present case, silicon powder was used as the internal standard and 10 wt% of silicon powder was added to the composite powder. Figure 4 shows the XRD data of the surface and the bulk of the composite that was tested in water vapor at 1300 °C for 100 hr. It must be noted that the bulk data was obtained by crushing the tested composite along with 10 wt% Silicon powder in a mortar and pestle, whereas the surface data was from the as-tested sample. Hence, the surface data does not show a silicon peak. Figure 4 reveals that the surface does not have any detectable silica. However, there was appreciable amount of silica in the interior of the hydrothermal tested sample even after 100 hrs. This indicates that the volatilization of silica is significantly retarded within the composite.

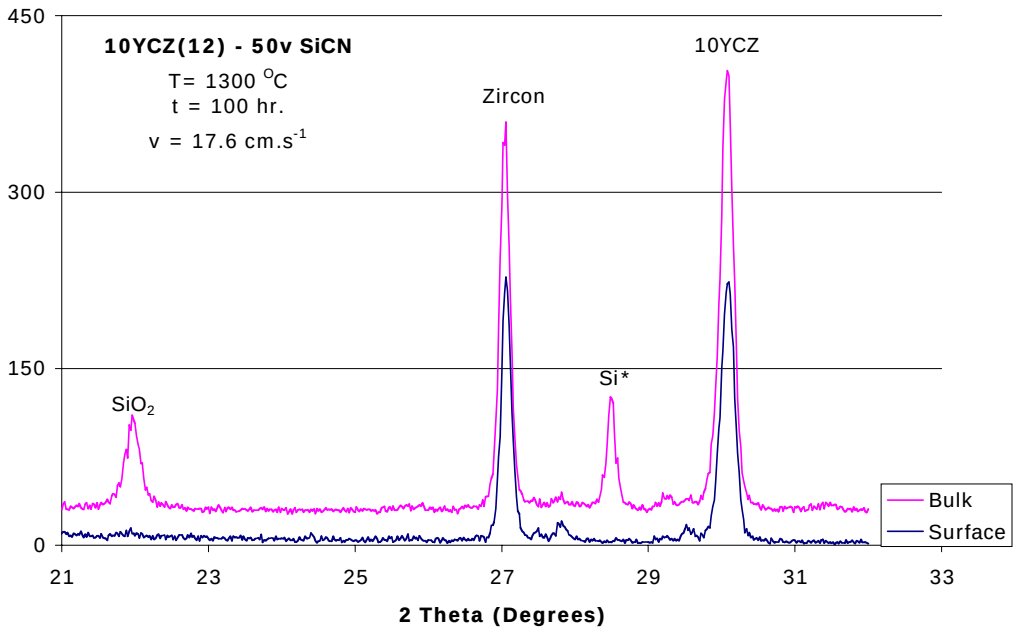

Figure 4 Phase evolution on the surface and bulk of the composite tested in hydrothermal conditions. The Silicon peak in the XRD scan of the bulk is from the internal standard added to the crushed composite powder.

The integrated area under each peak was calculated by a standard software provide with the XRD control software. The ratio of the intensity of zirconia (10YCZ), zircon and silica, to that of silicon is plotted as a function of testing time in figure 5 for the case of the hydrothermal oxidized sample. As seen in the figure, the zircon wt% increases at the expense of zirconia. Similar behavior was also observed in samples oxidized in dry air. Another interesting observation from Figure 5 is that the silica wt% shows only a marginal decrease even after 100 hrs., indicating the continued oxidation of SiCN.

(c) Microscopy studies:

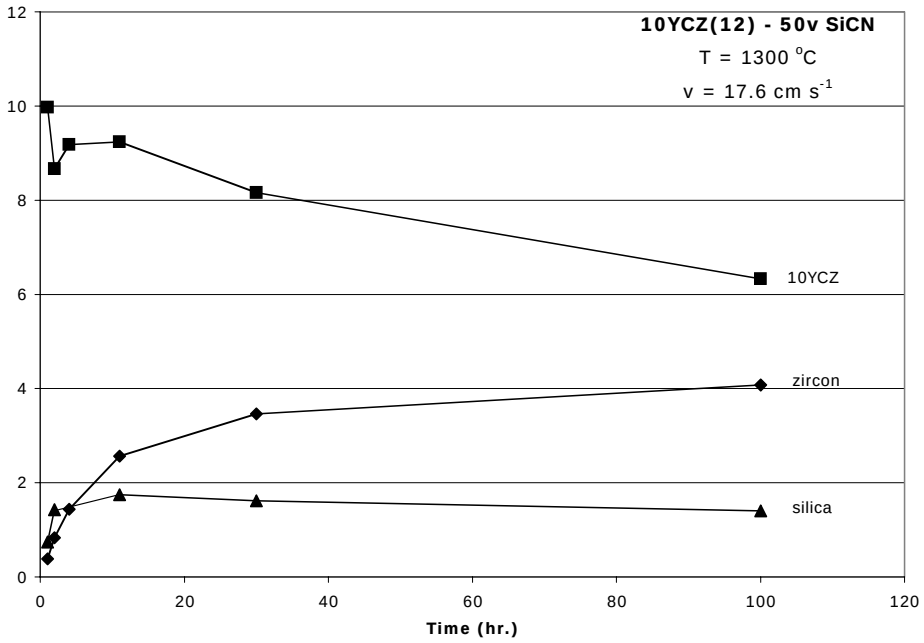

Figure 5 : The time dependent phase evolution of zirconia, zircon and silica in the case of hydrothermal oxidized sample. The zircon forms at the expense of zirconia. The nearly constant amount of silica may be due to the continued oxidation of SiCN to form silica.

Figure 6 shows the SEM micrographs of the as-sintered and the air oxidized sample. As seen in the figure, there is good adhesion between the zirconia and SiCN particles due to the formation of zircon. Figure 7 shows a line scan of zirconium and silicon along a zirconia – SiCN interface for both dry and wet oxidized samples. As seen in the figure, both the samples show comparable profiles, indicating that the microstructural evolution inside the hydrothermal tested sample is similar to that of the dry oxidized one.

The combination of weight change, XRD and microstructural studies indicate that the zirconia – SiCN composite is a potential EBC material. However, the key feature would be to get a reliable bonding between silicon nitride and the coating. Studies have been initiated to determine this aspect.

(iii) Zirconia-SiCN Composite Coatings on Silicon Nitride

Preliminary coating studies have been conducted to test the adherence of the composite coating to silicon nitride. In the preliminary trials 50-50 vol% composite mixture were added to Ceraset™ so as to form a viscous slurry. This slurry was brush coated on to a silicon nitride substrate that was cleaned in HF and then washed in boiling acetone and then methanol. The coating was air dried for ~ 1 hr. and then heated at a slow rate of 2 °C min^{-1} to 1000 °C and soaked for 3 hr.

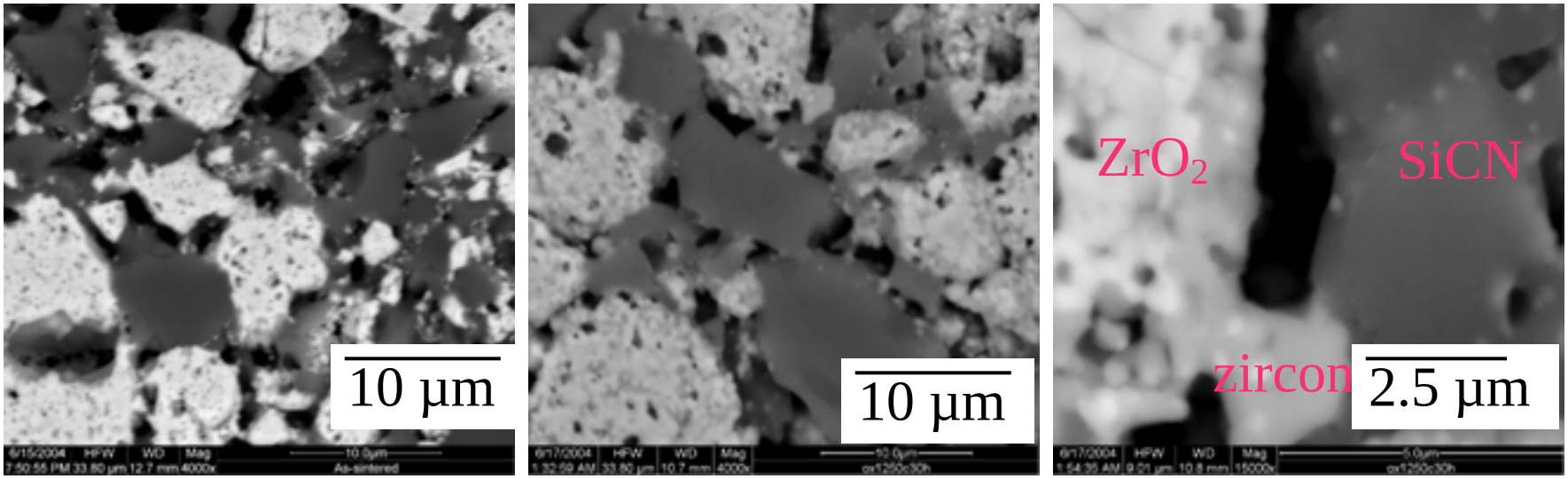

As-Sintered (1300 °C, 2 h)
Density ~ 77%

Oxidized 1250 °C, 30 h

Figure 6: SEM micrographs of the composite in the as-sintered and air oxidized conditions.

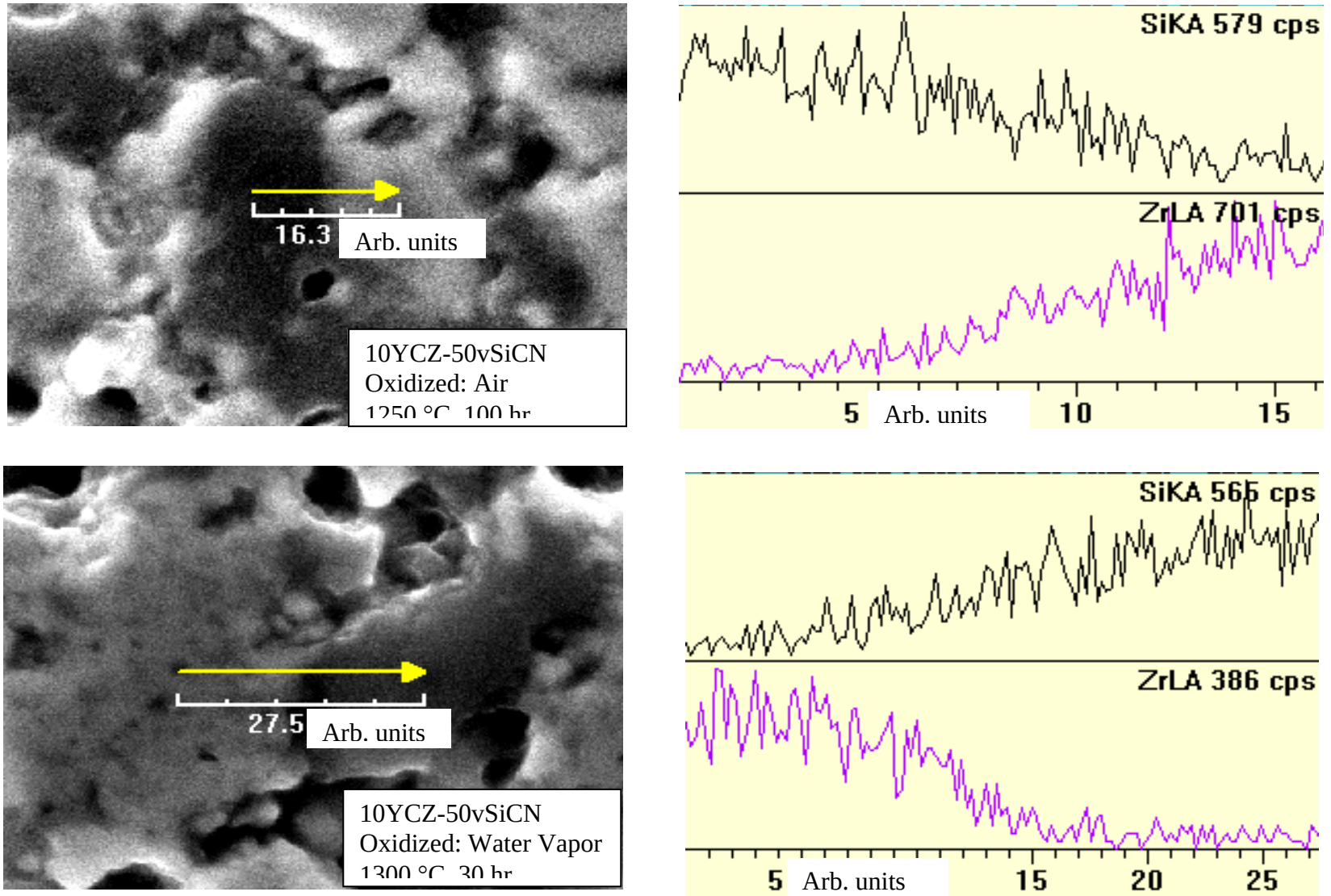

Figure 7 : Elemental line scans on the dry and wet oxidized composite showing that the microstructural evolution is comparable in both cases.

Optical microscopic observations revealed that the coating did not show any cracks. The sample was then polished along the cross-section to determine the coating thickness. Figure 8 shows the SEM micrograph of the composite coating on silicon nitride. As seen in the figure, the coating is not uniform, which is due to the coarse method used to apply the slurry. However, it is interesting to note that the coating is continuous and crack-free and at least 5 μm thick. Further efforts are on to increase the coating thickness and study the EBC properties.

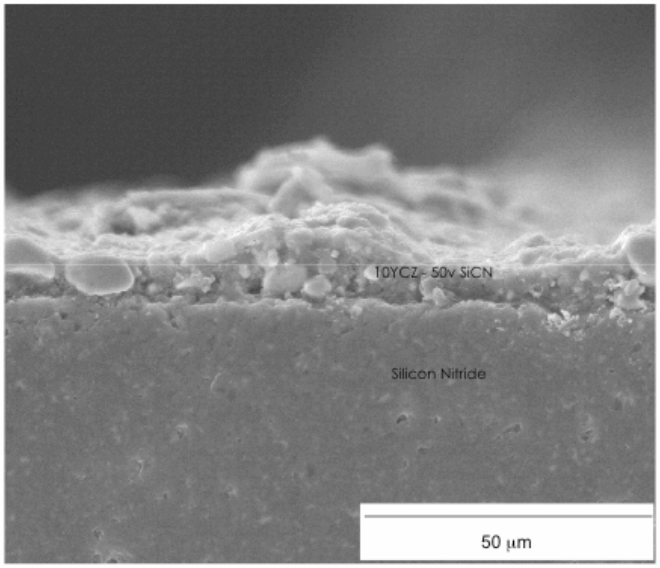

Figure 8 : SEM micrograph of the composite coating on the silicon nitride substrate.

Status of Milestones

Evaluate the oxidation kinetics of oxide-SiCN structures in the Keiser Rig to discern if the information of silica at oxide-SiCN interface can be averted by strong interfacial bonding. (September 2004)

Industry Interactions

None

Problems Encountered

None

Publications and Presentations

None

EBC Development for Silicon Nitride Ceramics for Enhanced Hydrothermal Corrosion Resistance

B. Nair, C. Lewinsohn and Q.Zhao
Ceramatec, Inc.
Salt Lake City, UT 84092
Phone: (801) 956-1000, E-mail: bnair@ceramatec.com

Objective

Ceramic materials such as silicon nitride (Si_3N_4) have the potential to substantially enhance the operating temperatures, and therefore operating efficiencies, of next generation turbines. While these materials have been shown to have excellent mechanical and thermomechanical properties, there are still technological barriers that need to be overcome before the use of monolithic ceramics becomes practical in turbine environments. One of the primary problems is the limited hydrothermal oxidation/corrosion resistance of silicon based ceramics. In order to enhance the oxidation/corrosion resistance, the main strategy has been the development of environmental barrier coatings (EBCs) with improved thermochemical stability in the turbine operational environment. While substantial progress has been made, there are still hurdles to be overcome to make EBCs viable. One issue is that most candidate EBC materials that have been studied such as mullite and stabilized celsian, primarily selected due to thermal expansion match with silicon nitride, are themselves corroded in the high temperature hydrothermal environment. Further, the coating processes that have been studied widely to date, such as plasma spraying, have several drawbacks. Plasma spraying is a line of sight process, cannot provide desirable top coat densities and generally results in substantial degradation of substrate strength during the coating process.

The goal of the current program at Ceramatec is to develop a functional environmental barrier coating system for silicon nitride ceramics, processed using non-line of sight techniques, which will provide substantially improved hydrothermal corrosion resistance without degradation of bulk mechanical properties.

Highlights

In the first four months of the program, which constituted the Phase I period, a number of significant accomplishments were achieved. Multilayered EBC-coatings were applied on NT154 Si_3N_4 coupons and bars received from Saint-Gobain, and it was demonstrated that after bond coat application, the Si_3N_4 coupons retained nearly 100% of their strength, and after complete EBC system application, the coated bars retained >75% of the flexural strength. Recession tests at Saint-Gobain demonstrated that selected geomimetic compositions had recession resistance comparable to hot pressed yttria.

Technical Progress

In the Phase I project, a number of low-silica activity top coat compositions that are expected to be stable in turbine environments were selected using the geomimetic approach. In addition, an oxide composition with proven thermochemical resistance in the turbine environment was also

selected. Bond coat compositions that show good adhesion to the top coat material and the silicon nitride substrate, as well as show intermediate thermal expansion between the top coat and substrate were also identified. After identifying the compositions, a processing route was developed for the EBC system, which utilizes simple non-line of sight coating application routes such as dip-coating and painting for both the bond coat and top coat layers.

ASTM cross-hatch tests were used to demonstrate good adhesion of the bond coat to the substrate. Flexural testing of as-received bars compared with EBC-coated bars revealed the absence of significant degradation in strength of the substrate as a result of the coating process. It was demonstrated that both as-processed and machined NT154 Si_3N_4 bars retained nearly 100% of their strength after bond coat application. After complete EBC system application, the coated bars retained >75% of the flexural strength.

Sintered monolithic compositions of the oxide and geomimetic compositions were sent to Saint-Gobain to evaluate recession resistance of these materials. Tests in their recession rig in flowing steam containing air at 1200^{o}C suggested that some of the geomimetic compositions had recession resistance comparable with hot pressed yttria. Since these compositions also showed excellent thermal expansion match with silicon nitride, and showed promise for application as thick EBC coatings on silicon nitride (See Figure 1), these set of compositions were selected for further optimization in Phase II. Saint-Gobain is exploring secondary densification techniques for the EBC coatings. Coated samples have been supplied to Argonne National Laboratory for indentation tests and to oak Ridge National Laboratory for recession tests in the Keiser rig.

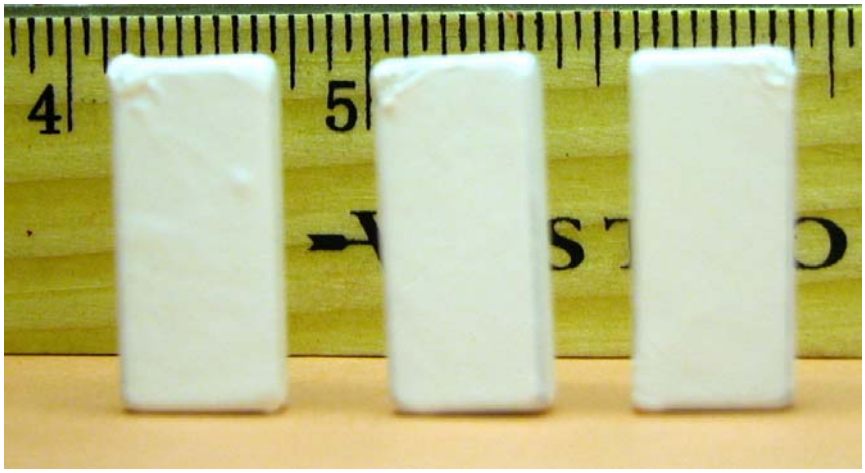

Figure 1 Geomimetic EBC-coating applied on Si_3N_4 coupons received from Saint-Gobain.

Industry Interactions

Dr. Vimal Pujari from Saint-Gobain Industrial Ceramics visited Ceramatec and reviewed our progress. A strategy was defined for collaboration between Ceramatec and Saint-Gobain which has been in effect for the last couple of months. The teaming strategy involves supply of sintered Si_3N_4 tiles from Saint-Gobain to Ceramatec, coating of the samples by Ceramatec using oxide and geomimetic coatings, and post-processing and evaluation of the coated specimens at Saint-Gobain. Saint-Gobain also evaluated recession resistance of sintered monolithic oxide and geomimetic coating compositions, as well as bond coat compositions.

Problems Encountered

None

Publications and Presentations

None

Failure Mechanisms in Coatings

J. P. Singh, K. Sharma, and P. S. Shankar
Energy Technology Division
Argonne National Laboratory
Argonne, IL 60439
Phone: (630) 252-5123, E-mail: jpsingh@anl.gov

Objective

The purpose of this research is to identify failure mode(s), understand and evaluate failure mechanisms, and develop appropriate test methods and protocols to characterize the integrity and predict failure of environmental and thermal barrier coatings for advanced turbine applications.

Technical Highlights

The effect of barium-strontium-aluminosilicate (BSAS) environmental barrier coating (EBC) on the strength and fracture behavior of EBC-coated SN282 Si_3N_4 specimens has been analyzed. The four-point flexure strength of BSAS EBC-coated SN282 was 357±17 MPa, which is lower than the strength of uncoated SN282 specimens (500±74 MPa). The measured flexure strength of the EBC-coated SN282 specimens was confirmed by finite element analysis and by fracture mechanics calculations. The decrease in strength of the EBC-coated Si_3N_4 specimens is believed to be due to the presence of tensile residual stresses in the EBC arising from thermal expansion mismatch between the EBC and the substrate. These stresses cause failure initiation at reduced applied stresses from pre-existing flaws in the EBC (silicon bond coat) at the Si/Si_3N_4 interface, as confirmed by fractographic observations.

Technical Progress

Effort this quarter concentrated on analyzing the effect of BSAS EBC on the strength and fracture behavior of the EBC-coated SN282 silicon nitride (Si_3N_4) specimens. In a related program, mechanical characterization of the BSAS-coated SN282 Si_3N_4 specimens had been performed. Four-point flexure strength of EBC-coated Si_3N_4 bar specimens (of lateral dimension 26 mm x 2 mm and substrate thickness 1.5 mm) was evaluated with the BSAS top coat in tension. The loading and support spans were 10 mm and 20 mm, respectively. The crosshead speed was maintained at 0.2 mm/min. The total thickness of the EBC was ≈ 500 μm. The flexure strength of the EBC-coated SN282 Si_3N_4 specimens was determined to be 357±17 MPa with a Weibull modulus of 23.34. It is to be noted that the flexure strength was determined using the simple beam bending equation by considering only the substrate thickness.

In order to confirm the validity of strength estimation by the simple beam bending equation (where the EBC thickness has been neglected), a finite element analysis (FEA) was performed to determine the stress profile at fracture under four-point loading of the

BSAS EBC-coated Si_3N_4. The FEA simulations considered both the effects of elastic and thermal expansion mismatch between the substrate and the EBC layers. This ensured that the effect of residual stress is taken into account in the analysis. The elastic modulus of the EBC layers used in the present analysis was relatively small as compared with that of the substrate. The EBC-coated Si_3N_4 specimen was considered to have been cooled to room temperature from a processing temperature of 1000ºC. Fig. 1 shows the stress profile at fracture in the different layers of the EBC and the substrate, as estimated by FEA. The stresses are in a direction parallel to the Si_3N_4/EBC interface. From the figure, it is clear that maximum tensile stresses are present in the Si-bond coat. In addition, the stress in the Si_3N_4 substrate at the Si_3N_4 /Si interface is about 300 MPa, which is in reasonable agreement with the measured strength (357±17 MPa).

Furthermore, the results of FEA suggest that fracture is likely to initiate in the Si-bond coat at the Si/ Si_3N_4 interface. Fig. 2 represents a typical fracture surface of a failed SN282 flexure bar coated with BSAS EBC, showing a critical flaw outlined by a dotted line. It is clear from the figure that failure originated in the silicon bond coat, confirming the prediction of FEA. Also, from the measured critical flaw size (c) on the fracture surface, the strength can be determined using a fracture mechanics equation,

$$\sigma_f = K_{IC}/Y\sqrt{c}, \qquad (1)$$

where, Y = 1.35 for four-point loading, and K_{IC} is the fracture toughness. Based on the measured K_{IC} (5.5 MPa$\sqrt{m}$) of SN282 Si_3N_4, σ_f was calculated to ≈300MPa, which agrees with the FEA prediction.

Therefore, as discussed above, the simple beam bending equation can be reliably used to estimate the flexural strength of EBC-coated Si_3N_4 specimens for relatively low elastic modulus values of EBCs. However, for EBCs with elastic modulus comparable to that of the substrate, the simple beam bending equation should be carefully evaluated for its applicability to flexural strength prediction. The above-noted measured strength of the BSAS EBC-coated specimens (357±17 MPa) was lower than the strength of the uncoated SN282 Si_3N_4 specimens (500±74 MPa). This reduction in strength is believed to be due to the presence of large tensile residual stresses in the EBC (specifically in the Si-bond coat) arising from thermal expansion coefficient mismatch between the substrate and the EBC. These stresses are believed to cause failure initiation at reduced applied stresses from pre-existing flaws in the EBCs. This is confirmed by fractographic observation of the failure initiating critical flaw in the silicon bond coat at the Si/Si_3N_4 interface (Fig. 2). To delineate the effects of individual EBC layers, future effort will focus on studying the mechanical behavior of Si_3N_4 specimens coated with silicon coating alone.

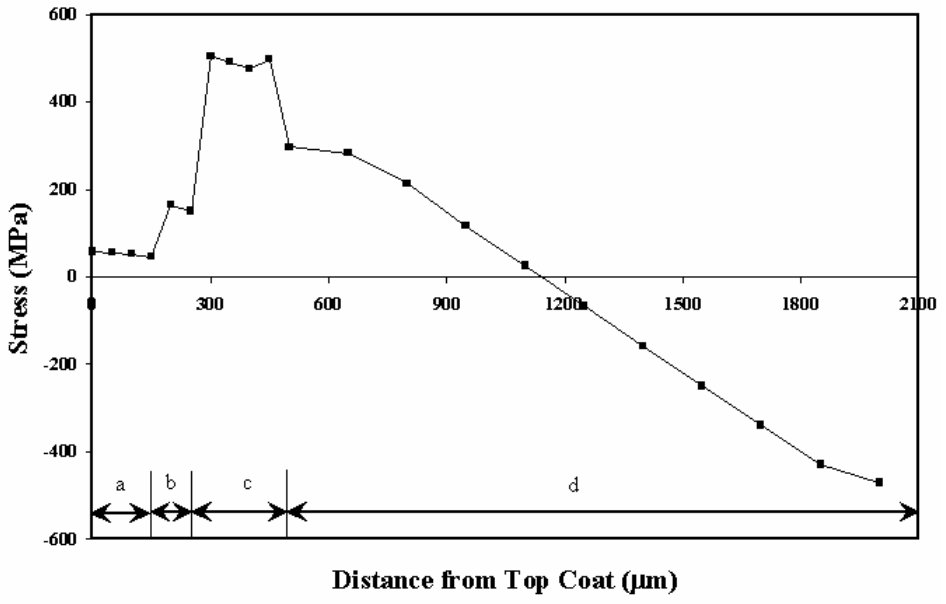

Figure 1. Variation of stresses at fracture in the different layers of a BSAS-coated SN282 Si_3N_4 substrate as estimated by FEA under four-point loading. a, b, c, and d represent the thickness of BSAS top coat, BSAS+Mullite layer, silicon bond coat, and Si_3N_4 substrate, respectively.

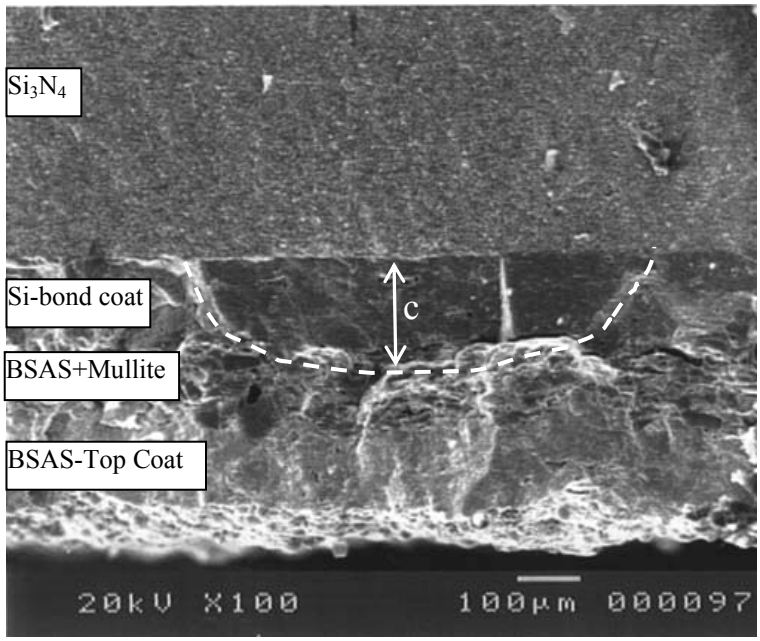

Figure 2. SEM micrograph of the fractured cross-section of SN282 Si_3N_4 flexure bar coated with BSAS EBC. Failure initiation at the Si_3N_4/silicon bond coat is clearly evident.

Status of Milestones

Complete evaluation of the effects of compositional variations in Ta_2O_5-based EBCs on mechanical behavior of the coated Si_3N_4 substrates that are being developed at Northwestern University/Honeywell. September 2004. On Schedule

Industry Interactions

Discussion on the results of mechanical and microstructural evaluation of BSAS-coated SN282 Si_3N_4 specimens was continued with Oak Ridge National Laboratory/United Technologies Research Center.

Problems Encountered

None

Publications/Presentations

K. Sharma, P. S. Shankar, and J. P. Singh, "Mechanical and Fractographic Evaluations of Si_3N_4 substrates with Environmental Barrier Coatings," Poster presented at the 106th American Ceramic Society Annual Meeting and Exposition, Indianapolis, IN, April 18-21, 2004.

High-Temperature Diffusion Barriers for Ni-Base Superalloys

B. A. Pint, K. M. Cooley and J. A. Haynes
Metals and Ceramics Division
Oak Ridge National Laboratory
Oak Ridge, TN 37831-6156
Phone: (865) 576-2897, E-mail: pintba@ornl.gov

Objective

Nickel-base superalloys require coatings to improve their high temperature oxidation resistance, particularly when a thermal barrier coating is employed. The underlying oxidation-resistant metallic coating or bond coat is degraded by the loss of Al due to oxidation, but much more Al is lost due to interdiffusion with the superalloy. Loss of Al causes diffusion aluminide coatings to undergo phase transformations, which likely cause deformation of the bond coat surface and subsequent loss of the protective alumina scale and the overlying thermal protection layer. The goal of this program is to fabricate and assess potential compounds for use as high-temperature diffusion barriers between coating and substrate. Ideally, the barrier would act to reduce the inward diffusion of Al, as well as the outward diffusion of substrate elements (such as Cr, Re, Ta, W), which generally degrade the oxidation resistance of the coating. The work is motivated by previous experimental results which suggested some compositions that exhibited diffusion-barrier capabilities. A secondary objective is to demonstrate routes to fabricating diffusion aluminide coatings incorporating a diffusion barrier using chemical vapor deposition (CVD).

Highlights

A heat treatment has been developed which reduces the residual stress in the sputtered Pt-Hf coatings, thereby reducing buckling of the coating during aluminizing. Cyclic and isothermal oxidation testing of coated specimens was initiated. Isothermal results showed the detrimental effect of coating buckling and cracking. A final series of substrates with Pt-Ni and Ir-Hf coatings has been ordered to complete work in this area.

Technical Progress

Heat treatments of Pt-Hf Coatings

The deposition of Pt and Hf layers on low sulfur René N5 substrates was described in prior reports. After numerous attempts to develop an effective heat treatment for reducing buckling in the as-aluminized coatings, a successful heat treatment was identified. Initial stage annealing for 1h at 500°C was used to reduce residual stress in the as-sputtered Pf-Hf layer followed by 2h at 1100°C in order to diffusion bond the coating to the substrate and form the desired $HfPt_3$ phase. The annealed specimen was then aluminized via a low activity CVD process described in previous reports. A specimen (NA070904-PHA8) with a 3µm Pt layer and a 1µm Hf layer showed no buckling after aluminization. A specimen with a thicker starting coating (5µm Pt, 1µm Hf, NA0709042-PHB7) showed slight buckling after aluminization but was better than any previous treatment. Exposure of both specimens under cyclic oxidation conditions has begun.

Oxidation Testing

Two aluminized specimens with Pt-Hf coatings on one side were isothermally oxidized for 200h at 1150°C in order to determine the effect of the Pt-Hf layer on oxidation behavior. These specimens both had a pre-aluminizing anneal of 30min at 900°C followed by 30min at 950°C. Because the specimen was only coated on one side, the mass gain was a combination of the coated and uncoated

behavior. Therefore, the most effective means of evaluating the effect of the Pt-Hf coating is to examine the reaction product and coating cross-section after the test. While 1150°C is a significantly higher metal temperature than anticipated in service, these accelerated conditions were used because of an extensive database of prior results for aluminide coatings at this temperature.

Figures 1 and 2 show SEM secondary electron images of a cross-section of an aluminized superalloy specimen with an initial 3µm Pt/1µm Hf sputter coating. Figure 1a indicates that significant coating buckling occurred. Coating buckles were observed after aluminizing and the delaminated areas beneath the buckles showed internal oxidation (Figure 1b) indicating that the buckled coating integrity was poor. A standard Pt-modified aluminide coating would typical form a thin protective external scale with little or no internal oxidation after this type of exposure. The oxide beneath the buckle appears thicker likely due to spallation of the outer scale. However, some of the increased thickness could be attributed to the incorporation of HfO_2 into the scale. Hafnia is known to be a fast oxygen conductor. Typical internal oxidation "stringers" or pegs were observed with Al_2O_3 encapsulated HfO_2 particles (which appear brighter), Figure 2. The presence of significant number of pegs could suggest a higher than optimal Hf content. However, this issue needs to be further investigated with unbuckled coatings.

Figure 3 shows SEM images of a cross-section from a similarly aluminized and oxidized superalloy specimen but with a thicker sputtered coating, 5µm Pt/1µm Hf. This specimen had an even greater amount of buckling and more extensive internal attack, Figures 3a-3c. However, the outer scale appeared to have fewer oxide pegs. For comparison, Figure 3d shows the opposite surface of the specimen, which was aluminized but without the Pt-Hf coating. On this side, there is no internal oxidation observed and a relatively thin adherent alumina layer formed on the surface. The need for the improved heat treatment is obvious from these results.

Because of the problems with coating buckling, no further oxidation testing had been attempted with the Pt-Hf coatings. However, with the improved annealing treatment, cyclic testing was attempted on a series of specimens with various heat treatments, Table I. Results from the first 100, 1h cycles at 1150°C in dry flowing O_2 are shown in Figure 4. For comparison, the mass gain for aluminized specimens without Pt-Hf coatings were included. The mass gains for the specimens without the optimized heat treatment are all significantly higher than those for the aluminized specimens without a Pt-Hf coating. The specimen with the optimized heat treatment showed a low mass gain consistent

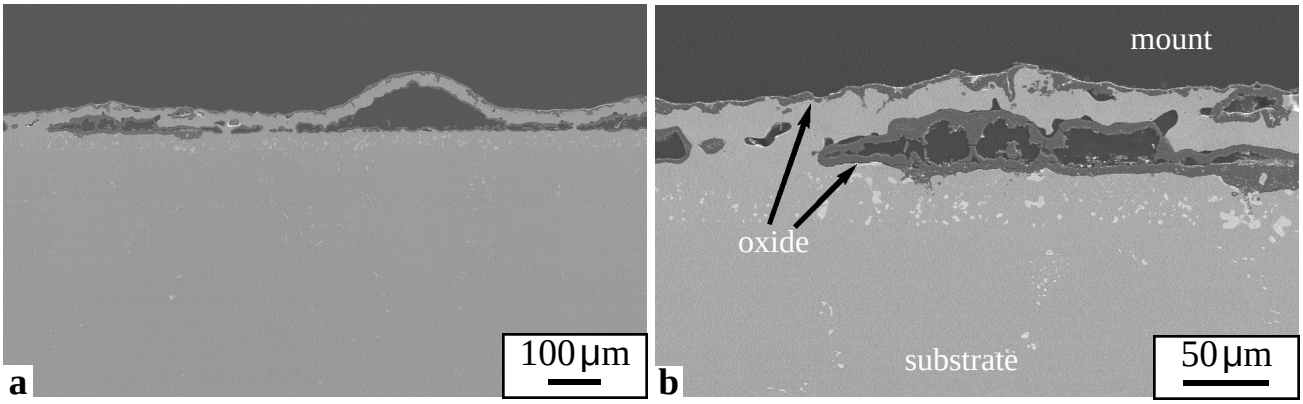

Figure 1. SEM secondary electron images of a cross-section of an aluminized superalloy specimen with an initial 3µm Pt/1µm Hf sputter coating after isothermal oxidation for 200h at 1150°C in dry flowing O_2. Significant coating buckling and internal oxidation was observed.

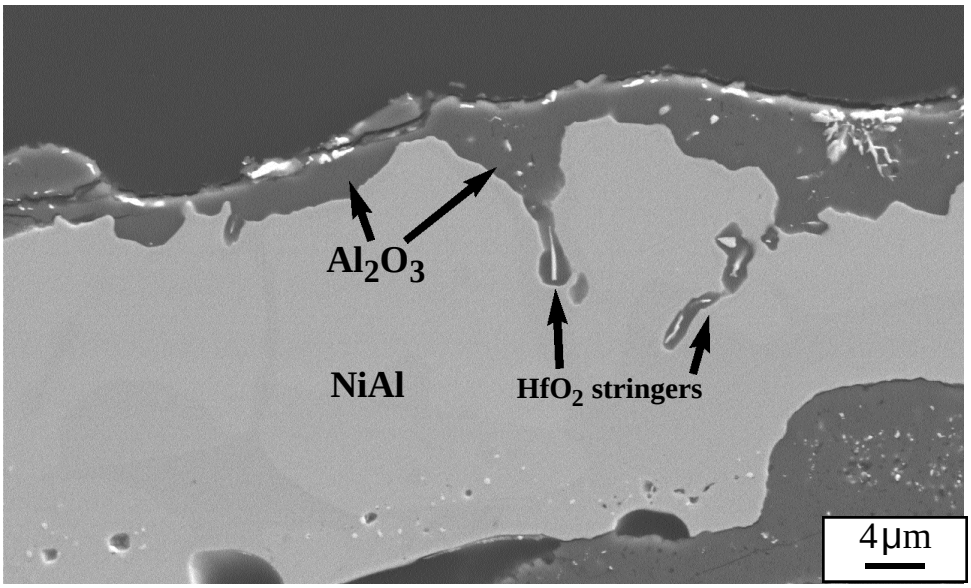

Figure 2. Cross-section of the scale formed on specimen in Figure 1. Al_2O_3-encased HfO_2 stringers were observed in the scale.

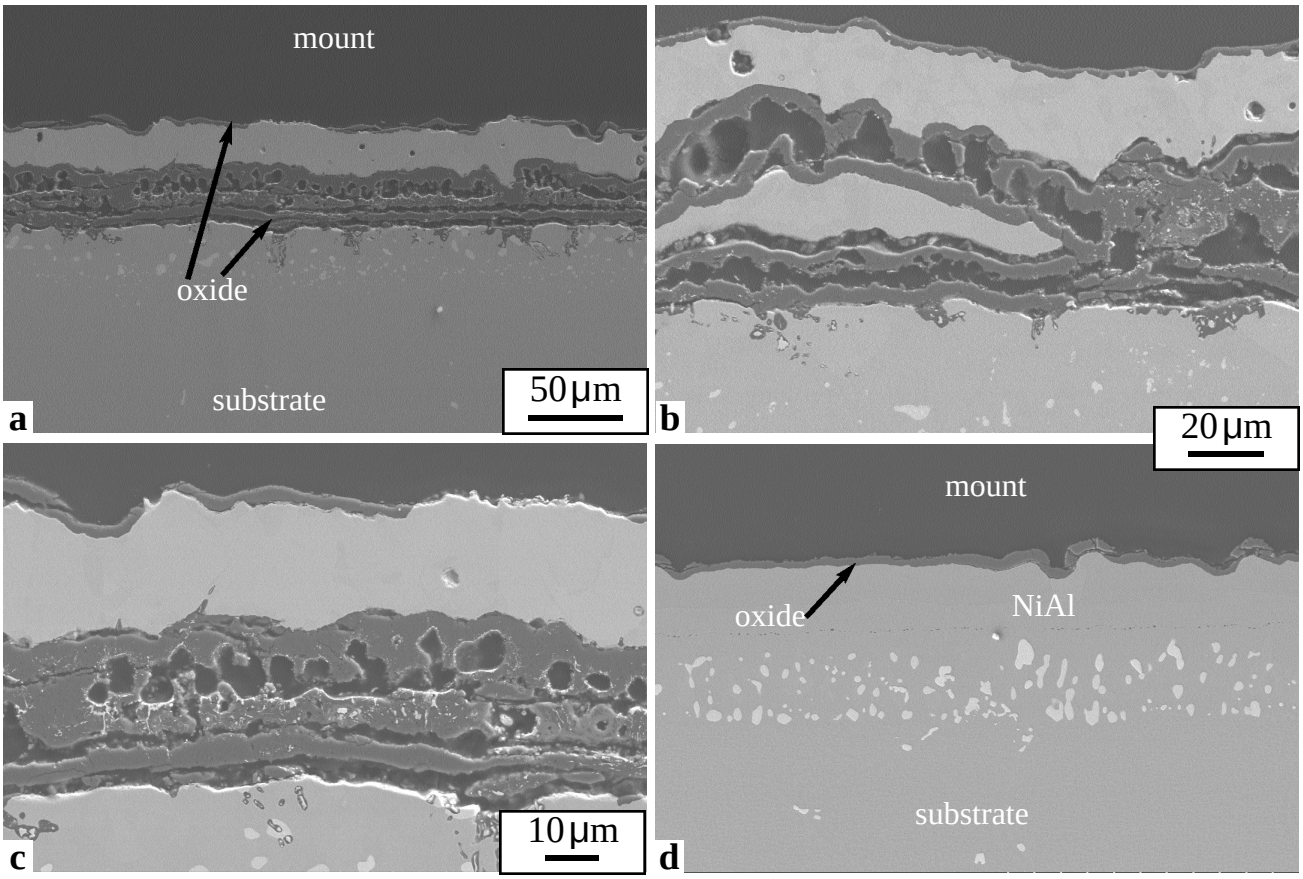

Figure 3. SEM secondary electron images of a cross-section of an aluminized superalloy specimen with an initial 5µm Pt/1µm Hf sputter coating on one side after isothermal oxidation for 200h at 1150°C in dry flowing O_2. (a-c) Significant coating buckling and internal oxidation was observed on the coated side while the side without a Pt-Hf coating (d) showed no internal attack.

Table I. Coating thicknesses and heat treatment conditions for cyclic oxidation specimens.

Specimen	Hf* (µm)	Pt* (µm)	Pre-treat Temp. (°C)	Pre-treat Time (h)	Aluminizing Time (h) at 1100°C
PHA-4	1	3	800, 1000	1, 2	6
PHB-4	1	5	None	n/a	6
PHB-7	1	5	700, 900	1, 2	6
PHA-8	1	3	500, 1100	1, 2	6

* Specimens were sputter coated on one side prior to aluminizing.

with the aluminized superalloy specimens. The surface oxide formed on these specimens is now being characterized.

Preparation for Next Series of Coatings

A significant portion of this quarter's work focused on preparation for deposition of Ir-based coatings. In this series, coatings will be sputtered onto both bare superalloys and pre-oxidized specimens. Pre-oxidation was used to form a thin, high-purity alumina scale as a surrogate diffusion barrier. These specimens were sent to Surmet Corp. for sputter deposition and are expected back in August.

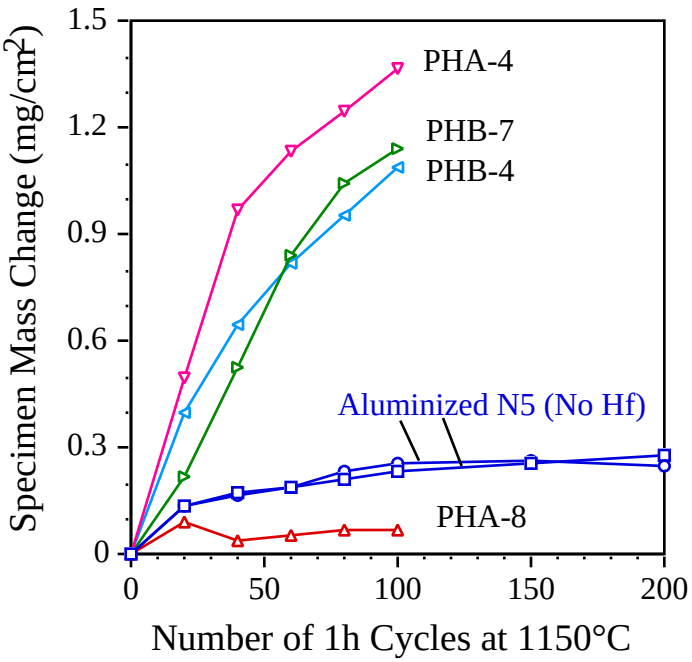

Figure 4. Mass change curves during 1150°C oxidation testing of CVD NiAl coatings with a 1µm Hf and 3 or 5µm Pt sputter coating and various pre-aluminizing heat treatments.

Status of Milestones

FY 2004
Complete characterization and testing of the first batch of precious metal-based diffusion barriers and report disclosable findings in an open literature publication.
(September 2004)

Industry Interactions

Substrates with and without pre-oxidation were sent to Surmet Corporation (Burlington, MA) for sputtering coating of Ir-Hf and Pt-Ni respectively.

Problems Encountered

None

Publications

None

POWER ELECTRONICS

High Temperature Heat Exchanger

E. Lara-Curzio, J. G. Hemrick, A. Zaltash, N.C. Gallego, C.A. Walls
Metals and Ceramics Division
Oak Ridge National Laboratory
P.O. Box 2008, Oak Ridge, TN 37831-6069
Phone: (865) 574-1749, E-mail: laracurzioe@ornl.gov
B.E. Thompson
University of Western Ontario

Objectives

As part of a collaborative effort between ORNL and the University of Western Ontario, graphite-based heat exchangers will be designed and evaluated for heat recovery systems in microturbine applications. In particular, it is desired to improve the efficiency of heat recovery systems based on aluminum fin heat exchangers that are currently being used in commercial units. In coordination with modeling efforts, the microstructure of graphite-based heat exchangers will be designed in order to maximize heat transfer while minimizing pressure drop. The efficiency of the new designs will be compared against currently used aluminum fin heat exchangers and eventually evaluated using a Unifin Microgen heat recovery unit couple to a Capstone C60 microturbine.
Work will be supplemented with experiments to gain a better understanding of the effect of heat exchanger material microstructure on gas flow penetration, pressure drop, and mechanical strength.

Highlight

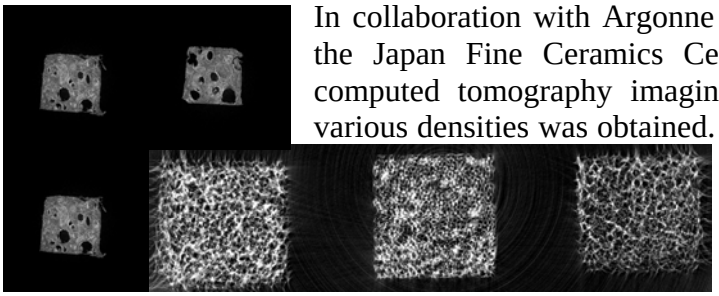

In collaboration with Argonne National Laboratory (ANL) and the Japan Fine Ceramics Center (JFCC) in Nagoya, Japan computed tomography imaging of carbon foam materials of various densities was obtained. Carbon foam materials produced at Oak Ridge National Laboratory under 500, 1000, and 1500 psig of pressure were analyzed. Low spatial resolution (28μm) X-ray tomography scans were performed at ANL, while higher spatial resolution (3μm) X-ray tomography scans were performed at JFCC. Examples of resulting digital maps are shown above.

Technical Progress

Upon consideration of the costs and labor associated with connecting the Unifin Microgen heat exchanger to ORNL's 60 kW Capstone microturbine, discussion was held regarding the feasibility of using the current microturbine/heat exchanger system already in place at the ORNL Cooling, Heating, and Power Facility (bldg. 3115). This option

would utilize the already existing infrastructure and instrumentation, while allowing alteration to the current equipment to facilitate the testing of new heat exchanger concepts.

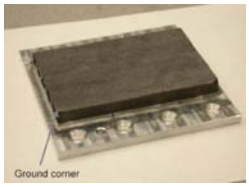

Efforts to fabricate a "miniature wind tunnel" device were combined with expertise at the University of Western Ontario. Carbon foam samples with varying densities were prepared at ORNL and supplied to Materials Resources International for S-bond joining to aluminum plates. These joined samples will be provided to the University of Western Ontario for testing in their existing wind tunnel facility. Information on the depth of gas penetration in these systems, which will be obtained from the wind tunnel tests is important to optimize material usage.

Development and implementation of a method to evaluate and compare the mechanical properties of individual foam ligaments using X-ray tomography and rapid prototyping techniques has been continued. Low spatial resolution (28μm) CT scans were performed at Argonne National Laboratory. High spatial resolution (3μm) CT scans were performed at the Japan Fine Ceramics Center in Nagoya, Japan. Estimates are still being sought for file conversion and rapid prototyping services. One company, Javelin 3D Digital Manufacturing Company, has been identified thus far who can perform the needed file conversion and rapid prototyping services.

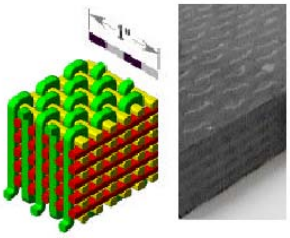

High thermal conductivity graphite fiber samples have been obtained. Lower thermal conductivity/lower modulus fiber materials have also been identified and samples have been obtained. A commercial company (3-Tex, Inc. of Cary, NC) has been identified as a partner in the project. They have a unique weaving process (3-Weave) which is capable of producing 3-dimensional fiber preforms. A visit was made to 3-Tex and possible preform weaving techniques and designs were discussed. Out of the meeting, it was decided that a series of preforms would be woven with and without metallic tubing incorporated in the structure. Initial weavings will use 50 Msi/lower thermal conductivity fibers. Subsequent weavings will be attempted with higher modulus/higher thermal conductivity fibers. Fiber has been ordered for the initial weavings and production time is being scheduled at the 3-Tex Rutherfordton, NC facility.

Brian Thompson and Qijun Yu, from the University of Western Ontario, visited ORNL in early May. Both presented seminars outlining their work and progress in regard to the modeling of carbon foam and the design of alternative carbon foam heat exchangers. The design of microturbine/heat exchanger experiments, the base-line performance of the current Unifin heat exchanger, and the cooling of power electronics were also discussed.

A test rig has been designed and constructed to evaluate heat transfer, permeability, and pressure drops associated with experimental graphite foams and woven fiber preform structures. Results will be used to optimize the pore structures of foams and fiber preforms to maximize performance and to verify model predictions.

Status of Milestones

In Progress.

- Fabrication and joining of samples for wind tunnel analysis at University of Western Ontario. Eight samples have been provided for analysis and additional samples are in preparation (July 2004)
- Alteration of current equipment in place at the ORNL Cooling, Heating, and Power Facility (bldg. 3115) to facilitate the testing of new heat exchanger concepts. (August 2004)
- Development and implementation of a method to evaluate and compare the mechanical properties of individual foam ligaments using X-ray tomography and rapid prototyping techniques. (August 2004)
- Testing of carbon foam and fiber performs in test rig. (August 2004)
- Fabrication of carbon-fiber preform prototypes. (September 2004)

Problems Encountered

None

Publications/Inventions/Meetings

Visit to 3-Tex, Inc., Cary, NC to discuss 3-dimensional weaving process (4/04)
Visit by Brian Thompson and Qijun Yu, from the University of Western Ontario (5/04)

Industrial Interactions

Technical discussions have been held with the following organizations:
Albany International Techniweave Inc.
Cytec Carbon Fibers
Ford Motor Company
Javelin 3D Digital Manufacturing Company
Nippon Graphite Fibers
3-Tex, Inc.
Unifin

Heat Exchange Concepts Utilizing Porous Carbon Foam

B. E. Thompson
University of Ottawa
Ottawa, Ontario, Canada K1N 6N5
A. G. Straatman
The University of Western Ontario
London, Ontario, Canada N6G 4K1
Phone: (613)562-5800, E-mail: Thompson@eng.uottawa.ca

Objective

To produce engineering models for design of heat exchangers made from porous carbon-foam materials. Knowledge and understanding of the effects of carbon foam on convective heat transfer is crucial to the development of appropriate engineering approximations for these design models. The overall objective is to explore new ideas for heat-exchanger configurations, especially for situations in which current technology is marginally cost effective. A thermo-economic model and a strategic design study are planned to provide new understanding for assessment in a stage-gate approach to further prototype development.

Highlights

Measurements have begun to quantify the enhancement of heat transfer with carbon foam coatings. Preliminary results with flat plates cooled by simple flow over the surface of the foam quantifies enhancement in the range from about 10 to 50% that depend sensibly on carbon-foam characteristics, Reynolds number, and foam thickness. Enhancement with geometric configurations that force flow through the foam, is anticipated to be larger and will need to be quantified as a function of pressure drop.

Technical Progress

Experiments to quantify heat transfer from heated plates coated with porous carbon foam have been configured in a 2x3 ft wind tunnel in the Boundary-Layer Wind Tunnel Laboratory at the University of Western Ontario. After validating the heat transfer was two-dimensional and after ascertaining that experimental uncertainty was within acceptable tolerances, tests began to investigate a range of foam thickness, air speed, heating rate and foam materials. Results will quantify enhancement of heat transfer that can be achieved with porous carbon-foam coatings. Preliminary results suggest that even in simple flow over top of a flat plate, there is natural enhancement of heat transfer, albeit over the range 10 to 50% depending on Reynolds number, material characteristics, and thickness. Conclusions about enhancement as a function of the thickness are still pending however results to date show no advantage for the use of very thick layers of foam, as was suspected from the outset.

Second, validation of the carbon foam model was complete as well as can be done with currently available experimental data. Results were used to select the best design of a carbon-foam heat exchanger concept for replacement of a conventional finned aluminium heat exchanger in a commercial microturbine. Significant progress was also made to resolve practical factors that include, for example, the inherent gradients of porosity in carbon-foam materials that result from its manufacturing processes. Similarly, concepts for use of carbon foam in electronic cooling were also improved.

Status of Milestones

The next two milestones are the completion of the carbon-foam heat exchanger design for a commercial microturbine, the completion of measurements with simple flow over flat plates coated with carbon foam, and the analysis of these wind tunnel measurements to quantify heat transfer from the surface of carbon foam, especially for the effect of thickness.

Industry Interactions

None during this period of intense effort to configure the experiments, select design concepts in collaboration with ORNL technical personnel, and the design of carbon-foam recuperator and electronic cooling devices.

Problems Encountered

The wind tunnel measurement program has required 3 times more wind tunnel time than was anticipated, in part, because eight samples were tested and, in part, because of the high standards in experimental uncertainty that were applied to produce reliable, repeatable, engineering results. Also, the cost of machining the eight carbon-foam plates exceeded expectations by 4 fold and this was due to difficulties that were not anticipated, specifically the extra care and cleaning needed to accurately machine the surfaces precisely: to obtain the required foam thicknesses with appropriate accuracy for the wind tunnel tests (i.e. to have no leading edge lip or deficit at the required thickness) cleaning had to be done during the machining process and not just afterwards. Greater care was required than anticipated to machine and clean all eight carbon-foam samples however this has resulted in excellent geometric configurations and reduced experimental uncertainty significantly. No further problems are anticipated.

Publications/Presentations

Yu, Q., Thompson, B. E, and Straatman, A. G.: Thermal engineering model of a heat exchanger with finned tubes made from porous carbon foam. CSME Forum 2004, June 1-4, 2004. University of Western Ontario, London, Canada.

MATERIALS FOR ADVANCED RECIPROCATING ENGINES

Spark Plug Erosion and Failure

H. T. Lin and M. P. Brady
Oak Ridge National Laboratory
Oak Ridge, TN 37831-6068
Phone: (865) 576-8857, E-mail: linh@ornl.gov

Objective

The subtask focuses on two major parallel efforts. The first task will characterize the electrode near-surface region microstructure in spark plugs before and after engine testing to understand corrosion/erosion mechanisms as a function of engine condition (environment) and time in determining the lifetime limiting processes. The information gained from the first task will feed into an exploratory alloy development effort for electrode materials with improved corrosion/erosion resistance to extend the long-term durability and lifetime performance of spark plugs for advanced reciprocating engines.

Highlights

A partnership was initiated with Federal Mogul (Champion) Corp. for development of natural gas spark plug electrode materials with improved erosion resistance during this reporting period. Wire of a microalloyed Ir alloy and a novel Cr-base alloy was delivered to Federal Mogul for assessment of manufacturability, with the goal of making several test spark plugs with these materials as electrode insert tips. Characterization of electrode materials after bench rig tests will be performed by ORNL.

Technical Progress

Microstructure characterization of spark plugs after 2020h field tests was carried out during this quarterly report period. These 2020h field-tested spark plugs, manufactured by Champion, Federal Mogul Corp., were acquired from Caterpillar Inc. The objective of this characterization was to provide insight into the effect of engine test time on the corrosion/erosion behavior of spark plug electrodes. SEM results of both ground (Pt-W alloy) and central (Ir) electrode inserts showed that the features of surface oxidation and substantial Ca-containing glassy phase formed on the side surfaces were similar to those reported previously for spark plugs after 4386h field test, as shown in Fig. 1 and 2. The presence of Ca was from the lubricant oil in the engine. Note that Ca was well known to be the glass modifier and could result in significant decrease in softening point and viscosity of glassy phase formed on the exposed surfaces, resulting the accelerated erosion process. The feature of droplet morphology, indicating the melting of electrode material, plus the micro cracking was also observed on the Pt-W electrode insert surface (Fig. 1b). In addition, the generation of mud cracks covered with Ir-containing oxide film was observed on Ir electrode insert surface (Fig. 2b). SEM examinations of polished cross sections showed extensive oxidation and crack generation occurred along the Pt-W alloy insert and Ni-base electrode interface after field test (Fig. 3b). Examinations also showed the generation of intergranular cracking in both Ir and Pt alloy insert after 2020h spark plugs, similar

to those observed in 4386h tested plugs (Fig. 4). Findings obtained from spark plugs with > 2000h of field test time suggest that it is necessary to acquire spark plugs with shorter test times (in 100h range) in order to understand the role of formation of Ca-containing glass on the erosion process and the onset of crack initiation.

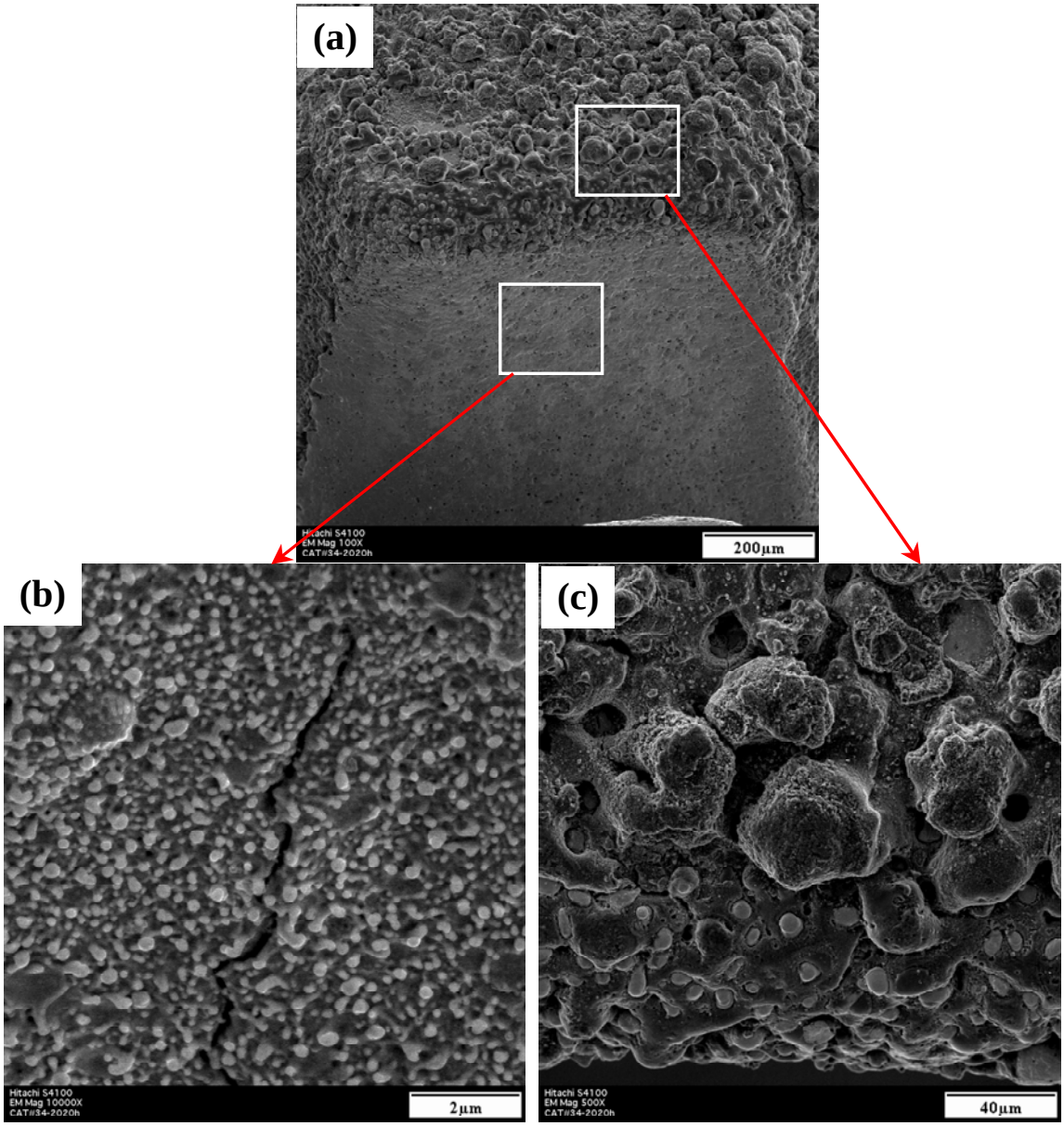

Figure 1. SEM micrographs of Pt-W insert after 2020h field test. (a) General oxidation feature of Pt-W electrode insert. (b) Pt-W electrode insert tip surface showing the droplet-like morphology with micro cracks. (c) Formation of Ca-containing glassy phase on the side surface of Pt-W electrode insert.

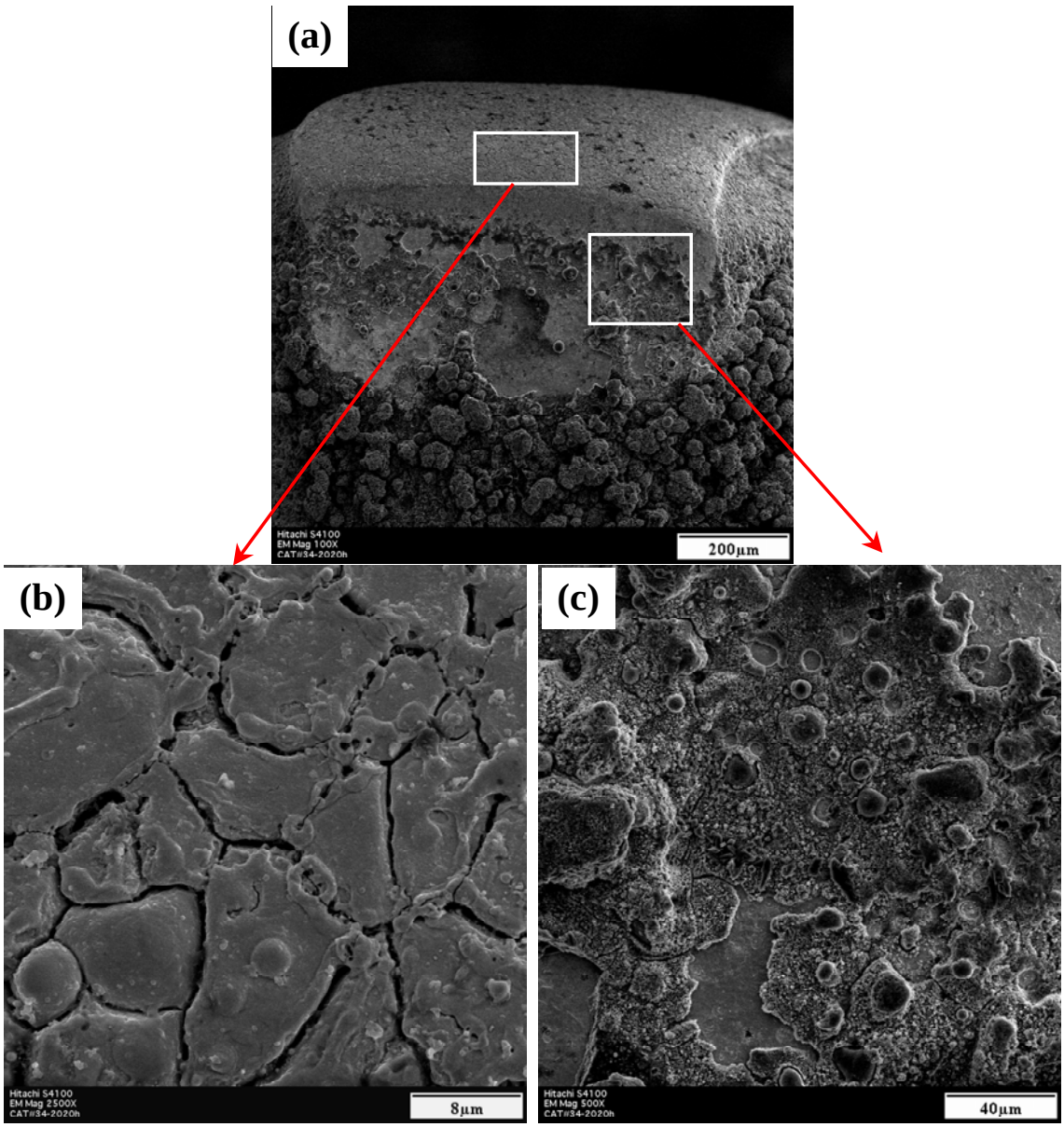

Figure 2. . SEM micrographs of Ir insert after 2020h field test. (a) General oxidation feature of Ir electrode insert. (b) Ir electrode insert tip surface showing the mud-like crack morphology plus glassy phase formation. (c) Formation of Ca-containing glassy phase on the side surface of Ir electrode insert.

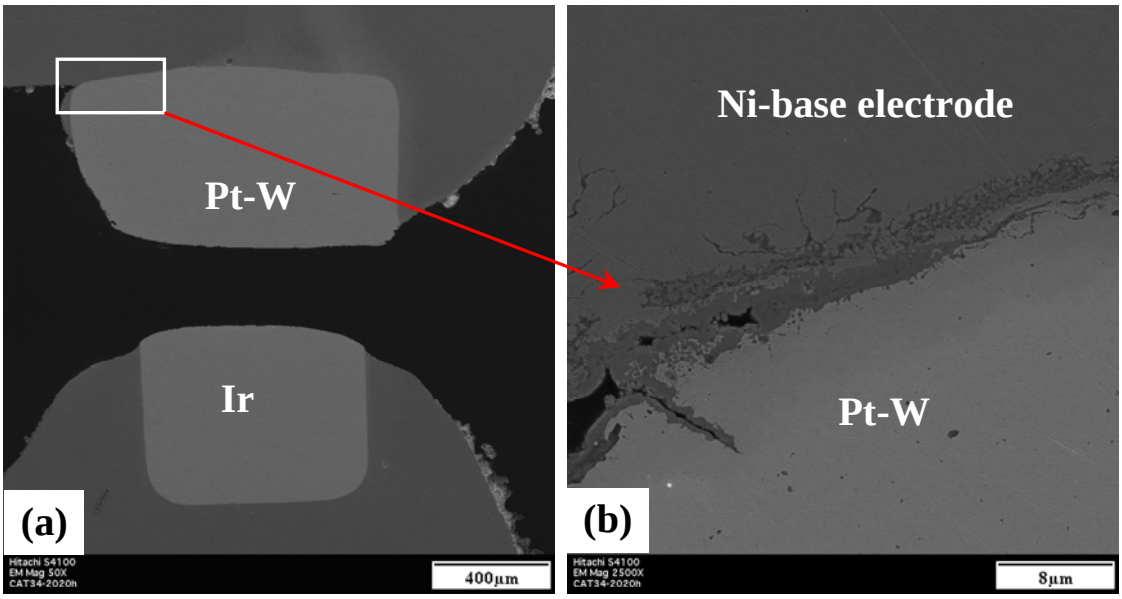

Figure 3. (a) SEM micrograph of polished cross-section of spark plug after 2020h field test. (b) Extensive oxidation and crack initiation occurred along the Ni-base alloy electrode and Pt-W alloy tip insert after field service.

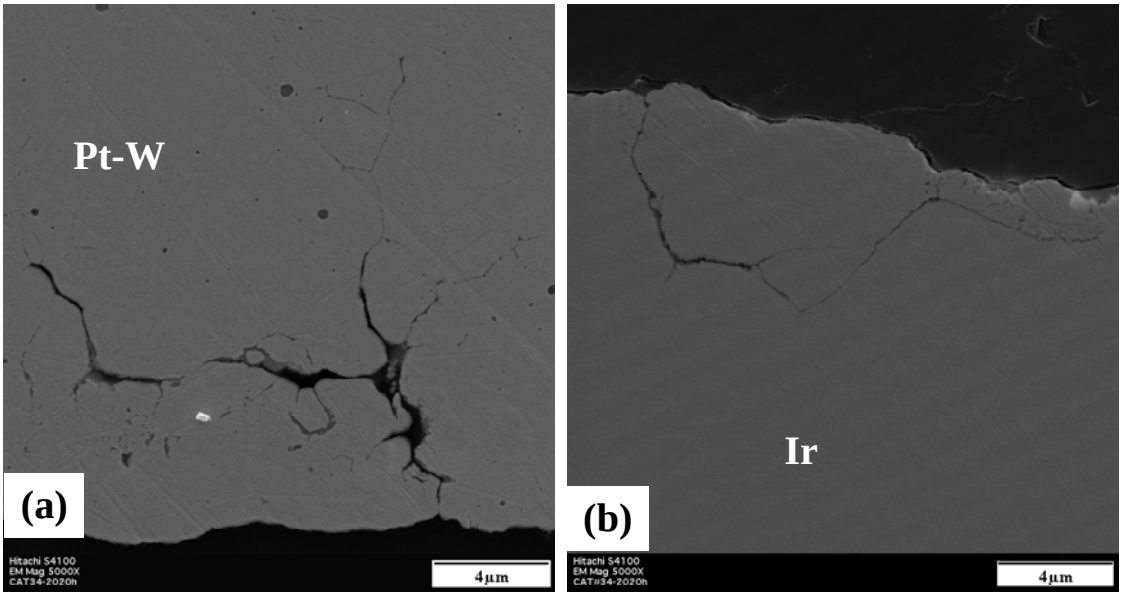

Figure 4. SEM micrographs show generation of extensive intergranular cracks in the subsurface region in both Pt-W alloy (a) and Ir (b) tip insert after field service.

Test coupons were manufactured from a stainless steel alloy in the solution treated and carbide precipitated conditions to explore the effect of nano carbide dispersions on sparking erosion. Study of this issue is based on literature reports of improved sparking resistance in precious metal and platinum group alloys with fine dispersions. This work makes use of findings from

other ORNL programs/efforts devoted to carbide dispersions for steels with improved high temperature creep resistance.

A partnership was initiated with Federal Mogul (Champion) for development of natural gas spark plug electrode materials with improved erosion resistance. Wire of a microalloyed Ir alloy and a novel Cr-base alloy was delivered to them for assessment of manufacturability, with the goal of making several test spark plugs with these materials as electrode insert tips. The selection of the Ir and Cr materials was based on ongoing characterization studies of worn, field tested spark plugs from natural gas engines. Those studies have found extensive electrode insert cracking, particularly with Pt inserts. Currently Ir inserts are used only on the central electrode due to poor manufacturability. The ORNL microalloyed Ir offers improved mechanical properties that may permit use of Ir inserts for both electrodes. The Cr alloy was selected because it offers the potential for significantly improved corrosion and cracking resistance in these environments over the Pt insert material. It is also significantly less expensive than the Pt.

Status of Milestones

Establish test protocol for rapidly screening developmental alloys for resistance to spark erosion and complete initial assessment of at least one material class/protection phenomenon for improved erosion resistance. September 2004. On schedule.

Industry Interactions

Drs. McMurray, Lykowski, and Levina from Federal Mogul (Champion) Corp. visited ORNL an on May 6th to discuss the spark plug electrode oxidation/erosion issues and potential collaborative research areas.

Communication with Caterpillar on the microstructure characterization results for spark plugs after 2020h field service.

Problems Encountered

None

Publications/Presentations

R. K. Richards, H. T. Lin, and M. P. Brady, “Characterization of Erosion Mechanisms of Natural Gas Engine Spark Plugs” accepted for presentation and publication at ASME International Combustion Engine Division, 2004 Fall Technical Conference, Long Beach, CA, October 24-27, 2004.

Advanced Materials for Exhaust Components of Reciprocating Engines

P. J. Maziasz, N. D. Evans, J. J. Truhan, and K. L. More
Metals and Ceramics Division
Oak Ridge National Laboratory
P.O. Box 2008, Oak Ridge, TN 37831-6115
Phone: (865) 574-5082, E-mail: maziaszpj@ornl.gov

Objective

This program is expanding to consider limitations of various critical in-cylinder and exhaust system components due to performance, temperature capability, and tribology for advanced natural gas reciprocating engine systems (ARES). While initial efforts focused only on exhaust valves, recent input from engine manufactures has expanded the scope to include intake and exhaust valves and their respective seats, as well as other exhaust components. Currently, this program is engaged in active dialog to define the long-term needs and priorities of engine makers.

Highlights

This quarter new work on engine cylinder components began with Waukesha Engine Division, Dresser Industries, including new and engine-tested components. For exhaust system materials creep-rupture data is summarized for the new CF8C-Plus cast austenitic stainless steel compared to SiMo cast iron, showing the great advantage of the cast stainless above 600^{o}C.

Technical Progress

Microcharacterization of exhaust valves of Pyromet 31V (Ni-22Cr-15Fe alloy with Ti and Al for γ' precipitation hardening), provided previously by Waukesha Engine Division, Dresser Industries, Inc. has been completed. That initial work will form a basis for comparison for follow-on work.

This quarter, new work employing a system approach for studying in-cylinder materials and considering both bulk metallurgical and surface and wear properties began with Waukesha Engine Division, Dresser Industries, Inc. The study encompasses intake and exhaust valves, and their corresponding seats, and compares both new and engine-tested components to determine changes occurring during service.

Last year, ORNL and Caterpillar developed a new cast austenitic stainless steel, CF8C-Plus, that has the potential for use as exhaust component applications in advanced diesel engines. Typical exhaust manifolds and turbocharger housings are made from SiMo cast iron, which has poor strength above 550-600^{o}C, and can be susceptible to thermal fatigue cracking during severe cycling after prolonged use. Standard CF8C steel (Fe-19Cr-9Ni-0.7Nb-0.07C), has good castability and sufficient strength up to about 600-625^{o}C, but is

not strong enough at higher temperatures. CF8C steel contains a large amount (20-25 vol.%) of δ-ferrite, which then transforms into σ-phase during aging at 600°C and above, and severely reduces ductility. CF8C-Plus steel was developed to be stronger and much more resistant to creep, fatigue and thermal fatigue for use in severe thermal cycling conditions. CF8C-Plus has an "engineered microstructure" that contains no δ-ferrite in the as-cast microstructure, and hence no σ-phase forms during aging.

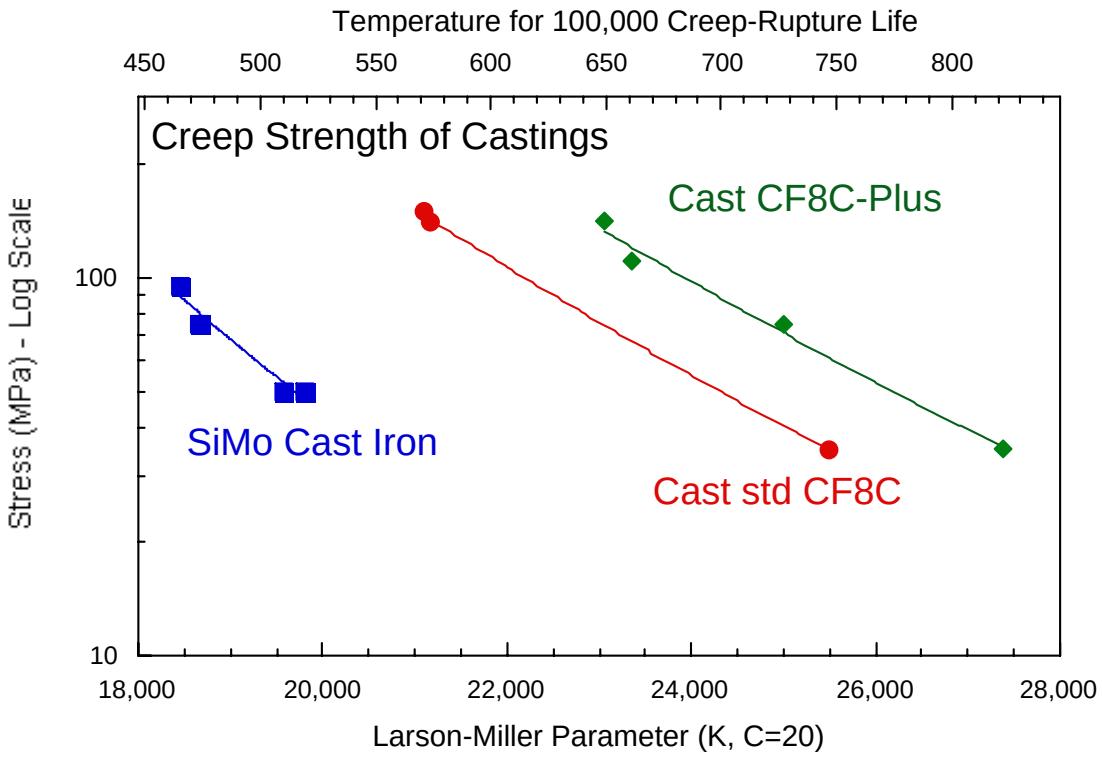

Figure 1 – Larson-Miller Parameter (LMP) plot of creep-rupture test data of commercial standard SiMo cast iron, CF8C cast austenitic steel, and ORNL lab-scale heats of new CF8C-Plus stainless steels. The SiMo cast iron was tested at 550-650°C, while the cast stainless was tested at 750-850°C. The CF8C-Plus has far better creep-rupture resistance than SiMo cast iron, and has almost twice the creep strength of the standard CF8C steel at these conditions. The upper axis is a projection of rupture temperature at a give stress for extrapolation of the current data to 100,000 h lifetime.

The creep-rupture resistance of a new commercial heat of the CF8C-Plus steel at 750-850°C is far better than SiMo cast iron, and better by almost a factor of two in rupture strength than standard CF8C steel (Fig. 1). The new CF8C-Plus steel is currently being commercialized, and should be applicable for exhaust components of advanced ARES engines.

Status of Milestones

FY 2004 – Complete characterization Ni-based superalloy (Pyromet 31V) valves to define aging effect during engine service. Define aging effects at weld overlay and coating bond regions (December 2003) – completed.

Industry Interactions

New discussions with Waukesha Engine Dresser, Inc. (Jim Drees, Joe Derra, Roger Rangarajan, and others) about materials needs and interests for advanced ARES engines with ORNL (Tom King, Tim Theiss, Phil Maziasz and John Truhan) began last quarter, and defined a clear set of initial tasks that began this quarter.

Problems Encountered

None

Publications/Presentations

None

Development of Catalytically Selective Electrodes for NOx and Ammonia Sensors

T. Armstrong, F. Montgomery, and D. West
Oak Ridge National Laboratory
P.O. Box 2008, Oak Ridge, TN 37831-6084
Phone: (865) 574-7996, E-mail: armstrongt@ornl.gov

Objective

This project seeks to develop materials and technologies useful for NO_x and ammonia sensors.

Highlights

As the project has progressed, the major focus has been on DC, electrical-biased sensing elements with compositionally identical electrodes, with secondary emphasis on sensing elements with two different electrode materials.

Elements with two electrode materials (conductive oxide/Pt)

Recent investigations on these types of elements have focused on the impact of replacing $La_{0.85}Sr_{0.15}CrO_3$ (LSC) with other La-containing perovskites. Some of the findings are given in Fig. 1, which shows that the response to 450 ppm NO_x (600°C, 7 vol% O_2) was qualitatively the same for $La_{0.85}Ba_{0.15}CrO_3$ (LBC)/Pt and LSC/Pt with DC current bias, but quite different for Sr-modified $LaFeO_3$ (LSF). LBC, LSC, and $La_{0.8}Sr_{0.2}FeO_3$ (LSF) are all p-type oxides, therefore the reason for the differing response of LSF relative to the chromites may be due either to the presence of oxygen vacancies in the LSF, or to the fact that the B-site ion (Fe^{3+}) in LSF is already in its highest common valence state.

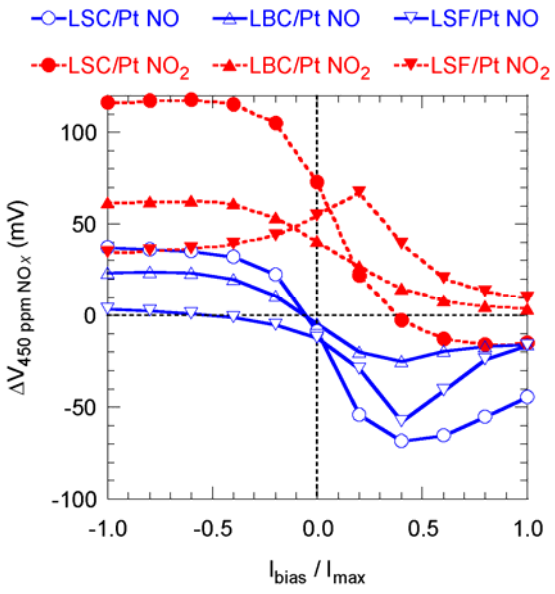

Figure 1: Voltage changes produced by 450 ppm_V NO_x (600°C, 7 vol% O_2, balance N_2) as a function of DC bias for dual-materials sensing elements with $La_{0.85}Sr_{0.15}CrO_3$ (LSC), $La_{0.85}Ba_{0.15}CrO_3$ (LBC), and $La_{0.8}Sr_{0.2}FeO_{3-}$ (LSF) in conjunction with Pt.

Elements with compositionally identical electrodes

The temperature dependence of the NO_x sensing response was investigated. Data collected to study this dependence are shown in Fig. 2. The data indicate that the measured resistance[1] (R) is an exponential function of T whereas the changes in R_{meas} (ΔR) due to NO_x are a linear function of temperature.

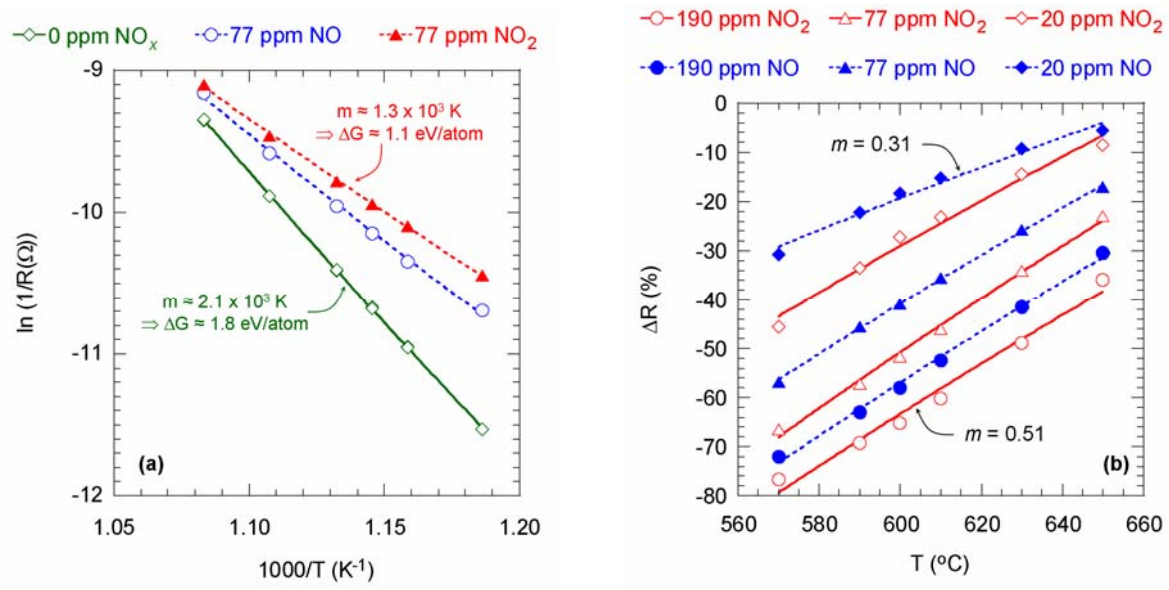

Figure 1: "Arrhenius" plot of log admittance (1/R) vs. 1/T (a) and changes in resistance (ΔR) due to the presence of NO_x as a function of T (b). Data collected in 7 vol% O_2.

Status of Milestones

Elements with two electrode materials (conductive oxide/Pt)
For these type of elements the focus will be on n vs. p type oxides. As mentioned previously, most work at ORNL has focused on p-type oxides and the effect(s) of pairing a n-type oxide (such as ZnO or WO_3) with Pt is unknown. Depending on the outcome of the initial experiments, sensing elements which pair off n and p type oxides (no Pt) could also be fabricated and tested.

[1] The data in Fig. 1 were collected with voltage biasing. The measured currents were converted to resistances.

Elements with compositionally identical electrodes

Four specific series of experiments are planned:

1. Electrode thickness effects will be studied by fabricating electrodes with wet thicknesses of 30, 75 (current ORNL wet print thickness), and 130 μm.
2. A "small footprint" element geometry in will be explored. The current plan is to attach Pt leads and seal the connector surface with glass in an attempt to more closely simulate actual sensor geometry.
3. Experiments aimed at elucidating the mechanism for "total NO_x" sensing are being planned.

Problems Encountered

None

Publications/Presentations

D. L. West, F. C. Montgomery, and T. R. Armstrong. "Electrically biased NO_x sensing elements with co-planar electrodes," *205th Meeting of the Electrochemical Society*, San Antonio, TX, May 2004.

D. L. West, F. C. Montgomery, and T. R. Armstrong. "Electrically biased NO_x sensing elements with co-planar electrodes," (companion paper to above presentation, submitted to *Journal of the Electrochemical Society* June 2004).

Trips/Meetings

A meeting was held in Washington DC with Ford (J. Visser, R. Soltis, D. Kubinski, R. Novak, E. Murray), and ORNL (T. Armstrong and D. West) to discuss our progress.

Internal Distribution

B. L. Armstrong, 4515, MS-6063, armstrongbl@ornl.gov
T. R. Armstrong, 4508, MS-6084, armstrongt@ornl.gov
P. F. Becher, 4515, MS-6068, becherpf@ornl.gov
T. M. Besmann, 4515, MS-6063, besmanntm@ornl.gov
C. A. Blue, 4508, MS-6083, blueca@ornl.gov
M. P. Brady, 4500S, MS-6115, bradymp@ornl.gov
M. A. Brown, 4500N, MS-6186, brownma@ornl.gov
M. K. Ferber, 4515, MS-6069, ferbermk@ornl.gov
J. A. Haynes, 4515, MS-6063, haynesa@ornl.gov
D. R. Johnson, 4515, MS-6066, johnsondr@ornl.gov
M. A. Karnitz, 4500N, MS-6186, karnitzma@ornl.gov
J. O. Kiggans, 4508, MS-6087, kiggansjojr@ornl.gov
T. J. King, 4515, MS-6065, kingtjjr@ornl.gov
J. W. Klett, 4508, MS-6087, klettjw@ornl.gov
E. Lara-Curzio, 4515, MS-6069, laracurzioe@ornl.gov
H. T. Lin, 4515, MS-6068, linh@ornl.gov
R. A. Lowden, 4515, MS-6063, lowdenra@ornl.gov
P. J. Maziasz, 4500S, MS-6115, maziaszpj@ornl.gov
K. L. More, 4515, MS-6064, morekl1@ornl.gov
R. D. Ott, 4515, MS-6083, ottr@ornl.gov
S. D. Nunn, 4508, MS-6087, nunnsd@ornl.gov
B. A. Pint, 4500S, MS-6156, pintba@ornl.gov
D. T. Rizy, 3147, MS-6070, rizydt@ornl.gov
D. P. Stinton, 4515, MS-6063, stintondp@ornl.gov
R. W. Swindeman, 4500S, MS-6155, swindemanrw@ornl.gov
T. N. Tiegs, 4508, MS-6087, tiegstn@ornl.gov
P. F. Tortorelli, 4500S, MS-6156, tortorellipf@ornl.gov
I. G. Wright, 4500S, MS-6157, wrightig@ornl.gov
A. Zaltash, 3147, MS-6070, zaltasha@ornl.gov

External Distribution

ALLISON ADVANCED DEVELOPMENT CO., 1100 Wilson Blvd., Suite 1450, Arlington, VA 22209
J. Miles, r.jeffrey.miles@allison.com

ALM SYSTEMS, INC, 1920 N Street, NW, Suite 750, Washington, DC 20036
M. Kalin, mkalin@ibek.com

ARGONNE NATIONAL LABORATORY, 9700 S. Cass Ave., Argonne, IL 60439-4838
W. Ellingson, ellingson@anl.gov
J. P. Singh, jpsingh@anl.gov

BATTELLE MEMORIAL INSTITUTE, 505 King Avenue, Columbus, OH 43201
D. Anson, ansond@battelle.org

BAYSIDE MATERIALS TECHNOLOGY, 21150 New Hampshire Ave., Brookville, MD 20833
D. Freitag, dfreitag@ix.netcom.com

BCS, INC., 5550 Sterrett Place, Suite 216, Columbia, MD 21044
D. Bartley, dbartley@bcs-hq.com

BOWMAN POWER, 20501 Ventura Boulevard #285, Woodland Hills, CA 91364
T. Davies, tdavies@bowmanpower.co.uk
T. Hynes, ahynes.bowmanpower@att.net
D. Flaxington, dflaxington@bowmanpower.co.uk

CALIFORNIA ENERGY COMMISSION
A. Soinski, asoinski@energy.state.ca.us

CANNON-MUSKEGON CORP., Box 506, Muskegon, MI 49443-0506
J. Wahl, jwahl@canmkg.com

CAPSTONE TURBINE CORP., 6430 Independence Ave., Woodland Hills, CA 91367
P. Chancellor, pchancellor@capstoneturbine.com
K. Duggan, kduggan@capstoneturbine.com
M. Stewart, mstewart@capstoneturbine.com
J. Willis, jwillis@capstoneturbine.com
M. Rodrigues, mrodrigues@capstoneturbine.com
B. Treece, btreece@capstoneturbine.com

CERAMATEC INC., 2425 South 900 West, Salt Lake City, UT 84119
C. Lewinsohn, clewinsohn@ceramatec.com
B. Nair, bnair@ceramatec.com

CLEMSON UNIVERSITY, South Carolina Institute for Energy Studies, 386-2, Clemson, SC 29634-5180
L. Golan, glawren@clemson.edu
R. Wenglarz, rwnglrz@clemson.edu
J. Hinson, jhinson@clemson.edu

CONNECTICUT RESERVE TECHNOLOGIES, 2997 Sussex Ct., Stow, OH 44224
E. Baker, baker@crtechnologies.com
S. Duffy, sduffy@crtechnologies.com
J. Palko, jpalko@crtechnologies.com

DTE ENERGY, 37849 Interchange Dr., Suite 100, Farmington Hills, MI 48335
M. Davis, davism@dteenergy.com

ELECTRIC POWER RESEARCH INSTITUTE, 3412 Hillview Ave., Palo Alto, CA 94303
J. Stringer, jstringe@epri.com

ELGILOY SPECIALTY METALS, 1565 Fleetwood Drive, Elgin, IL 60123

T. Bartel, terryb@elgiloy.com

ELLIOTT ENERGY SYSTEMS, 2901 S.E. Monroe Street, Stuart, FL 34997
D. Burnham, dburnham@elliott-turbo.com
D. Dewis, ddewis@elliott-turbo.com

ENERGETICS, INC., 501 School St., SW, Suite 500, Washington, DC 20024
R. Scheer, rscheer@energeticsinc.com

ENERGY TECHNOLOGIES APPLICATIONS, 5064 Camino Vista Lujo, San Diego, CA 92130-2849
T. Bornemisza, borneger@ix.netcom.com

GAS TURBINE ASSOCIATION, 1050 Thomas Jefferson St., NW, 5th Fl, Washington, DC 20007
J. Abboud, abboud@advocatesinc.com

GENERAL ELECTRIC (GE) CR&D, 1 Research Circle, Building K1-RM 3B4, Niskayuna, NY 12309
S. Correa, correa@crd.ge.com
K. Luthra, luthra@crd.ge.com
M. VanDerwerken, vanderwerken@crd.ge.com
C. Johnson, johnsonca@crd.ge.com

GENERAL ELECTRIC AIRCRAFT ENGINES, One Neumann Way, Mail Drop M89, Cincinnati, OH 45215-1988
R. Darolia, ram.darolia@ae.ge.com

GENERAL ELECTRIC POWER SYSTEMS, One River Rd., 55-127, Schenectady, NY 12345
R. Orenstein, robert.orenstein@ps.ge.com

GENERAL ELECTRIC POWER SYSTEMS, Gas Technology Center, 300 Garlington Road, Greenville, SC 29615
P. Monaghan, philip.monagham@ps.ge.com

HAYNES INTERNATIONAL, INC., 1020 W. Park Avenue, P.O. Box 9013, Kokomo, IN 46904-9013
V. Ishwar, vishwar@haynesintl.com
D. Klarstrom, dklarstrom@haynesintl.com

HONEYWELL CERAMIC COMPONENTS, 2525 W. 190th St., Torrance, CA 90504
D. Foley, dan.foley@honeywell.com
C. Li, chien-wei.li@honeywell.com
D. Newson, danielle.newson@honeywell.com
M. Savitz, MaxineSavitz@aol.com
J. Wimmer, jim.wimmer@honeywell.com
M. Mitchell, michele.mitchell@honeywell.com

HONEYWELL COMPOSITES, 1300 Marrows Rd., PO Box 9559, Newark, DE 19714-9559
L. Connelly, liz.connolly@ps.ge.com
P. Gray, paul1.gray@ps.ge.com
D. Landini, dennis.landini@ps.ge.com

HONEYWELL ENGINES, SYSTEMS, & SERVICES 2739 E. Washington St., PO Box 5227, Phoenix, AZ 85010
B. Schenk, bjoern.schenk@honeywell.com
HONEYWELL POWER SYSTEMS, 8725 Pan American Freeway NE, Albuquerque, NM 87113
S. Wright, e.scott.wright@honeywell.com

HOWMET RESEARCH CORP., 1500 South Warner St., Operhall Research Center, Whitehall, MI 49461-1895
B. Mueller, bmueller@howmet.com
R. Thompson, rthompson@howmet.com

INGERSOLL-RAND ENERGY SYSTEMS, 32 Exeter St., Portsmouth, NH 03801
A. Kaplau-Colan, alex_haplau-colan@ingersoll-rand.com
M. Krieger, michael_krieger@irco.com
J. Johnson, jay_johnson@ingersoll-rand.com
J. Kesseli, jim_kesseli@ingersoll-rand.com
J. Nash, jim_nash@ingersoll-rand.com

KENNAMETAL INC. 1600 Technology Way, P.O. Box 231, Latrobe, PA 15650-0231
R. Yeckley, Russ.yeckley@kennametal.com

KINECTRICS NORTH AMERICA, 124 Balch Springs Circle, SW, Leesburg, VA 20175
B. Morrison, blake.Morrison@kinectrics.com

KRUPP VDM TECHNOLOGIES CORP., 11210 Steeplecrest, Suite #120, Houston, TX 77065-4939
D. Agarwal, dcagarwal@pdq.net

NASA GLENN RESEARCH CENTER, 21000 Brookpark Rd., MS 49-7, Cleveland, OH 44135
D. Brewer, david.n.brewer@grc.nasa.gov
J. Gykenyesi, john.p.gyekenyesi@lerc.nasa.gov
S. Levine, stanley.r.levine@lerc.nasa.gov
N. Nemeth, noel.n.nemeth@grc.nasa.gov
B. Opila, opila@grc.nasa.gov

NATIONAL RURAL ELECTRIC COOPERATIVE ASSOC., 4301 Wilson Blvd., SS9-204, Arlington, VA 22203-1860
E. Torrero, ed.torrero@nreca.org

NATURAL RESOURCES CANADA, 1 Haanel Drive, Nepean, Ontario, Canada K1A 1M1
R. Brandon, rbrandon@nrcan.gc.ca

PCC AIRFOILS, INC., 25201 Chagrin Blvd., Suite 290, Beachwood, OH 44122
C. Kortovich, ckortovich@pccairfoils.com

PENN STATE UNIVERSITY, Applied Research Laboratory, PO Box 30, State College, PA 16823
J. Singh, jxs46@psu.edu

RICHERSON AND ASSOC., 2093 E. Delmont Dr., Salt Lake City, UT 84117
D. Richerson, richersond@aol.com

ROLLS-ROYCE ALLISON, 2925 W. Minnesota St., PO Box 420, Indianapolis, IN 46241
S. Berenyi, steve.g.berenyi@allison.com
P. Heitman, peter.w.heitman@allison.com
F. Macri, francis.g.macri@allison.com
J. Oswald, jim.oswald@rolls-royce.com

SAINT-GOBAIN CERAMICS & PLASTICS, INC., Goddard Road, Northboro, MA 01532
B. LaCourse, Brian.C.LaCourse@saint-gobain.com
R. Licht, robert.h.licht@saint-gobain.com
M. Abouaf, Marc.Abouaf@saint-gobain.com
V. Pujari, Vimal.K.Pujari@saint-gobain.com
A. Vartabedian, Ara.M.Vartabedian@saint-gobain.com

SEBESTYEN, T., Consultant, 6550 Mission Ridge, Traverse City, MI 49686-6123
T. Sebestyen, sebestyen@chartermi.net

SIEMENS WESTINGHOUSE POWER CORP., 1310 Beulah Rd., Pittsburgh, PA 15235-5098
M. Burke, michael.burke@swpc.siemens.com
C. Forbes, christian.forbes@swpc.siemens.com

SOLAR TURBINES, INC., TurboFab Facility, 16504 DeZavala Rd., Channelview, TX 77530
B. Harkins, harkins_bruce_d@solarturbines.com

SOLAR TURBINES INC., 818 Connecticut Ave., NW, Suite 600, Washington, DC 20006-2702
R. Brent, solardc@bellatlantic.net

SOLAR TURBINES, INC., 2200 Pacific Highway, PO Box 85376, MZ R, San Diego, CA 92186-5376
P. Browning, browning_paul_f@solarturbines.com
M. Fitzpatrick, fitzpatrick_mike_d@solarturbines.com
P. Montague, montague_preston_j@solarturbines.com
M Van Roode, van_roode_mark_x@solarturbines.com
M. Ward, ward_mike_e@solarturbines.com
J. Price, jeffprice@solarturbines.com

SOUTHERN CALIFORNIA EDISON COMPANY, 2244 Walnut Grove Avenue, Rosemead, CA 91770

S. Hamilton, hamiltsl@sce.com

SOUTHERN COMPANY, 600 N. 18th Street, 14N-8195, P.O. Box 2641, Birmingham, AL 35291

S. Wilson

STEVEN I. FREEDMAN, Engineering Consultant, 410 Carlisle Ave., Deerfield, IL 60015

S. Freedman, sifreedman@aol.com

STAMBLER ASSOCIATES, 205 South Beverly Drive, Suite 208, Beverly Hills, California 90212

I. Stambler

THE BOEING COMPANY, Rocketdyne Propulsion & Power, 6633 Canoga Avenue
MC: GB-19, P.O. Box 7922, Canoga Park, CA 91309-7922

G. Pelletier, gerard.pelletier@west.boeing.com

TELEDYNE CONTINENTAL MOTORS, 1330 W. Laskey Rd., PO Box 6971, Toledo, OH 43612-0971

J. T. Exley, texley@teledyne.com

TURBEC

L. Malmrup, lars.malmrup@turbec.com

UCI COMBUSTION LABORATORY, U. of CA, Irvine, Irvine, CA 92697-3550

V. McDonell, mcdonell@ucic1.uci.edu

UDRI, Ceramic & Glass Laboratories, 300 College Park Ave., Dayton, OH 45469-0172

A. Crasto, allan.crasto@udri.udayton.edu
G. Graves, gravesga@udri.udayton.edu
N. Osborne, osborne@udri.udayton.edu
R. Wills, roger.wills@udri.udayton.edu

UNITED TECHNOLOGIES RESEARCH CENTER, 411 Silver Lane MS 129-24, East Hartford, CT 06108

H. Eaton, eatonhe@utrc.utc.com
J. Holowczak, holowcje@utrc.utc.com
T. Rosfjord, rosfjotj@utrc.utc.com
J. Smeggil, smeggijg@utrc.utc.com
G. Linsey, linseygd@utrc.utc.com
J. Shi, shij@utrc.utc.com
E. Sun, suney@utrc.utc.com
D. Mosher, mosherda@utrc.utc.com

UNIVERSITY OF CALIFORNIA, Department of Mechanical Engineering, Berkeley, CA 94720
R. Dibble, rdibble@newton.berkeley.edu

UNIVERSITY OF COLORADO, Department of Mechanical Engineering, Boulder, CO 80309-0427
R. Raj, rishi.raj@Colorado.edu

UNIVERSITY OF MARYLAND, Department of Mechanical Engineering, College Park, MD 20742-3035
R. Radermacher, rader@eng.umd.edu

UNIVERSITY OF OTTAWA, Department of Mechanical and Materials Engineering, Ottawa, Ontario, Canada K1N 6N5
B. E. Thompson, Thompson@eng.uwo.ca

UNIVERSITY OF WESTERN ONTARIO, Department of Mechanical and Materials Engineering, London, Ontario, Canada N6G 4K1
A. G. Straatman, astraat@engga.uwo.ca

US DOE-NETL, P. O. Box 880, MSO-D01, 3610 Collins Ferry Rd., Morgantown, WV 26507-0880
C. Alsup, Jr., charles.alsup@netl.doe.gov
A. Layne, abbie.layne@netl.doe.gov
L. Wilson, lane.wilson@netl.doe.gov

US DOE-NETL, PO Box 10940, Pittsburgh, PA 15236
N. Holcombe, norman.holcombe@netl.doe.gov
U. Rao, rao@netl.doe.gov

US DOE CHICAGO OPERATIONS OFFICE, 9800 S. Cass Ave., Argonne, IL 60439
J. Jonkouski, jill.jonkouski@ch.doe.gov
J. Mavec, joseph.mavec@ch.doe.gov
J. Livengood, joanna.livengood@ch.doe.gov
S. Waslo, stephen.waslo@ch.doe.gov

US DOE-HQ, 1000 Independence Ave., S.W., Washington DC 20585
R. Fiskum, ronald.fiskum@ee.doe.gov
D. Haught, debbie.haught@ee.doe.gov
P. Hoffman, patricia.hoffman@ee.doe.gov
W. Parks, william.parks@ee.doe.gov
M. Smith, merrill.smith@ee.doe.gov
C. Sorrell, charles.sorrell@ee.doe.gov

WILLIAMS INTERNATIONAL, 2280 West Maple Rd., PO Box 200, Walled Lake, MI 48390-0200
G. Cruzen, g.cruzen@williams-int.com
W. Fohey, w.fohey@williams-int.com

C. Schiller, cschiller@williams-int.com

WRIGHT PATTERSON AIRFORCE BASE,
R. Sikorski, ruth.sikorski@wpafb.af.mil